

②
FINAL REPORT

RESEARCH ON THE CORRELATION OF ALOUETTE-ISIS
SATELLITE DATA WITH GROUND-BASED MAGNETOMETER

DATA *final report*

by

Gordon Rostoker, Marie P. Hron, and R.P. Sharma

DOC Contract OSP3-0167

DSS File Number Sp2 36100-3-0328

March 31, 1975



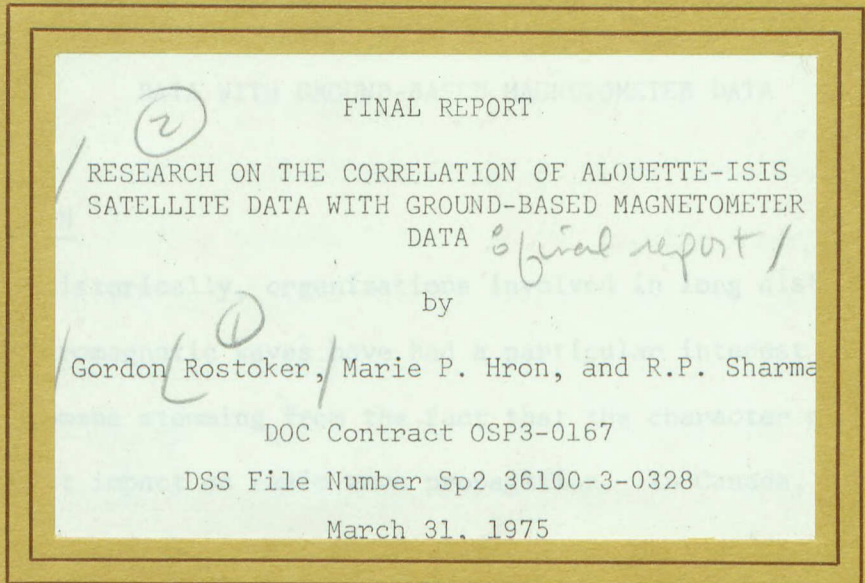
Geophysics

DEPARTMENT OF PHYSICS

**The University of Alberta
Edmonton, Alberta, Canada**

CRL-2243

P
91
C655
R688
1975



Geophysics

DEPARTMENT OF PHYSICS
The University of Alberta
Edmonton, Alberta, Canada

Queen
91
C655
R688
1975

(2) FINAL REPORT

RESEARCH ON THE CORRELATION OF ALOUETTE-ISIS
SATELLITE DATA WITH GROUND-BASED MAGNETOMETER

DATA *Final report*

by

Gordon Rostoker, Marie P. Hron, and R.P. Sharma

DOC Contract OSP3-0167

DSS File Number Sp2 36100-3-0328

March 31, 1975



P
91
C655
R688
1975

DD4610466
DL 4610489

FINAL REPORT ON DOC CONTRACT OSP3-0167

DSS FILE NUMBER Sp2 36100-0328

RESEARCH ON THE CORRELATION OF ALOUETTE-ISIS SATELLITE
DATA WITH GROUND-BASED MAGNETOMETER DATA

INTRODUCTION

Historically, organizations involved in long distance communications using electromagnetic waves have had a particular interest in magnetic storm phenomena stemming from the fact that the character of the ionosphere has a direct impact on radio wave propagation. In Canada, research into the influence of the ionosphere on radio wave propagation has been considered an active area of research since a large portion of the country lies at high magnetic latitudes where ionospheric effects associated with magnetic storms are most pronounced.

More recently, communications using H.F. radio waves have had less attention as the capability and facilities to transfer information using microwaves, UHF (via geostationary satellites), and hard line has been upgraded. Accordingly, there is less concern regarding the potential disruption of communications by ionospheric disturbance. Nonetheless, problems relating to magnetospheric storm and substorm activity are still of considerable importance in that spacecraft charging aboard geostationary spacecraft (DeForest, 1972) and induced earth currents in hard line communications networks (Anderson et al., 1974) may still cause disruptions in standard commercial communications networks. Accordingly, the Department of Communications still maintains an active interest in being able to relate the state of the magnetosphere (as controlled by the solar terrestrial

interaction) to the potential for disruption of communications networks. This interest demands an ability to monitor the level and character of energy transport and dissipation within the magnetosphere. Monitoring of this nature has been accomplished using ground based networks of instruments and using detectors flown in the topside ionosphere. It is of considerable importance to be able to relate in situ measurements of ionospheric and magnetospheric parameters to signatures in the various parameters measureable at the ground. In particular, the Department of Communications has operated the ISIS and Alouette series of satellites and has developed the ability to describe the state of the topside ionosphere. However, it is important to be able to relate the parameters of the topside ionosphere to the behaviour of the lower ionosphere when large currents may flow.

Ground based arrays of magnetometers have the capability of defining localized regions of significant current flow ($> 10^5$ A) in the lower ionosphere and associated with field-aligned currents. It is therefore useful to determine whether or not information recorded in the topside ionosphere is capable of defining the region of the ionospheric auroral electrojets and whether or not some measure of the strength of the electrojets can be established using such information. The research carried out under this contract attempts to answer these questions. Under the terms of the contract, magnetometer data from the University of Alberta meridian line were acquired, processed, and analysed to determine regions of electrojet flow in the auroral ionosphere over a period of some two months from November 1971 through February 1972. Data

from the topside sounder on ISIS II were subsequently analysed for passes where the satellite traversed a geographic meridian close to the station line at times when the magnetometer data yielded information about the character of the electrojets. The character of the topside ionosphere above the regions of electrojet flow were then investigated. This report deals with the results of this correlative study.

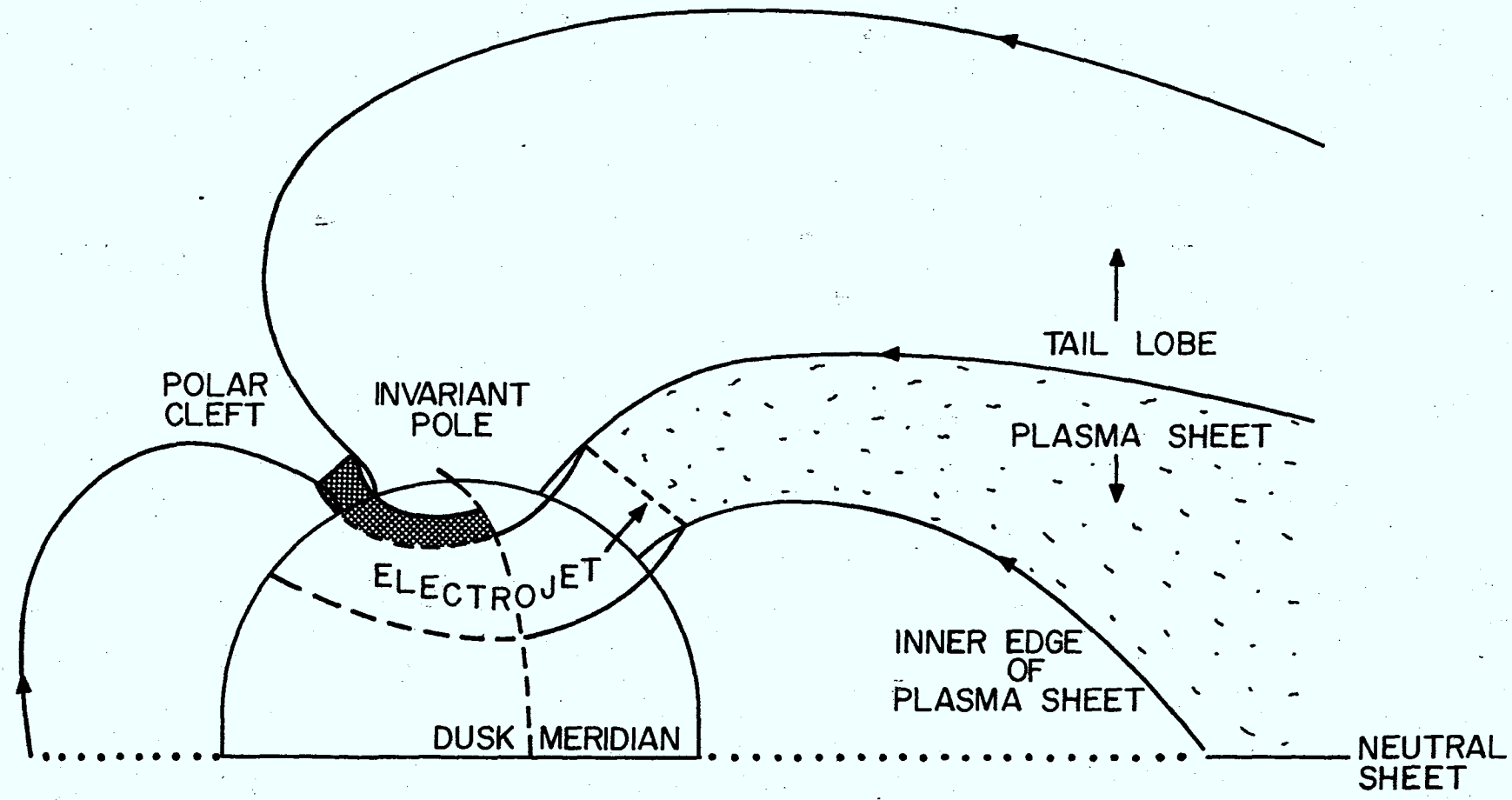
THE AURORAL ELECTROJETS

It is now well known that the magnetic field configuration of the earth is distorted by the flow of the solar wind emanating from the sun, and that this solar-terrestrial interaction causes the formation of a group of field lines distended in the anti-sunward direction in the lee of the earth (termed the magnetotail). In this way energy extracted from the solar wind as it flows past the earth is stored in the near earth environment (Figure 1). The energy is stored in the magnetotail as the kinetic energy of plasma sheet particles and in magnetic lines of force. This energy is eventually dissipated in the high latitude ionosphere and predominantly in the regions of the auroral electrojets. Hence the ability to monitor the character of the auroral electrojets is tantamount to the ability to monitor the solar terrestrial interaction.

Energy is transferred from one place to another within the magnetotail through the process of convection at velocities defined by the cross product of the electric and magnetic fields, viz

$$\underline{v} = \frac{\underline{E} \times \underline{B}}{B^2}$$

Figure 1 Schematic diagram (not to scale) showing regions of importance in the high latitude ionosphere and the regions in the magnetosphere and magnetotail to which they map. The northern hemisphere of the magnetosphere is shown with the situation being symmetric in the lower hemisphere.

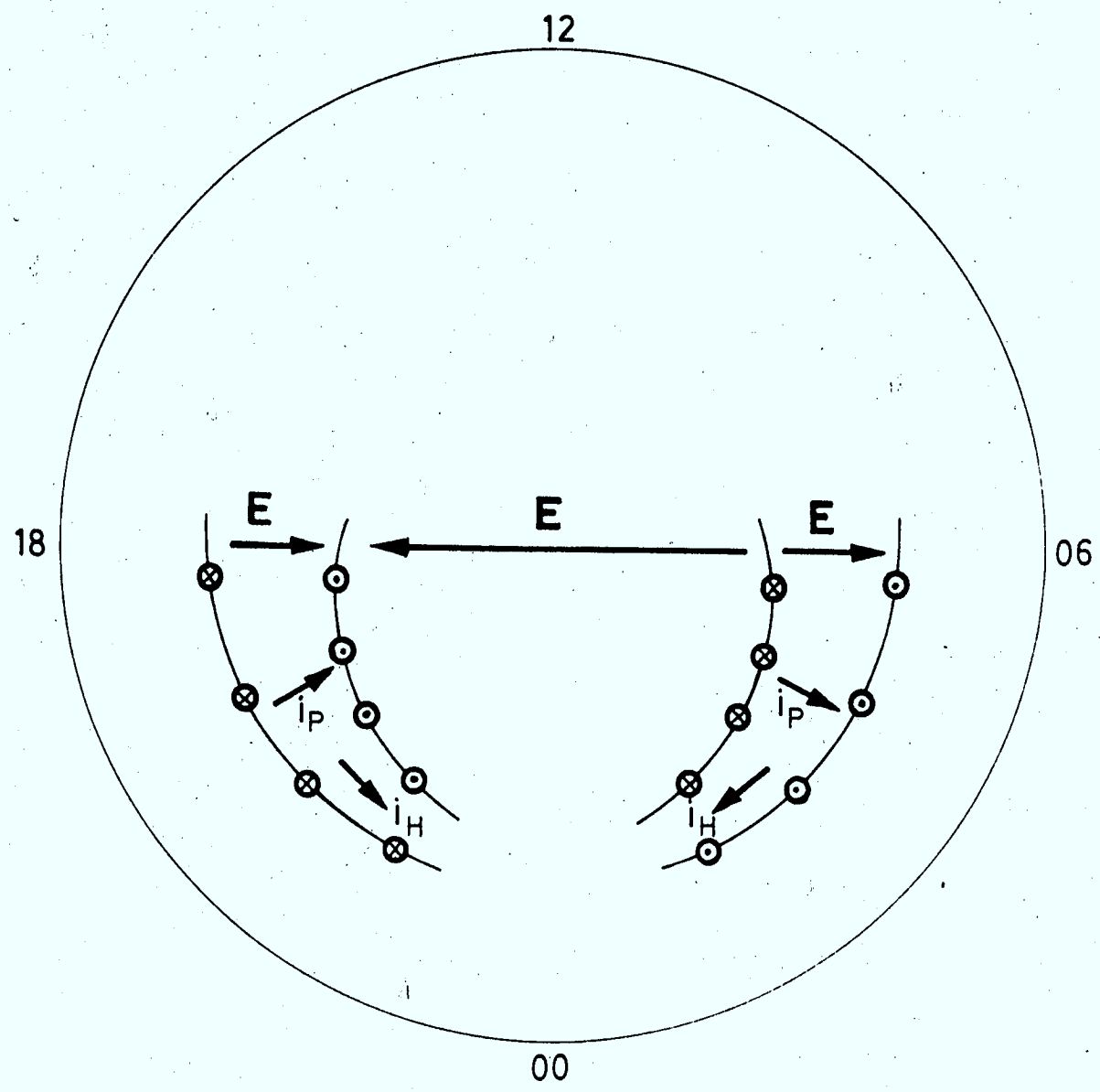


- 11 -

The electric field which is associated with convective motion in the magnetotail is thought to be the same electric field which drives the auroral electrojets. The distribution of key parameters utilized in this study is shown in Figure 2. In particular, we see that the ionospheric signature of magnetospheric convection is an eastward electrojet in the evening sector and a westward electrojet in the morning sector. The latitudinal extent of these electrojets is generally $5 - 10^{\circ}$ centered at a geomagnetic latitude of approximately 70° . The electrojets are penetrated by field aligned current flow (Zmuda and Armstrong, 1974) which is also detected far out in the magnetotail (Sugiura, 1974; Rostoker and Boström, 1975). The electric field that drives the Pedersen currents in the ionosphere which connect the upward and downward flowing currents, also drives Hall currents which are in fact the electrojets. It is the magnetic effect of these (Hall) electrojets which is detected at the earth's surface by the University of Alberta magnetometers.

The high conductivity channels which are the sites of the auroral electrojets are created by intense fluxes of precipitating electrons in the keV energy range. The higher is the energy of the precipitating electrons, the further into the ionosphere they penetrate. Thus it is the relatively low energy electrons which should have the major influence on the topside ionosphere. While it is well known that regions of the ionosphere below the peak of the F-layer exhibit markedly enhanced number densities of thermal plasma across the auroral electrojets, the situation in the topside ionosphere is less well defined. The topside sounder aboard the ISIS-II satellite is capable of yielding information about thermal

Figure 2 Polar plot showing the configuration of key parameters in the region of the high latitude ionosphere. Note that the field aligned currents flow away from the earth in the poleward portion of the evening sector eastward electrojet (i_H) and towards the earth in the poleward portion of the morning sector westward electrojet. The electric field transition at the poleward boundary of each of the electrojets marks the boundary between the polar cap (anti-sunward convection) zone and the auroral oval (sunward convection) zone.



plasma densities in the topside ionosphere, and we shall be particularly interested in the character of the thermal plasma at the satellite altitude of 1400 Km and whether or not the thermal plasma can be used to define the boundaries and strength of the auroral electrojets (and hence the level of the solar-terrestrial interaction).

DATA ACQUISITION AND PROCESSING

The University of Alberta magnetometers were arrayed along a common geomagnetic meridian ($\sim 300^{\circ}$ E) across the geomagnetic latitude range $60.6 < \Lambda < 84.0^{\circ}$ N. The coordinates of the observatories are given in Table 1. The data were recorded in digital form on seven track magnetic tape at each site. The details of the magnetometer system appears in Rostoker et al. (1972). The sample rate for the digital system was one data point per component every two seconds, the three components being the perturbation magnetic field in the local magnetic coordinate system (H (positive northward), D (positive eastward), Z (positive downward)). Approximately 45 days of data were recorded on each tape. Each tape was subsequently unpacked onto nine track tape using an IBM 360/67, and the data were timed using a WWVB signal which was recorded at regular intervals on each original data tape. All data points are timed within an accuracy of 0.1 sec.

The ISIS II satellite was launched into a nearly circular polar orbit at an altitude of 1400 Km on April 1, 1971. It carried on board a number of scientific experiments. Those experiments which will be referred to during the course of this report are the topside sounder (TS), the energetic particle detector (EPD), the soft particle spectrometer (SPS) and the noise detector (AGC). We shall study, in detail, the behaviour

Table 1

Coordinates and L Values of Magnetometer Line Sites

Site	Code Name	Geographic		Geomagnetic		L R_E
		Latitude ($^{\circ}$ N)	Longitude ($^{\circ}$ E)	Latitude ($^{\circ}$ N)	Longitude ($^{\circ}$ E)	
Resolute Bay	RESO	74.7	265.1	83.0	289.6	71.4
Cambridge Bay	CAMB	69.1	255.0	76.8	296.6	19.5
Contwoyto Lake	CONT	65.5	249.7	72.6	295.8	11.3
Fort Reliance	RELI	62.7	251.0	70.3	300.1	8.9
Fort Smith	SMIT	60.0	248.0	67.3	300.0	6.8
Fort Chipewyan	FTCH	58.8	248.0	66.3	303.1	6.2
Fort McMurray	MCMU	56.7	248.8	64.2	303.5	5.4
Meanook	MENK	54.6	246.7	61.9	300.8	4.5
Leduc	LEDU	53.3	246.5	60.6	302.9	4.2

of the topside ionosphere using the TS although we shall utilize data from the other experiments listed above when it is useful to do so.

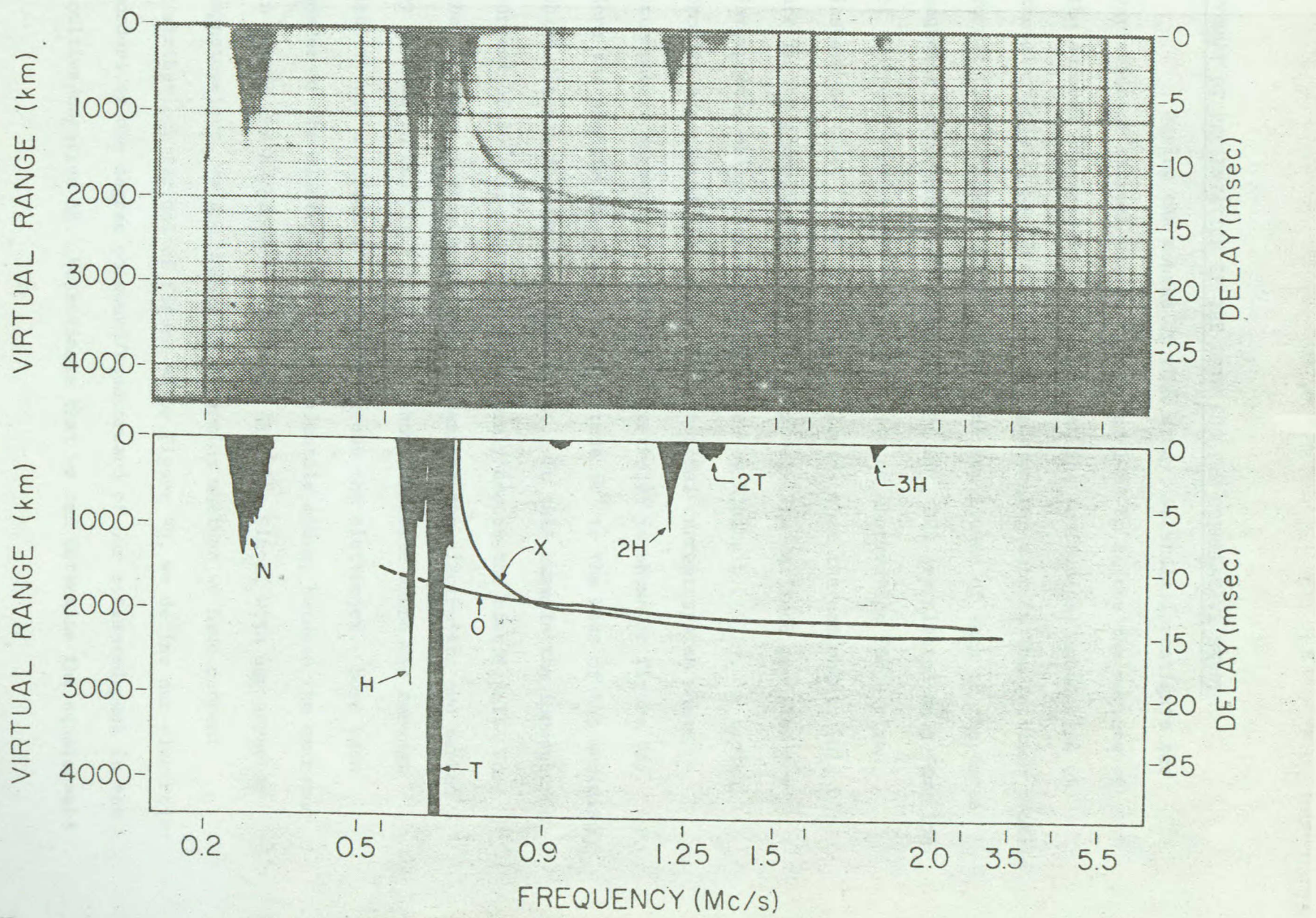
The topside sounder on board ISIS II uses a swept frequency signal in the frequency band $0.1 < f < 10$ MHz to probe the ionosphere around and below the satellite. By studying the character of the reflected signal it is possible to probe the ionospheric thermal plasma density down to the top of the F2 layer (nominally ~ 350 Km altitude). The data are recorded in the ionogram format (see Figure 3) in which it is possible to scale the X-wave trace and the plasma frequency spike so as to determine the thermal plasma densities at altitudes below the satellite and at the satellite altitude respectively. We shall be particularly concerned with the number density at 1400 Km, which may be obtained from the plasma frequency f_N by

$$n_e = \left(\frac{f_N}{8.98 \times 10^3} \right)^2 \text{ cm}^{-3}$$

where f_N is in Hz.

As well as looking at n_e at satellite altitude, the X-wave trace of the ionograms was scaled to yield values of n_e at heights ranging from the satellite altitude to the peak of the F2 layer. These data were used to check that thermal plasma enhancements observed at satellite altitude did, in fact, map down at least to the peak of the F2 layer.

Figure 3 Sample ionogram of the type processed in this study, and schematic indicating important frequency bands and spikes.
For the purposes of our project, the important parameters are N (the plasma frequency) and X (the X-wave trace).



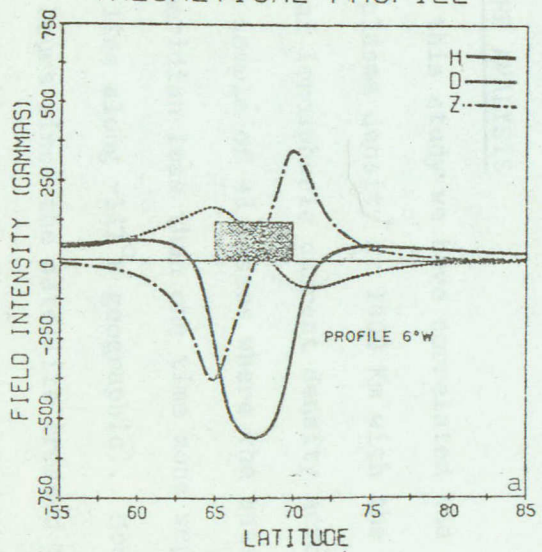
FORMAT OF PRESENTATION OF THE DATA FOR THE CORRELATIVE STUDY

During the course of this study, we shall investigate the variation of thermal plasma density at 1400 Km across the regions of the auroral electrojets. To establish the latitudinal boundaries of the electrojets, we first put the magnetometer data in the latitude profile format (see Rostoker, 1972). Here the amplitudes of each of the three magnetic perturbation components ($\Delta H'$, $\Delta D'$, ΔZ) are plotted as a function of the geomagnetic latitude of the site of observation for a given instant of time. Here the prime indicates that the components (H' , D') are in the geomagnetic coordinate system. The latitude profiles are interpreted using techniques developed by Kisabeth (1972). A typical profile associated with a three dimensional current system whose ionospheric segment is a westward electrojet is shown in Figure 4a. Here the profile is taken at a longitude 60° to the west of the meridian which bisects the westward electrojet. In this example the ionospheric current of $10^6 A$ is distributed uniformly across the electrojet. For the purposes of this study, the borders of the electrojets are marked by extrema in ΔZ . In Figure 4b we show a profile where the current density has a normal distribution across the electrojet. Here each border of the electrojet lies approximately midway between the extremum in ΔZ and the H -component crossover $\Delta H = 0$. Since, with our array of magnetometers, we are unable to determine whether we have current distributions typical of Figure 4a or Figure 4b, we define our electrojet borders as one degree poleward/equatorward of our estimated peak in the positive/negative ΔZ . We estimate that we can determine the equatorward

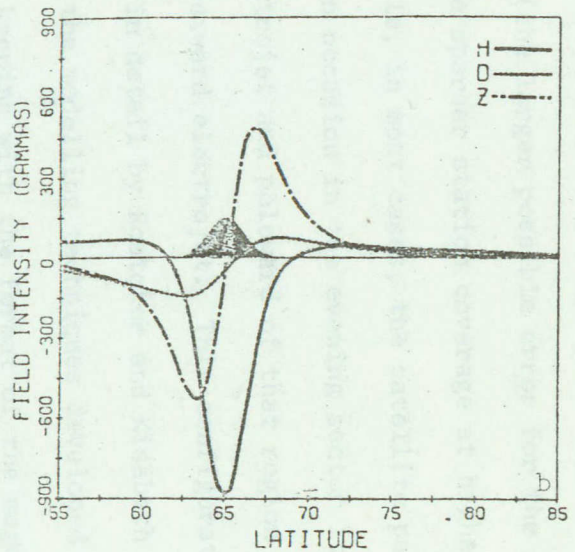
Figure 4a Latitude profile of the computed magnetic perturbation pattern along a meridian cutting a westward electrojet carrying 1.0 MA distributed uniformly across the current carrying region. The electrojet is coupled to the magnetosphere by field aligned current flow at its eastward and westward extrema. Note that the peaks in ΔZ mark the poleward and equatorward borders of the region of electrojet flow.

Figure 4b Latitude profile of the computed magnetic perturbation pattern along a meridian cutting a westward electrojet which is part of a current loop similar to that of Figure 4a except that the current has a normal distribution across the electrojet. Note that the peaks in ΔZ lie $\sim 1^\circ$ inside the borders of the electrojet flow.

THEORETICAL PROFILE



THEORETICAL PROFILE



borders of the electrojets to within $\pm 1^\circ$ and the poleward borders to within $\pm 1.5^\circ$ (the larger possible error for the poleward border estimate stems from the sparser station coverage at higher latitudes).

While, in most cases, the satellite passes across a single electrojet, on occasion in the evening sector it passes across the normal eastward electrojet and poleward of that region it crosses a substorm-associated westward electrojet. This configuration of electrojets has been studied in detail by Rostoker and Kisabeth (1973) and Rostoker et al. (1975) using the modelling techniques developed by Kisabeth (1972).

In keeping with the format of the magnetometer data, we shall plot the thermal plasma densities as a function of the invariant latitude of the point where the field line on which the satellite sits penetrates the ionosphere. (This invariant latitude is, for our degree of accuracy, equivalent to the geomagnetic latitude (see Table 1).) We shall also show data from the EPD and SPS in this format, while the noise will be interpreted directly from its format on the ionograms.

RESULTS OF THE ANALYSIS

In this study we have correlated the latitudinal variation of the thermal plasma density at 1400 Km with the latitudinal variation of the horizontal ionospheric current density across the auroral zone. We have used a sample of 43 passes where the satellite traversed a geographic meridian less than one time zone separated from the magnetometer line (which lies along $\sim 111^\circ\text{W}$ geographic). Most of the passes are during the evening hours since the satellite crossed the evening sector auroral zone when it was passing close to the station line during most of the

period during which magnetometer data were taken. The times of the passes treated in this study are shown in Table 2. Of the passes treated 21 occurred across the evening sector eastward electrojet, 8 occurred across the morning sector westward electrojet, 2 traversed the region between the two aforementioned electrojets (the Harang discontinuity) while 5 involved crossings of the cleft. In 2 cases no electrojet was identifiable. In addition there were 5 cases when the satellite traversed both an eastward electrojet and a westward electrojet to the north (consistent with evening sector substorm conditions).

In each case the latitudes of poleward and equatorward borders of the electrojets were estimated on the basis of the extrema in the Z-component. The maximum H-component perturbation across the electrojet regime was estimated in order to achieve a rough measure of the strength of the current flow in the electrojet. The latitudes of the poleward and equatorward borders of the electrojets and the magnitude of ΔH_{max} are shown in Table 3. In this table E signifies eastward electrojet flow, W westward electrojet flow, H the region near midnight between the two electrojets, E/W a configuration involving an eastward electrojet to the south and a westward electrojet to the north, and W/W a configuration of a westward electrojet with an intense poleward border.

In the Appendix, we show copies of all latitude profiles and all thermal plasma density profiles used in this study. On some of the thermal plasma density profiles, we shall also show noise data obtained from the automatic gain control (AGC) aboard the ISIS II satellite.

Table 2

Times and Geographic Longitudes of ISIS-II Passes Used in this Study

<u>Year</u>	<u>Day</u>	<u>UT of Most Poleward Point</u>	<u>Geographic Longitude of Pass (°W)</u>	<u>Level of Magnetic Activity (Kp)</u>
1971	308	0833	99	1+
"	318	0913	119	0o
"	343	0607	99	1o
"	344	0641	111	0o
"	346	0602	103	1-
"	349	0602	109	1-
"	350	0639	118	0o
"	351	0528	99	5+
"	352	0608	110	3+
"	354	0524	103	0o
"	355	0601	113	1o
"	360	0522	119	4-
1972	002	0407	97	2-
"	003	0444	108	1o
"	004	0516	120	3o
"	005	0406	102	2o
"	006	0443	112	2o
"	010	0328	101	1o
"	011	0405	108	4-
"	012	0250	91	3-
"	013	0327	103	1-
"	013	0519	130	1-
"	015	0252	93	1+
"	017	0403	115	4o
"	019	0326	109	3-
"	020	0403	118	3-
"	025	0309	115	4-
"	026	0357	125	4-
"	030	0247	110	3+
"	032	1508	111	2+
"	037	0130	99	1o
"	038	0207	109	2o
"	039	0244	120	3-
"	039	1554	127	1-

Table 2 (Cont'd)

<u>Year</u>	<u>Day</u>	<u>UT of Most Poleward Point</u>	<u>Geographic Longitude of Pass (°W)</u>	<u>Level of Magnetic Activity (Kp)</u>
1972	040	0129	103	1o
"	040	1438	110	0+
"	041	0206	112	3o
"	045	1359	106	1o
"	048	1357	110	4+
"	052	0123	116	2+
"	053	1319	106	1o
"	054	0048	108	1+
"	058	1240	102	1o

Table 3

Locations of Poleward and Equatorward Borders and Maximum ΔH
For Electrojets Identified Using the Magnetometer Line Data

Day	UT	Jet	PB (°N)	EB (°N)	$ \Delta H_{\text{max}} $ nT	Comments
71/308	0833	N/A	-	-	-	No electrojet
71/318	0913	N/A	-	-	-	No electrojet
71/343	0607	H	-	-	-	Harang discontinuity
71/344	0641	H	-	-	-	Harang discontinuity
71/346	0602	E	69	63	35	Near Harang
71/349	0602	E	72	63	20	
71/350	0639	E/W E	70	64	15	
			W	75	28	
71/351	0528	E/W E	71	?	>100	
			W	76	360	
71/352	0608	E/W E	70	64	>20	
			W	75	55	
71/354	0524	E/W E	69	66	25	Possible Harang
			W	75	69	?
71/355	0601	E/W E	70	65	25	Possible Harang
			W	75	70	30
71/360	0522	W/W W	69	63	200	Substorm
			W	75	69	Contamination
72/002	0407	E	77	66	25	
72/003	0444	E	75	66	30	
72/004	0516	E	74	66	60	
72/005	0406	E	76	67	25	
72/006	0443	E	72	66	15	
72/010	0328	E	75	66	85	
72/011	0405	E	74	64	150	
72/012	0250	E	73	65	75	
72/013	0327	E	75	64	40	Structure?
72/013	0519	E	75	66	50	
72/015	0252	E	73	65	65	
72/017	0403	E	68	61	150	
72/019	0326	E	73	63	25	Net field-aligned current flow Polar cap effects!
72/020	0403	E	71	65	50	
72/025	0319	E	71	63	75	
72/026	0357	E	73	64	75	

Table 3 (Cont'd)

Day	UT	Jet	PB (°N)	EB (°N)	$ \Delta H_{\text{max}} $ nT	Comments
72/030	0247	E	74	66	70	
72/032	1508	W	75	68	125	
72/037	0130	E	~79	~71	20	Cusp
72/038	0207	E	78	66	60	
72/039	0244	E	68	63	125	
72/039	1554	W	79	68	65	Eastward jet to south
72/040	0129	E	79	68	25	Cusp
72/040	1438	W	73	65	15	
72/041	0206	E	75	66	110	Cusp
72/045	1359	W	76	68	20	
72/048	1357	W	70	62	330	
72/052	0123	E	75	65	50	Cusp
72/053	1319	W	75	67	90	
72/054	0048	E	77	65	30	Cusp
72/058	1240	W	70	66	110	

PRESENTATION OF THE RESULTS

The correlation of the ISIS II thermal plasma measurements with the University of Alberta magnetometer line data has yielded the following two major conclusions:

- (1) The poleward borders of the auroral electrojets are marked by distinct peaks in the thermal plasma density.
- (2) In cases where net upward or downward field-aligned current flow is identified along a meridian across the electrojet, the peak in thermal plasma density across the electrojet generally contains the region of net field-aligned current flow.

Based on the available data which were analysed two secondary conclusions have been reached.

- (1) The thermal plasma peak at the poleward border of the electrojet is normally associated with markedly enhanced noise in the whistler range. This association is particularly marked near the poleward edge of the thermal plasma peak.
- (2) The peak in thermal plasma associated with the poleward border of the electrojet occurs in a region of soft electron precipitation, viz. $0.1 < E < 1$ keV.

In the following section we shall present individual cases demonstrating the validity of the general conclusions stated above. In addition we shall present summaries of the entire data suite which will demonstrate the validity of the two main conclusions stated above. Finally, in the Discussion section, we shall comment on the significance of our conclusions.

Case 1 Eastward Electrojet in the Evening Sector

Day 10, 1972 0328 UT

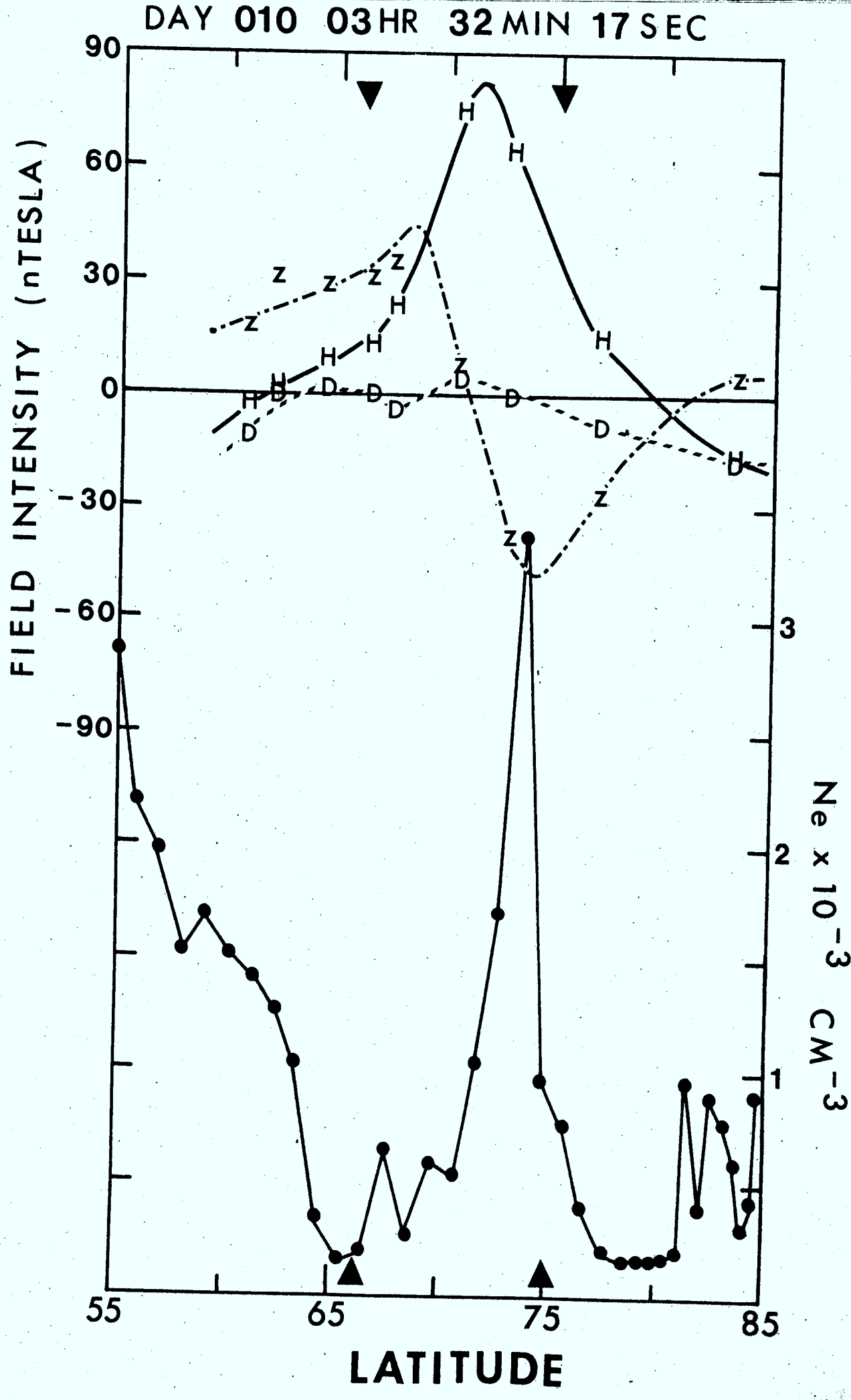
In this example the satellite was on a north-to-south pass along geographic meridian 101°W , approximately 10° east of the magnetometer line. The latitude profile, and the thermal plasma density and noise profiles synthesized from the ISIS II ionograms are shown in Figure 5.

It can be seen that the ISIS II satellite passed over an eastward electrojet flowing in the latitude range $66^{\circ} \leq \Lambda \leq 75^{\circ}\text{N}$ and having a net integrated current flow of $\sim 0.1 - 0.2\text{ MA}$. The fact that $\Delta D'$ follows $\Delta H'$ across the equatorward portion of the electrojet suggests that the current flow inclined slightly from due geomagnetic east, flowing from west north west to east south east. The separation of the peak in $-\Delta Z$ and the $\Delta H' = 0$ crossover suggests that the poleward border of the electrojet is not sharp, with the current density tapering off as one approaches the poleward border from the south.

It is clear that the poleward border of the electrojet is marked by a sharp spike in thermal plasma density at satellite altitude confined in the latitude range $71^{\circ} < \Lambda < 74.5^{\circ}\text{N}$. Thus the peak in thermal plasma density marks only the poleward half of the eastward electrojet. It should be noted that the thermal plasma density increases slowly (but consistently) from $\sim 77^{\circ}\text{N}$ to $\sim 74.5^{\circ}\text{N}$. It is quite possible that there is eastward current flow in this latitude although it would be quite weak and thus not easily detected by ground-based magnetometers. In fact, measurements by the ASP indicate that the poleward border of the diffuse aurora lay at $\sim 78^{\circ}\text{N}$ (Wallis et al., 1975) indicating enhanced conductivity up to that latitude.

Figure 5 Latitude profiles of the magnetic perturbation along the Alberta magnetometer line and the thermal plasma density measured along a meridian $\sim 10^\circ$ to the east of the Alberta line. Note the marked peak in thermal plasma density at ISIS altitude (1400 Km) near the poleward border of the eastward electrojet. See Figure A18 in the Appendix for information regarding whistler noise and auroral luminosity.

DAY 010 03HR 32MIN 17SEC



Finally we note that the noise level increases sharply from $\sim 77.5^{\circ}\text{N}$ to $\sim 76.5^{\circ}\text{N}$ reaching peak levels which are maintained down to $\sim 74.5^{\circ}\text{N}$ (or the edge of the steep gradient in thermal plasma density). Note that the noise peak is reached just before the thermal plasma density starts to rise. The noise level even decreases as the plasma density increases towards the peak value. Aside from a sharp isolated peak in noise at the equatorward border of the thermal plasma density peak, the noise level drops off and is certainly rather small across the equatorward portion of the eastward electrojet. It is also interesting to note that the sharp enhancements in n_e poleward of 81°N are not associated with enhanced noise levels. From this event, we may conclude that we may have noise but little thermal plasma, thermal plasma but little noise and finally thermal plasma with noise. We claim that the latter condition is a consistent feature at the poleward borders of the auroral electrojets.

Case 2 Westward Electrojet in the Morning Sector

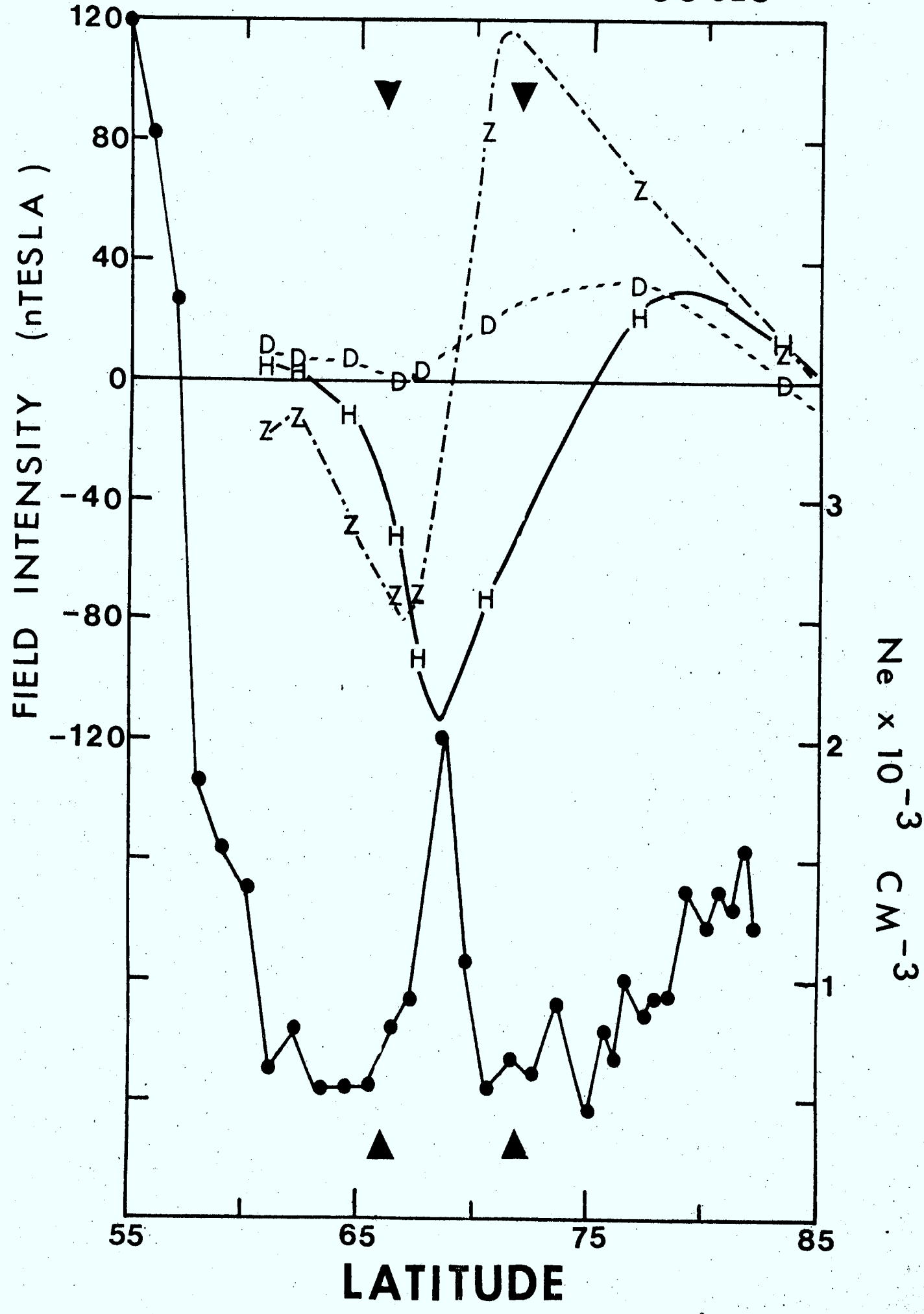
Day 58, 1972 1240 UT

In this case, the satellite was on a south-to-north pass along geographic meridian 102°W , approximately 9° east of the magnetometer line. The latitude profile, and the thermal plasma density and noise profiles synthesized from the ISIS II ionograms are shown in Figure 6.

It can be seen that the ISIS II satellite passed over a westward electrojet flowing in the latitude range $66^{\circ} \leq \Lambda \leq 70^{\circ}\text{N}$ and having a net integrated current flow of $\sim 0.1\text{ MA}$. Again we see that the poleward border of the electrojet is marked by a sharp spike in thermal plasma

Figure 6 Latitude profiles of the magnetic perturbation along the Alberta magnetometer line and the thermal plasma density measured along a meridian $\sim 9^\circ$ to the east of the Alberta line. Note the pronounced peak in thermal plasma density at 1400 Km in the poleward portion of the westward electrojet. See Figure A43 in the Appendix for information regarding whistler noise.

DAY 058 12HR 43MIN 00SEC



density confined in the latitude range $66.5^\circ \leq \Lambda \leq 70^\circ N$. Although there appears to be enhanced thermal plasma density across the entire electrojet, the sharp peak occurs in the poleward half of the electrojet (as in Case 1).

While the noise level is rather low for this event, there is clearly a peak at the poleward border of the electrojet, with the maximum value again lying at the poleward edge of the region of sharp gradient in n_e . In this example there is also a significant noise level in the polar cap, which may well be associated with the region of enhanced thermal plasma density found in that region.

Finally we note the positive gradient in ΔD on the latitude profile in the latitude range $67 \leq \Lambda < 76^\circ N$. The work of Hughes and Rostoker (1975) suggests that this is a region of net downward current flow, and thus there may be net current flow into the ionosphere across the entire electrojet and as much as 5° poleward of the electrojet border in this example. [Again we wish to emphasize that our electrojet borders mark the boundaries of the major portion of the ionospheric current flow. However, it is quite possible that very weak ionospheric current flow may occur outside our boundaries under conditions of low conductivity and/or low electric field.]

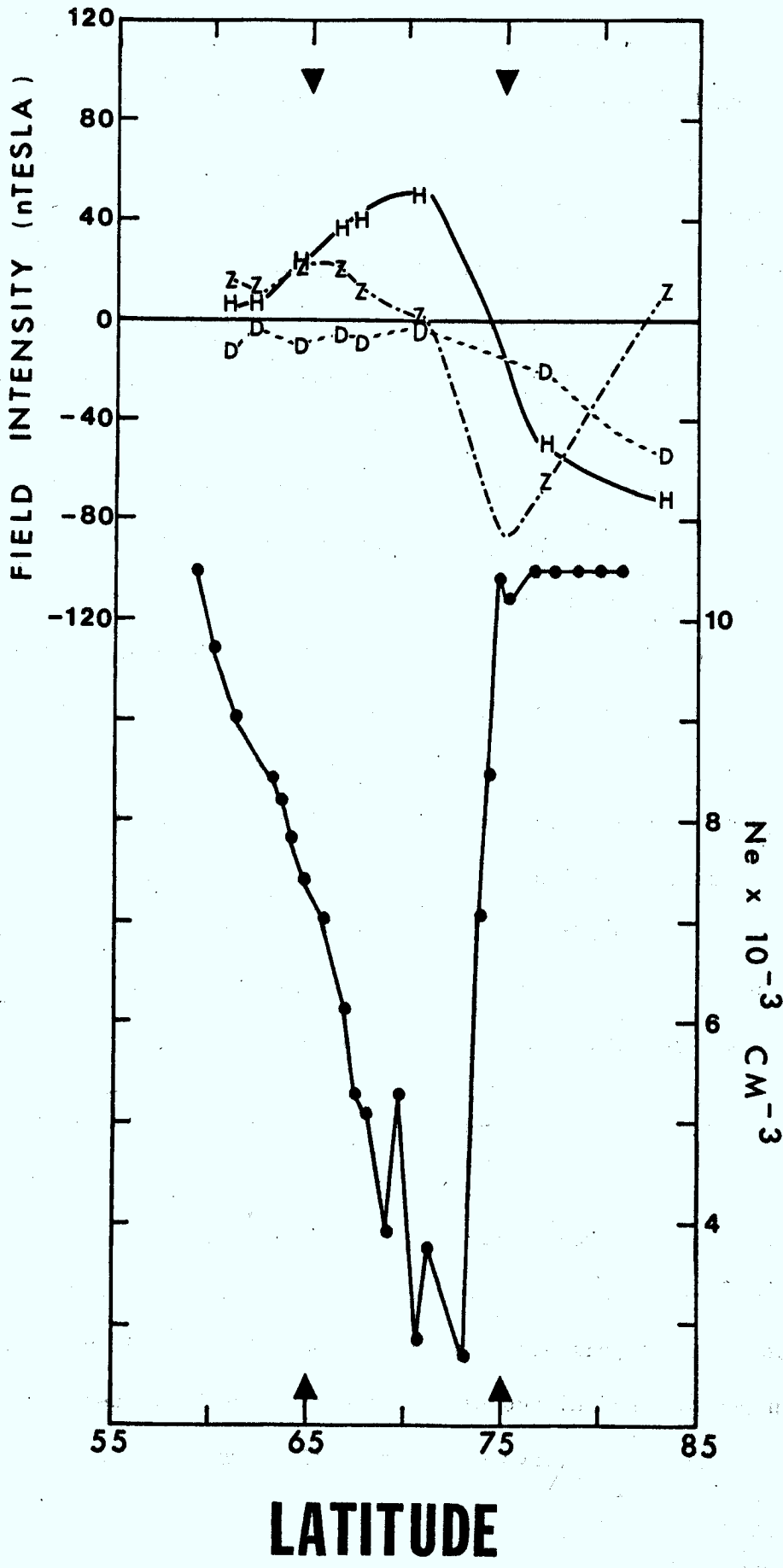
Case 3. The Polar Cleft in the Post-Noon Sector

Day 52, 1972 0123 UT

In this case the satellite was on a north-to-south pass along geographic meridian $116^\circ W$, approximately 4° west of the magnetometer line. The latitude profile, and the thermal plasma density and noise profiles synthesized from the ISIS II ionograms are shown in Figure 7.

Figure 7 Latitude profiles at the magnetic perturbation along the Alberta magnetometer line and the thermal plasma density measured along meridian $\sim 5^\circ$ to the west of the Alberta line. Note the sharp rise in thermal plasma density at the poleward border of the region of eastward ionospheric current flow. This rise marks the position of the equatorward boundary of the polar cleft. See Figure A40 in the Appendix for information regarding the whistler noise.

DAY 052 01 HR 30 MIN 51 SEC



It can be seen that the satellite passed over a broad region of eastward current flow in the latitude range $65 \leq \Lambda \leq 75^{\circ}\text{N}$ and having a net integrated current flow of ~ 0.1 MA. The lack of structure in ΔD across the electrojet suggests that there is no net field aligned current flow across this region of latitudinally confined eastward current flow.

The thermal plasma profile differs substantially from those seen in association with eastward electrojets in the evening sector. We suggest that this profile is associated with the polar cleft. If this is the case, the poleward border of the region of eastward current flow must mark the equatorward border of the cleft. This demarcation line separates the region of anti-sunward convection on the poleward side from the region of sunward (return) convection on the equatorward side. The thermal plasma signature of this important boundary is then a sharp rise in n_e to some peak value which is maintained across the cleft.

We note that the noise rises abruptly as one approaches the region of thermal plasma enhancement. The start of noise enhancement is observed just equatorward of the start of the rise in thermal plasma density at 1400 Km. Such enhancements in whistler noise associated with the polar cleft have been studied in detail by Hartz (1972) and James (1973).

Case 4 Eastward Electrojet in the Evening Sector

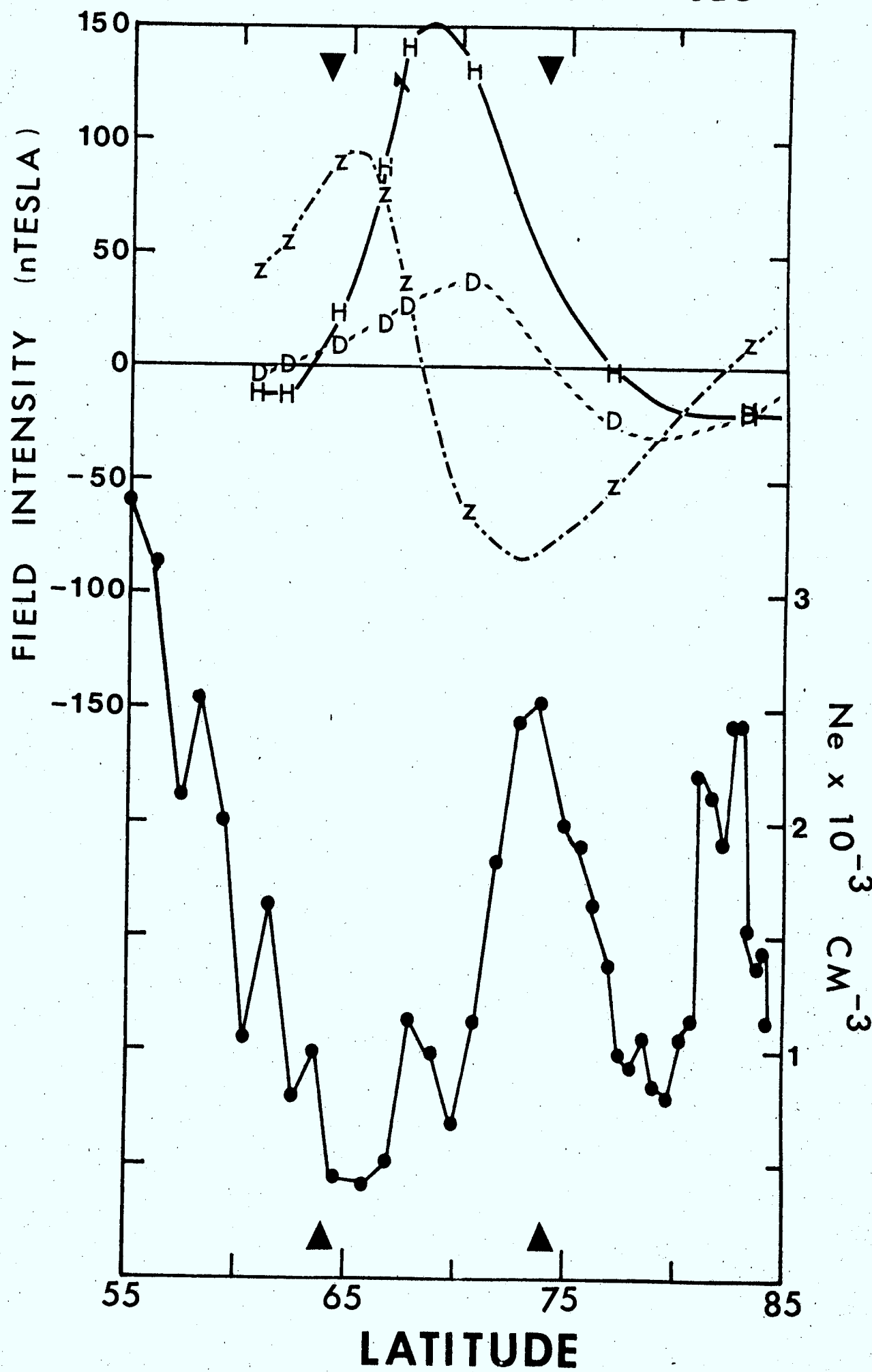
Day 11, 1972 0405 UT

In order to tie together as many physical parameters as possible relating to the physics of the poleward border of the auroral electrojet, we present this case of an evening sector eastward electrojet where the data were supplemented by energetic electron data and information regarding the distribution of auroral luminosity across the oval.

The satellite traversed the geographic meridian 102°W on a north-to-south pass, taking it approximately within 9° of the magnetometer line. The magnetic local time of the pass ranged from 1900 - 2000 UT as the satellite crossed the auroral oval. The latitude profile and the thermal plasma density and noise profiles synthesized from the ionograms are shown in Figure 8. From the latitude profile of the magnetometer data it was inferred that the eastward electrojet which flowed across the meridian traversed by the satellite was confined in the latitude range $64^{\circ} < \Lambda < 74^{\circ}\text{N}$. The large separation ($\sim 4^{\circ}$) between the peak in $-\Delta Z$ and the $\Delta H = 0$ crossover suggests that the current density tapers off approaching the poleward border of the electrojet from the south. The fact that ΔD follows ΔH across the equatorward portion of the electrojet suggests that the current channel is inclined with respect to the geomagnetic meridian such that the flow is from north west to south east. The large negative shift in ΔD across the poleward border of the electrojet suggests a net upward current flow in the poleward portion of the electrojet. The main peak in the thermal plasma density is confined within the latitude range $71^{\circ} < \Lambda < 77^{\circ}\text{N}$. It is interesting to note that the peak in thermal plasma density coincides exactly with the predicted poleward border of the eastward electrojet, however there are significantly enhanced thermal plasma densities in the latitude range $74^{\circ} < \Lambda < 77^{\circ}$ across which no significant electrojet flow is predicted. It is further interesting to note the existence of a marked thermal plasma peak in the latitude range $81^{\circ} < \Lambda < 84^{\circ}\text{N}$ which does not appear to be associated with any localized electrojet flow.

Figure 8 Latitude profiles of the magnetic perturbation along the Alberta magnetometer line and the thermal plasma density measured along a meridian $\sim 3^\circ$ to the east of the Alberta line. Note the peak in thermal plasma density at the poleward border of the eastward electrojet, and the addition thermal plasma peak in the polar cap. See Figure A19 in the Appendix for information regarding whistler noise and auroral luminosity.

DAY 011 04 HR 10 MIN 17 SEC



Consistent with the previous cases, we find that the polar cap peak in thermal plasma density has a weak level of noise associated with it, while the peak in n_e associated with the poleward border of the electrojet has intense noise associated with it. However, we note that the noise level attains peak strength in the latitude range $74^\circ < \Lambda < 76^\circ$ where little electrojet current is predicted. Thus we have in this case a situation where the noise does not correlate well with the predicted border of the eastward electrojet.

We may gain further insight into this event, by studying the behaviour of the energetic particles measured by the EPD and SPS. These data are shown in Figures 9a and 9b respectively. The EPD data show a rather soft spectrum for electrons near the poleward border of the electrojet, with the spectrum getting progressively harder as one approaches the equatorward border of the electrojet. There are strong fluxes of electrons in the energy range $0.15 < E < 6.0$ keV in the latitude range $74 < \Lambda < 77^\circ N$ where the enhanced thermal plasma density and enhanced noise are observed. The pitch angle distribution of the electrons is very anisotropic in this latitude range. There is a noticeable dropout in fluxes near $74^\circ N$ suggesting that there is a clear dividing line between the regions $74 < \Lambda < 77^\circ N$ and $\Lambda < 74^\circ N$, where the energetic electron fluxes appear to be considerably more isotropic.

A similar characteristic behaviour is noted in the lower energy electron fluxes recorded by the SPS (Figure 9b). Most noticeable are the intense bursts of energetic ($0.10 < E < 1.0$ keV) electrons poleward of $\sim 70^\circ N$. These intense soft electron fluxes lie in the latitude range of the thermal plasma peak and the large part of the net upward field-aligned

Figure 9a Energetic electron fluxes and the average energy of the electrons measured by the EPD aboard the ISIS II (courtesy Dr. J.R. Burrows) over the interval 0407-1417 UT on January 11, 1972. The fluxes are plotted as a function of invariant latitude and magnetic local time (MLT). The baselines of the various channels are indicated by B. The equatorward border of the electron fluxes in the 3.0 - 6.0 keV range lies at the predicted equatorward border of the eastward electrojet. Note the progressively softening energy spectrum poleward of $\sim 71^{\circ}$ N. Also note the intense soft electron fluxes and then anisotropic character in the latitude range $74 < \Lambda < 77^{\circ}$ N. The dropout of energetic electrons (particularly visible in the 6.0 keV electrons) separates the two regions $74 < \Lambda < 77^{\circ}$ N where little electrojet current is discernable and $\Lambda < 74^{\circ}$ N where the bulk of the electrojet current flows.

DAY 11, 1972

ISIS II

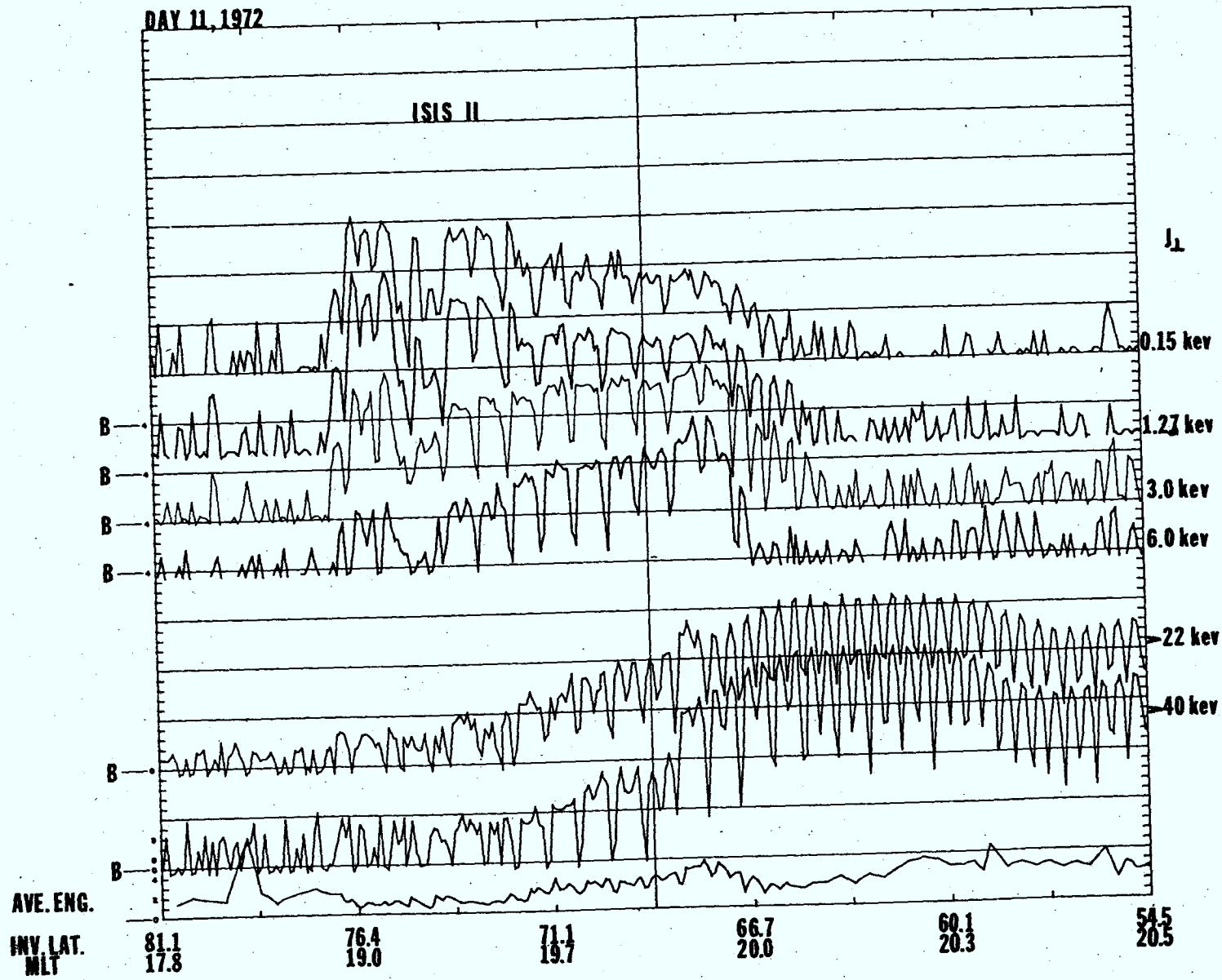
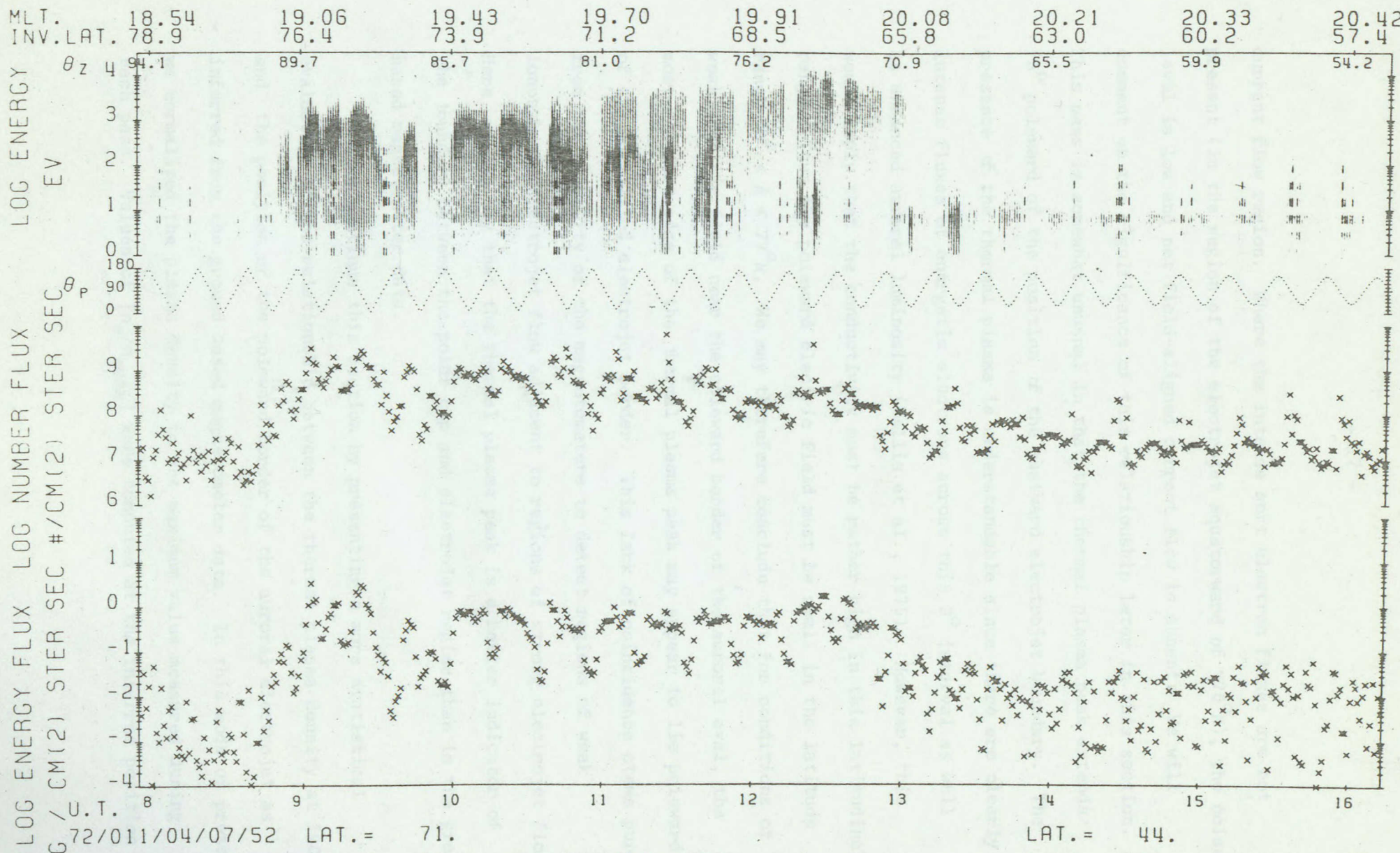


Figure 9b Spectrogram of the SPS electron fluxes measured over the interval 0408 - 0416 UT on January 22, 1972. Also shown is the number flux and energy flux of the electrons and an indication of their pitch angle distribution (for $\theta_p = 0^\circ$ the detector points up the field line). Note the intense fluxes of electrons in the energy range $300 < E < 1000$ eV poleward of $\sim 71^\circ N$, and the dropout in electron energy (and fluxes) just poleward of $\sim 74^\circ N$. Note that the soft electron fluxes, noise, and thermal plasma peak are confined within the same latitudinal regime.

TOP ELECTRON DATA

ISIS-II



72/011/04/07/52

LAT. = 71.

LONG. = -109.

20/43/10LT ECAL = 1

LAT. = 44.

LONG. = -108.

20/57/05LT

 $\eta_{\text{MAX}} = 0.8$

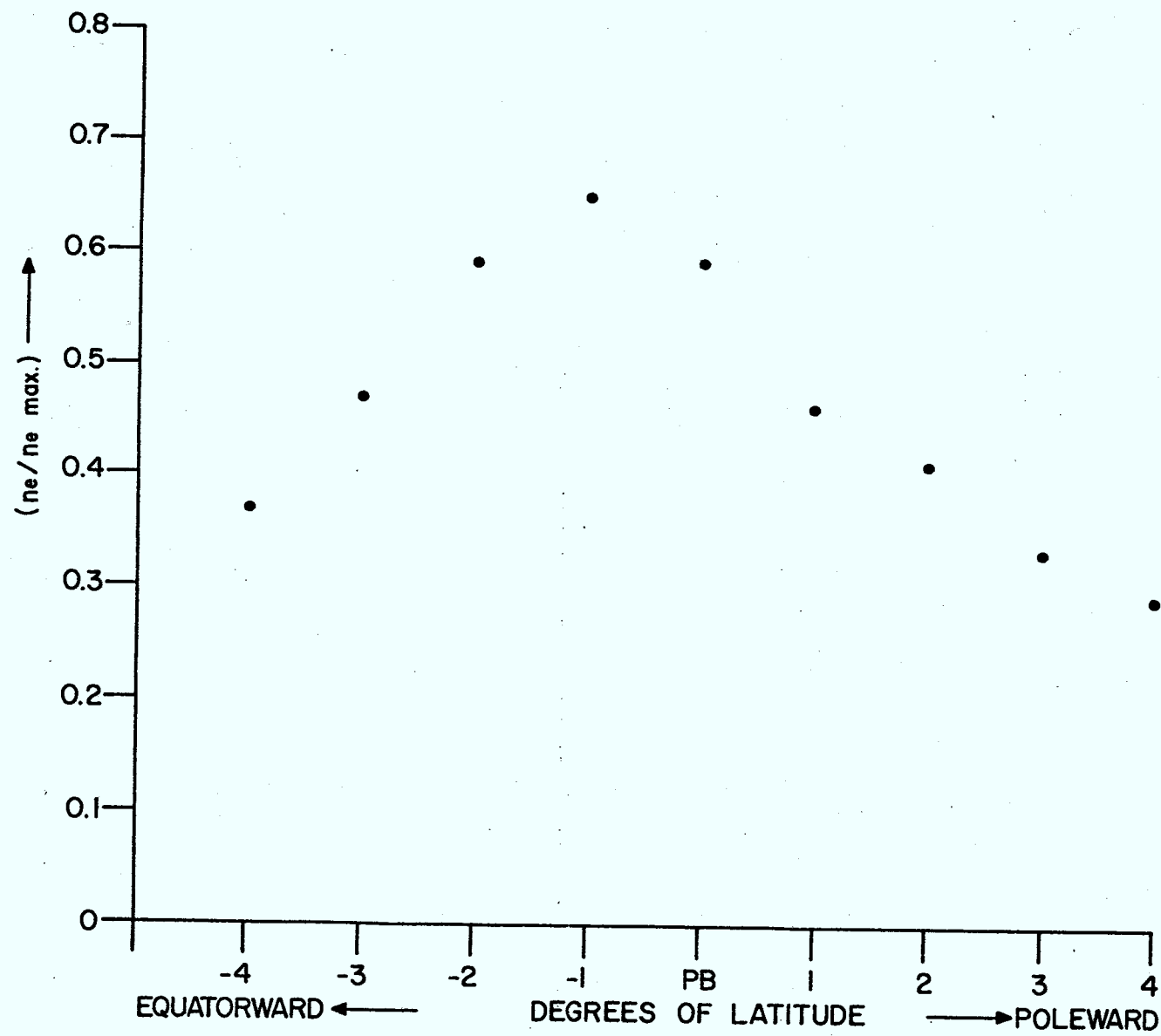
ORBIT = 3611 ALT. = 1394 N >= 0. TAPE NO. 2011AD DATE PROCESSED: 15-APR-74

current flow region. Where the intense soft electron fluxes are not present (in the region of the electrojet equatorward of $\sim 70^{\circ}$ N), the noise level is low and net field-aligned current flow is absent. We will comment on the significance of this relationship later in this section. This pass is somewhat unusual in that the thermal plasma peak extends $\sim 3^{\circ}$ poleward of the position of the eastward electrojet boundary. The presence of the thermal plasma is understandable since there are clearly intense fluxes of energetic electrons across this 3° interval as well as enhanced auroral luminosity (Wallis et al., 1975). However, this would imply that the conductivity must be rather high in this latitudinal range. Thus the poleward electric field must be small in the latitude range $74^{\circ} < \Lambda < 77^{\circ}$ N. We may therefore conclude that for conditions of weak electric field near the poleward border of the auroral oval, the most poleward edge of the thermal plasma peak may appear to lie poleward of the identified electrojet border. This lack of coincidence stems purely from the inability of the magnetometers to detect regions of weak ionospheric electrojet flow adjacent to regions of strong electrojet flow. Here we may say that the thermal plasma peak is a better indicator of the boundary between the polar cap and electrojet regime than is the ground based magnetometer data.

We continue this section by presenting a more statistical evaluation of the relationship between the thermal plasma density at 1400 km and the position of the poleward border of the auroral electrojet as inferred from the ground based magnetometer data. In this mode of presentation, we normalized the plasma density to the maximum value measured during each pass. Values of $[n_e/n_{e\max}]$ were computed at the inferred position

of the poleward border of the electrojet and at positions 1° - 4° poleward of and equatorward of the poleward border. The "superposed epoch" technique was then employed through addition of the values of $[n_e/n_{e\max}]$ for all events at each of the nine positions at and on either side of the poleward border of the electrojet. Events omitted in this procedure were those associated with the Harang discontinuity (8), those associated with the cusp (5), and those where no electrojet was present (2). In addition for some events (5 in all) large peaks in the polar cap sometimes dwarfed the maximum values of n_e attained across the electrojet region. Values of $[n_e/n_{e\max}]$ poleward of the poleward border of the electrojet were not used in the calculations involving the "superposed epoch" technique. The results of the analysis are shown in Figure 10. There is a clear peak here placed at 1° equatorward of the poleward border of the electrojet. In breaking down the sample used in this study, it was interesting to note that there was a pronounced difference in the positioning of the steep gradient in n_e relative to the poleward border of the electrojet for eastward and westward electrojets. In particular the plasma density was always low at the identified position of the poleward border of the westward electrojet, and started to rise rapidly in the degree interval equatorward of that poleward border. On the other hand, for the eastward electrojet either the peak in n_e lay at the poleward border of the electrojet or, at least, the value of n_e was already high at that poleward border. However, in the light of the potential error in identifying the poleward border of the electrojet using the data available for this study, we would claim that the poleward border of the electrojet coincides with the peak in thermal plasma density to within one degree of latitude.

Figure 10 Relationship of the peak value in thermal plasma density at 1400 Km across the electrojet region to the position of the poleward border of the electrojet. Positions northward of the poleward border are given in + degrees while positions equatorward of the poleward border are given in - degrees. The graph is constructed using the "superposed epoch" technique (see text).

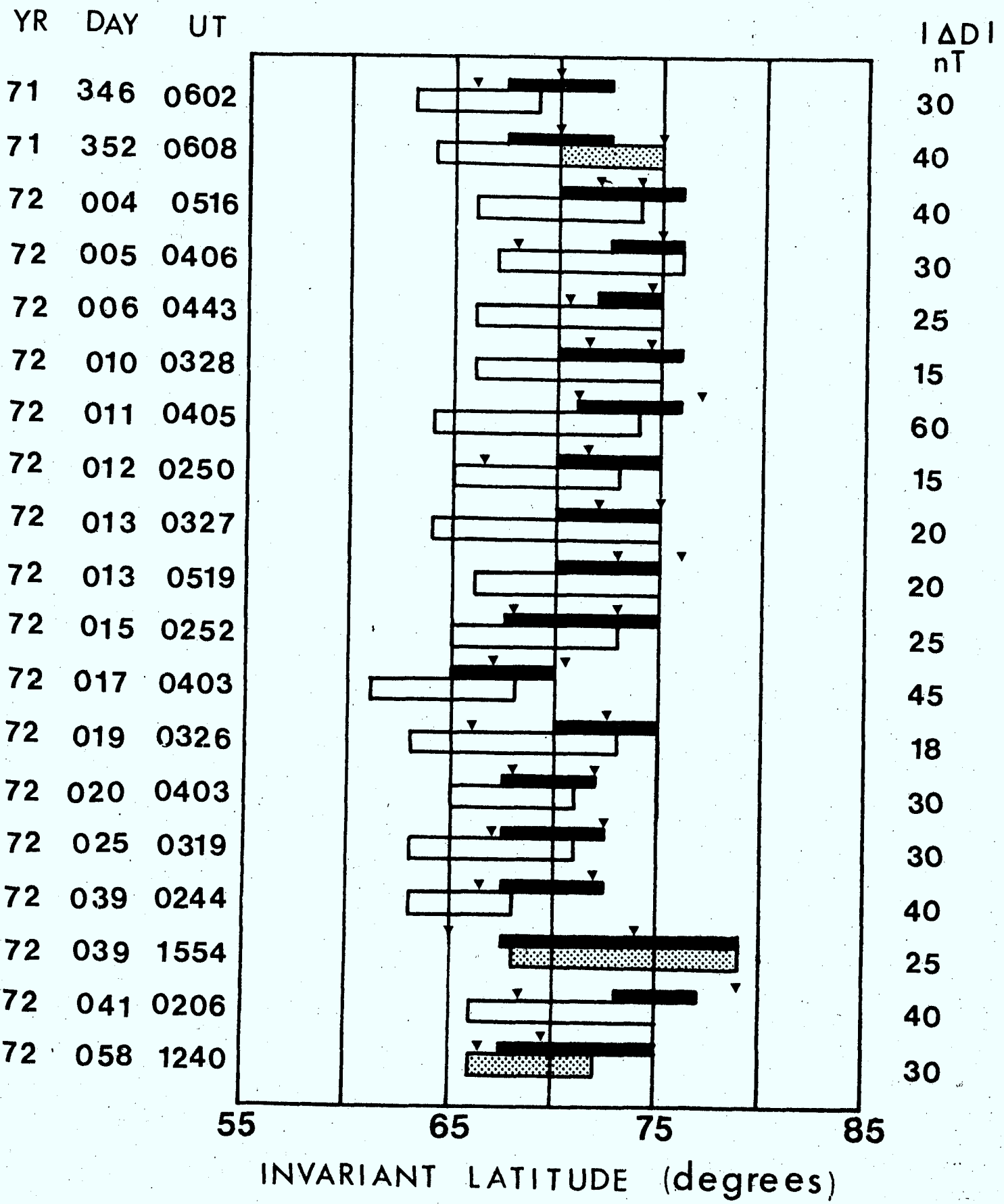


Only the study of a much larger data suite will permit one to decide whether the fact that the peak in Figure 10 lies one degree equatorward of our estimated position of the poleward border of the electrojet is significant. (We should point out here that our estimated position of the poleward border involved the assumption that the current density in the electrojet tapers off toward the poleward border. Under this assumption we placed the poleward border one degree poleward of the peak in ΔZ . If the current density is relatively constant across the electrojet and drops sharply at the poleward border, we would have placed the poleward border of the electrojet at the latitude of the peak in ΔZ . Then the peak in n_e shown in Figure 10 would have coincided precisely with the estimated position of the poleward border of the electrojet. Accordingly we do not believe it is feasible to assign a physical significance to the displacement of the peak in n_e from the poleward border of the electrojet seen in Figure 10).

We conclude this section by studying the ground based magnetometer data with a view to identifying regions of net field aligned current flow penetrating the electrojet region. Hughes and Rostoker (1975) have suggested that sheets of net current flow in the auroral oval would cause the magnetic D-component latitude profile to experience a step across the region of net current flow. The step would be positive going (moving from south to north) across a sheet of downward flowing current and negative going (moving from south to north) across a sheet of upward flowing current. Such regions of net field-aligned current flow have been noted in polar orbiter data by Zmuda (private communication) and Sugiura (1974) and the magnetic perturbation pattern described above

has been identified on the latitude profiles used in this study. In Figure 11 we show a synopsis of information synthesized from the ground-based magnetometer and ISIS II ionogram data in cases where this field-aligned current flow is clearly identifiable from the step-like signature in ΔD across the auroral oval region. In this figure we show for each event (listed on the left hand side of the figure) the latitudinal extent of the electrojet regime, the latitudinal extent of the net current flow regime as inferred from the D-component profiles (with the magnitude of the step $|\Delta D|$ shown on the left hand side of the figure) and the boundaries of the thermal plasma peak associated with each electrojet. It should be noted that the gaps in the ground-based magnetometer line make it possible only to define the upper limit of the latitudinal extent of the region of net field-aligned current flow. That is the step may well take place over a more confined latitudinal extent, but this would be impossible to prove using the existing data suite. Despite this limitation, it is clear that in the large majority of the events the net current flow is in the poleward portion of the electrojet associated with steady state convection in the magnetosphere. Furthermore, within the errors of identification of boundaries, the thermal plasma peak and the region of net field aligned current flow are coincident. This would imply that the intense soft electron fluxes responsible for the creation of the thermal plasma peaks may also be the current carriers associated with net field-aligned current flow into and out of the auroral oval. Of course, since some of the current carried in the closed three-dimensional sheet configuration (Boström, 1964; Zmuda and Armstrong, 1974) may also be carried by soft

Figure 11 Composite plot showing latitudinal extent of the electrojet regime (open rectangles indicating eastward current and hatched rectangles indicating westward current), the region of net field aligned current flow as inferred from the ΔD profile (solid bar), and the region of enhanced thermal plasma density (the boundaries of which are marked by solid triangles). Note the tendency for the thermal plasma peaks to delimit the region of net field-aligned current flow. Only cases of clearly defined net-current flow were used for this presentation.



electrons, we may also expect to see the regions of enhanced thermal plasma density extend to lower latitudes than the net field-aligned current flow on some occasions. However, the data shown in Figure 11 clearly show the tendency for the net field-aligned current flow to be confined to the poleward portion of the electrojet regions in the majority of cases.

Discussion

We have shown in the previous section, that only the poleward portion of the auroral electrojet is marked by enhanced thermal plasma densities at 1400 km. The absence of enhanced n_e at 1400 km above the equatorward portion of the auroral electrojet is very significant, in that it is consistent with the suggestion by Whitteker (1975) that the thermal plasma originates near the F-region peak and expands upward due to pressure effects. We point out that it is known that the energy spectrum of plasma sheet electrons becomes progressively softer moving from the neutral sheet toward the boundary between the tail like and the plasma sheet. Mapped into the high latitude ionosphere, this tendency would be reflected by a softening of the energy spectrum of precipitating electrons as one crosses the auroral oval moving toward the pole. Rees (1969) has shown that the harder the spectrum of the precipitating primary electrons is, the deeper in the ionosphere the secondary electrons will be created. We suggest that, only if the secondary electrons are produced high in the F-region will they have the opportunity to expand up the field lines to ISIS II altitude. Thus, while the hard electrons ($E > 1$ kev) precipitating in the equatorward portion of the auroral oval are capable of generating

secondaries in the E-region (thus enhancing the ionospheric conductivity in the height-range of the ionospheric electrojet currents), they will not create significant number of secondaries in the upper F-region and hence will not lead to enhanced fluxes of thermal plasma expanding into the topside ionosphere. However, near the poleward border of the electrojet, where the low energy ($0.1 < E < 1$ keV) fluxes of electrons are enhanced, large numbers of secondary electrons will be created in the upper F-region and these will expand upwards into the topside ionosphere generating a peak in thermal plasma above the poleward part of the electrojet. In this way, the spectrum of the precipitating electrons determines whether a thermal plasma peak in the topside ionosphere will be present across the auroral electrojet regime.

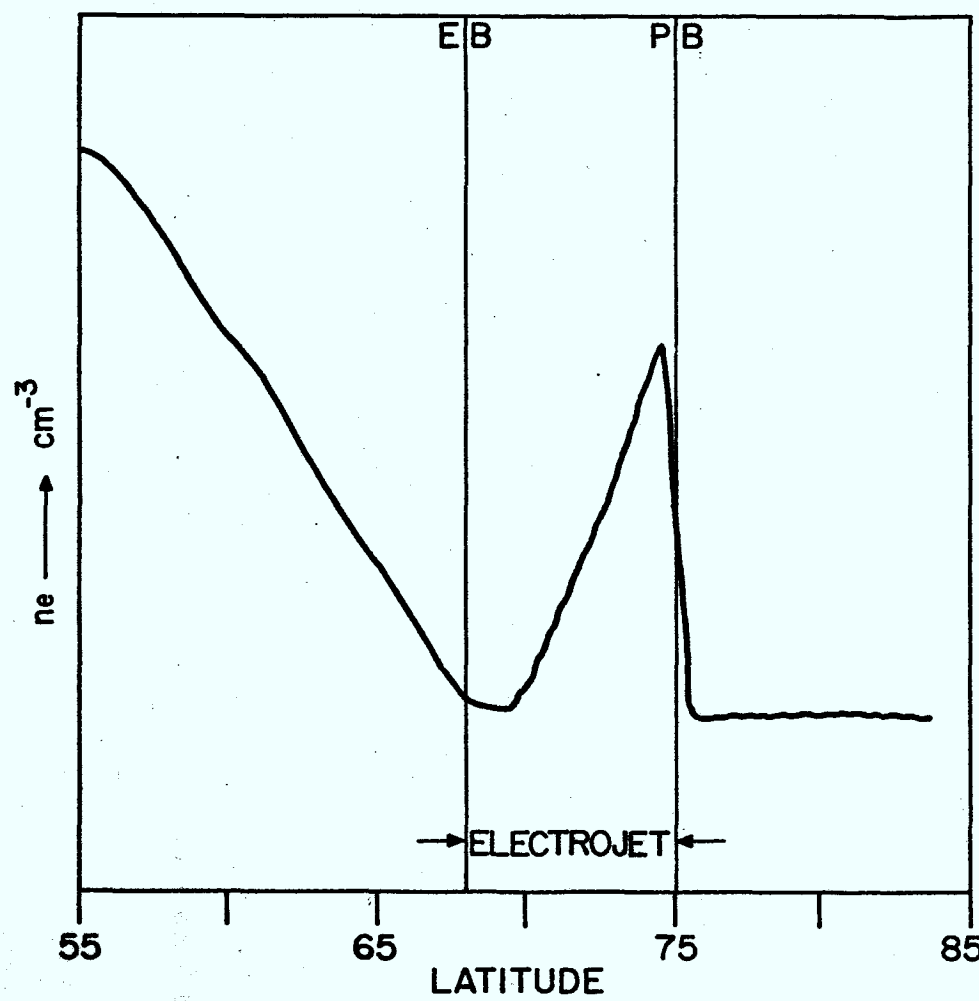
We have shown that we may have thermal plasma peaks in the topside ionosphere with or without the presence of whistler noise. However, those thermal plasma peaks associated with the poleward portion of the electrojet always have whistler noise associated with them. We suggest an important connection between this observation and the fact that we tend to observe any significant net field-aligned current flow in the poleward portion of the electrojet. We note that the presence of whistler noise suggests the possibility of regions of anomalous resistivity along the field lines. We further note that the region of whistler noise near the poleward border of the electrojet is also the region of enhanced bursts of electrons of energies of several hundred eV. We suggest that the noise and the enhanced low energy electron fluxes are causally related and that potential drop along the field lines

associated with region of anomalous resistivity is integrally related to the appearance of net field-aligned current flow in the poleward part of the electrojet. A further study of these interrelationships based on an adequate suite of SPS and EPD data is well warranted in the light of the important role which field-aligned current flow plays in the dissipation of energy in the magnetosphere.

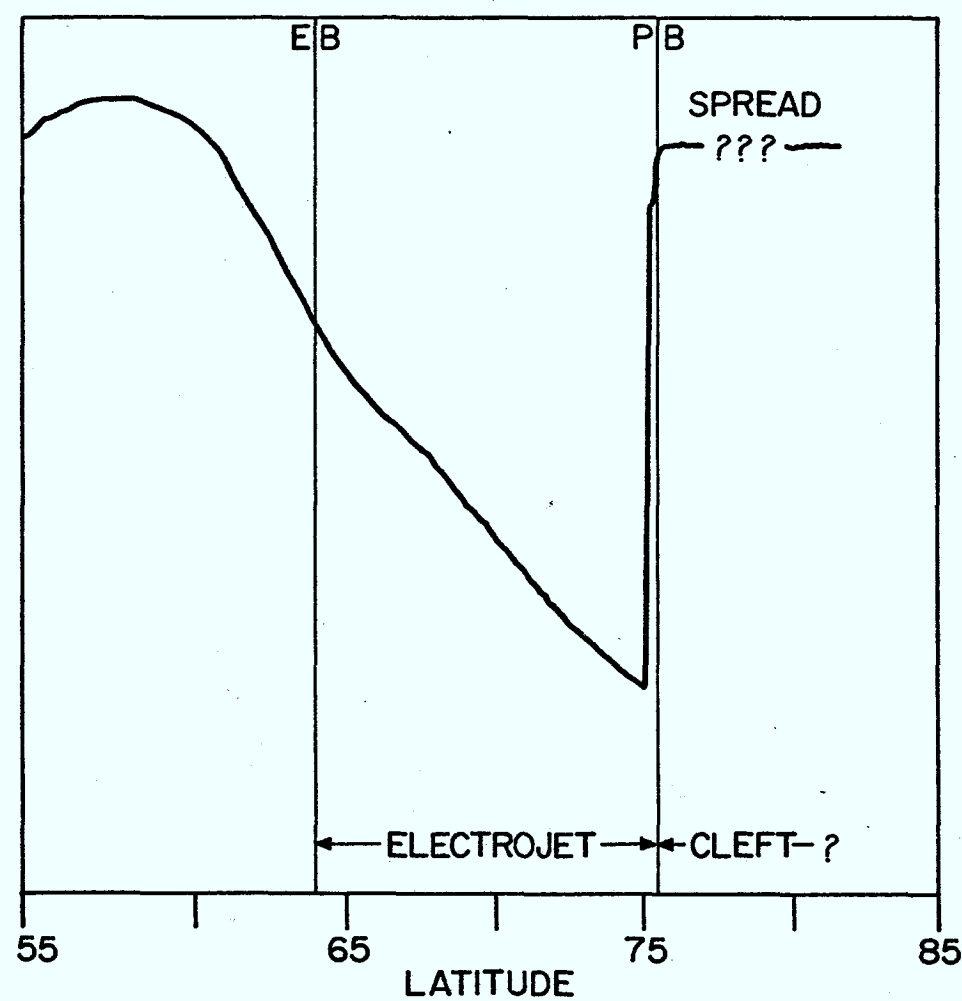
Finally, we wish to point out that the thermal plasma signature of the polar cleft is significantly different from that of the auroral electrojet. We show schematically in Figure 12 the two signatures which appear on opposite sides of the dusk meridian. First we note that the eastward electrojet regime in the post noon quadrant is significantly broader than in the pre-midnight quadrant. (In fact, some researchers (eg. Langel, 1974) tend to regard the magnetic signature of the ionospheric current flow in the post noon quadrant to be more representative of a vortex than an electrojet.) However, from our limited suite of data involving passes of ISIS II through the polar cleft, we may say that the poleward border of the eastward current flow in the post-noon quadrant marks the equatorward boundary of the cleft. The thermal plasma signatures are sufficiently different for the cleft and the electrojet, that we may use them to define whether the local time sector of the passes is dominated by cleft plasma, plasma sheet plasma or by both kinds. A further study of passes near the dusk meridian may be useful in furthering our understanding of how solar wind (magnetosheath) plasma enters the plasma sheet (if indeed it does).

Figure 12 Schematic thermal plasma latitude profiles indicating the behaviour of the thermal plasma at 1400 Km as the satellite traverses the high latitude region across the polar cleft and the eastward electrojet. Near the dusk meridian one might expect some profiles to exhibit aspects of both patterns.

EASTWARD ELECTROJET



POLAR CLEFT



Summary and Conclusions

In the study described in this report, we have attempted to correlate parameters measured in the topside ionosphere with the distribution of electrojet current in the high latitude ionosphere.

We have shown that the poleward portion of the auroral eastward or westward electrojet is the site of enhanced thermal plasma density at satellite altitude (1400 km for ISIS II) and we have shown that thermal plasma enhancements near the poleward border of the electrojet have associated with them enhanced whistler noise and soft electron fluxes as well as any net field aligned current flow which may penetrate the latitudinal regime of the electrojet.

The ability to define the poleward edge of the electrojet is important, in that this position also marks a transition in electric field polarity associated with the boundary between the polar cap (where anti-sunward convection takes place) and the auroral electrojet regime (where sunward convection is present). The ability to define the poleward border of the electrojet regime also reflects the possibility of defining the field line which maps back into the magnetotail along the boundary between the tail lobe and the plasma sheet. The latitudinal position of this field line is determined by the level of convection in the magnetosphere, and hence by the efficiency of the solar-terrestrial interaction.

Therefore, in conclusion, we may say that the region from the peak in thermal plasma density to the poleward edge of the enhanced thermal plasma regime accurately defines the boundary between the auroral electrojets and the polar cap, and hence is an effective monitor of the solar-terrestrial interaction.

References

- Anderson, C.W., III, I.J. Lanzerotti and C.G. MacLennan, Outage of the L-4 system and the geomagnetic disturbance of 4 August 1972, Bell Labs Preprint, 1974.
- Boström, R., A model of the auroral electrojets, *J. Geophys. Res.*, 69, 4983, 1964.
- Calvert, W. and J.R. McAfee, Topside-sounder resonances, *Proc. IEEE*, 57, 1089, 1969.
- DeForest, S.E., Spacecraft charging at synchronous orbit, *J. Geophys. Res.*, 77, 651, 1972.
- Hartz, T.R., Morphology of radio-radar polar propagation effects, in Radar Propagation in the Arctic, AGARD-CP-97, January, 1972.
- Hughes, T.J., and G. Rostoker, Ground-based magnetometer evidence for regions of net downward field aligned current flow in the morning sector, *J. Geophys. Res.*, manuscript in preparation.
- James, H.G., Whistler-mode hiss at low and medium frequencies in the dayside-cusp ionosphere, *J. Geophys. Res.*, 78, 4578, 1973.
- Kisabeth, J.L., The dynamical development of the polar electrojets, Ph.D. Thesis, Univ. of Alberta, Edmonton, Canada 1972.
- Langel, R.A., Near-earth magnetic disturbance in total field at high latitudes 2. Interpretation of data from Ogo 2, 4, and 6, *J. Geophys. Res.*, 79, 2373, 1974.
- Rees, M.H., Auroral electrons, *Space Sci. Rev.*, 10, 413, 1969.
- Rostoker, G., Interpretation of magnetic field variations during substorms, in Earth's Magnetospheric Processes, ed. B.M. McCormac, D. Reidel Publ. Co., 379, 1972.

Rostoker, G., W. Sherrard and R. Mah, The Killam Earth Sciences magnetometer system, Killam Earth Sciences Internal Report #32, September 15, 1972.

Rostoker, G., and J.L. Kisabeth, Response of the polar electrojets in the evening sector to polar magnetic substorms, J. Geophys. Res., 78, 5559, 1973.

Rostoker, G., J.C. Armstrong, and A.J. Zmuda, Field-aligned current flow associated with intrusion of the substorm intensified westward electrojet into the evening sector, J. Geophys. Res., in press, 1975.

Rostoker, G., and R. Boström, A mechanism for driving the gross field-aligned current configuration in the auroral oval, J. Geophys. Res., submitted for publication, 1975.

Sugiura, M., Identification of the polar cap boundary and the auroral belt in the high latitude magnetosphere; a model for field-aligned currents, Goddard Space Flight Center Report X-625-74-195, 1974.

Wallis, D.D., C.D. Anger and G. Rostoker, The spatial relationship of auroral electrojets and visible aurora in the evening sector, J. Geophys. Res., submitted for publication, 1975.

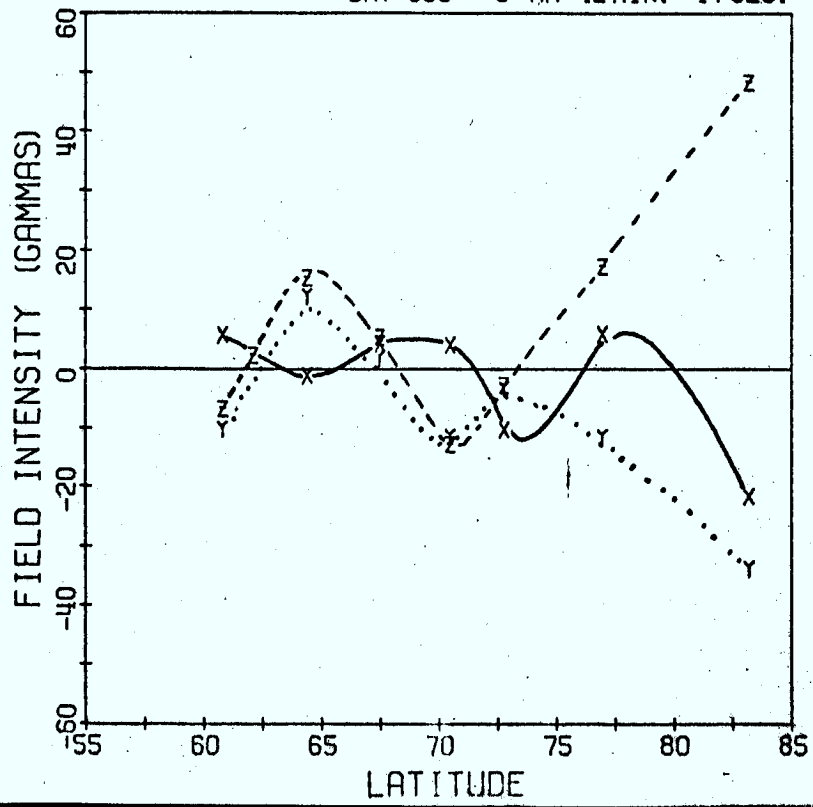
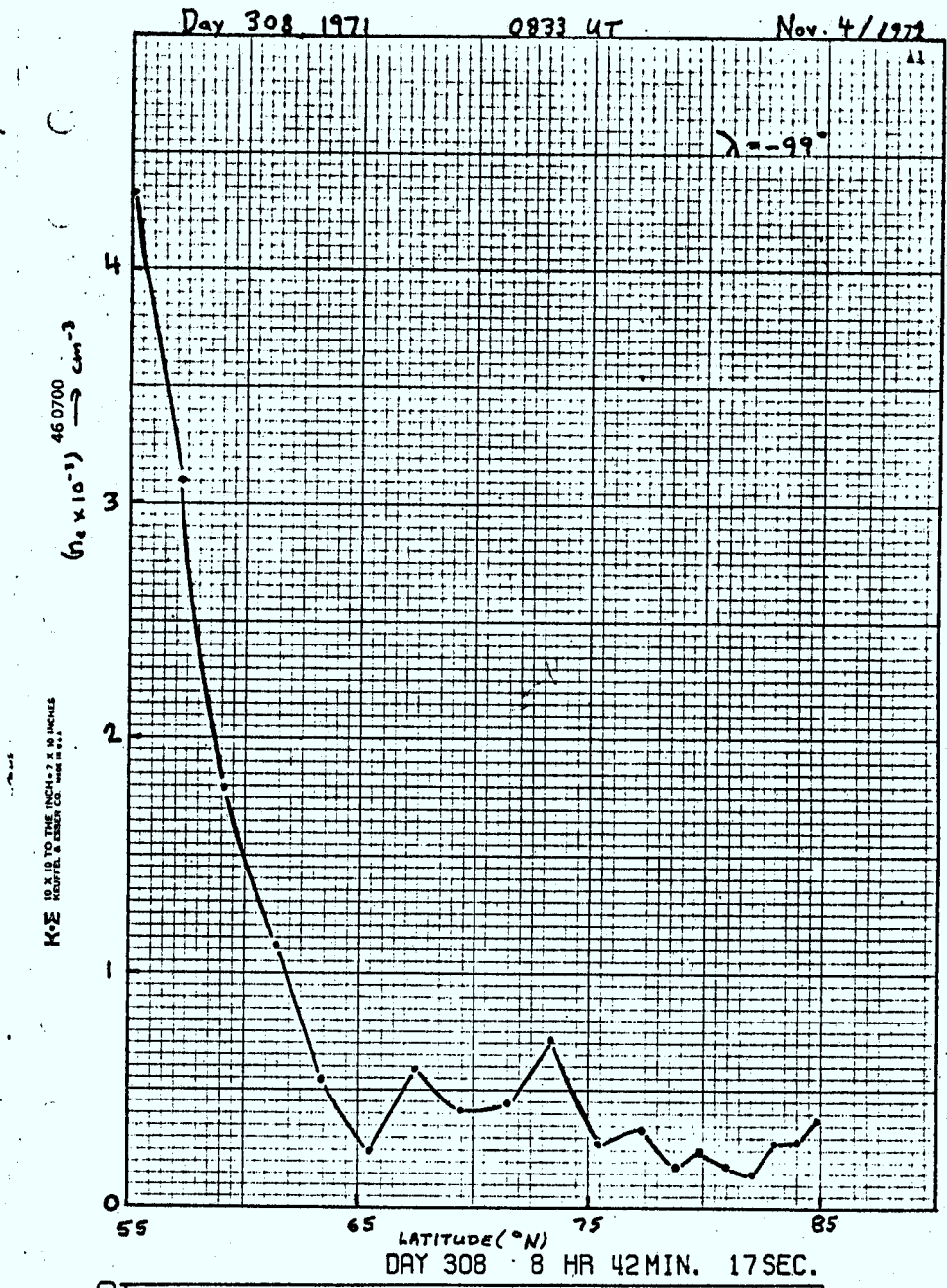
Whitteker, J.H., The magnetospheric cleft-ionospheric effects, J. Geophys. Res., manuscript in preparation, 1975.

Zmuda, A.J., and J.C. Armstrong, The diurnal flow of field-aligned currents, J. Geophys. Res., 79, 4611, 1974.

APPENDIX

In this appendix we show all latitude profiles, thermal plasma density and noise profiles used in this study. Each event plot shows the day of the pass, the UT when the satellite was at the most poleward position during the pass, and the geographic longitude λ of the pass (in degrees east). The borders of the auroral electrojets are shown by vertical arrows at the top of each plot of n_e vs latitude. Values of n_e which were too low to be established quantitatively are indicated by the symbol \downarrow . Cases where n_e was not easily evaluated due to spread conditions are indicated by ?.

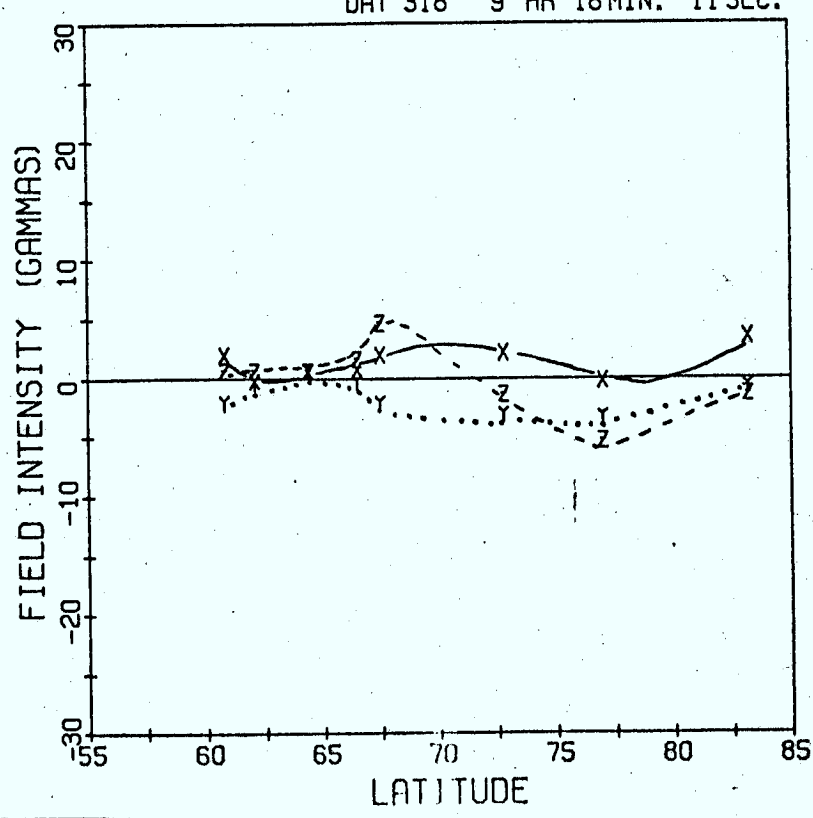
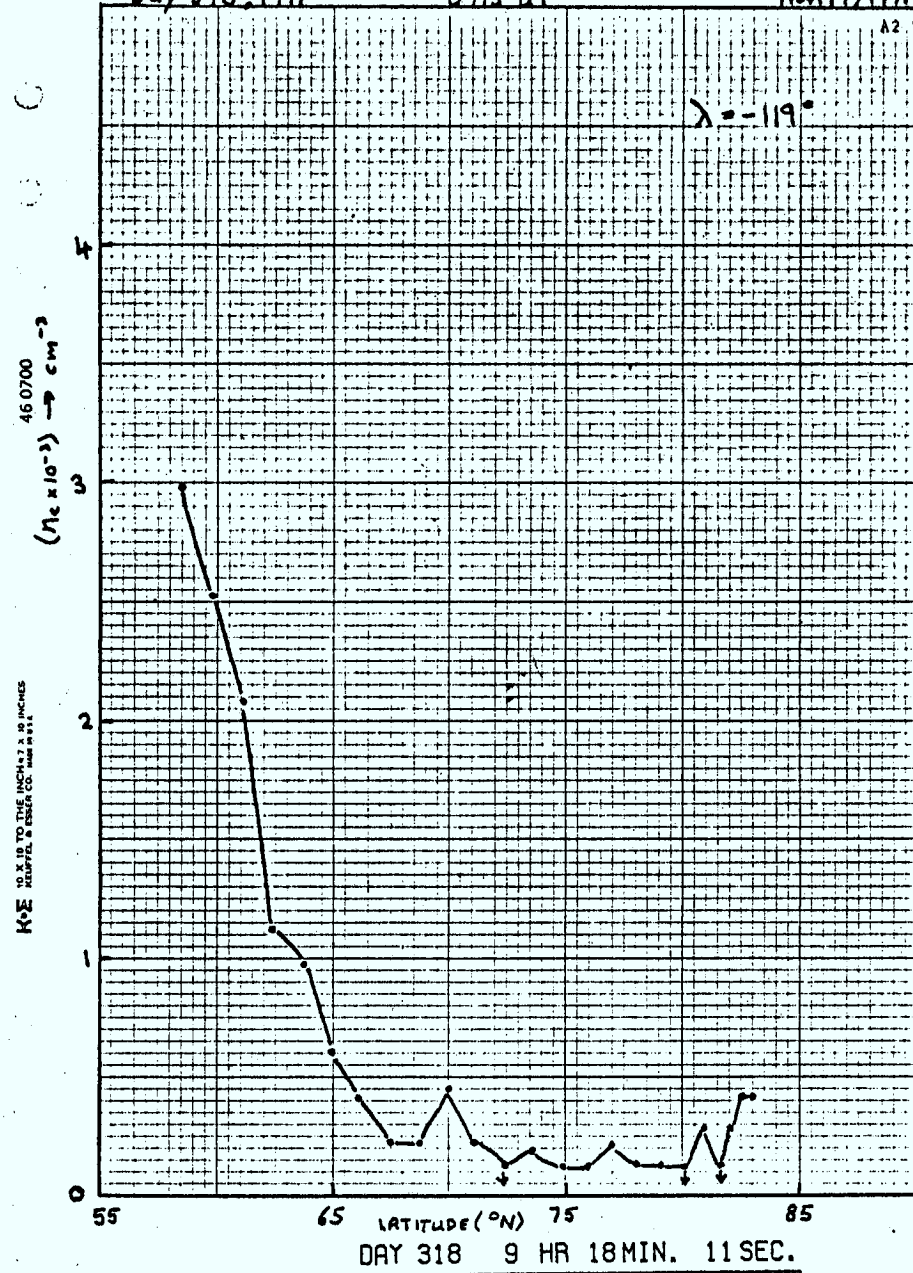
The times at the top of each latitude profile indicate the time at which the data were recorded from which the profile was constructed. On each profile points marked X give the perturbation in the geomagnetic north direction, points marked Y give the perturbation in the geomagnetic east direction, and points marked Z give the perturbation in the vertical direction.



Day 318, 1971

0913 UT

Nov. 14/1971

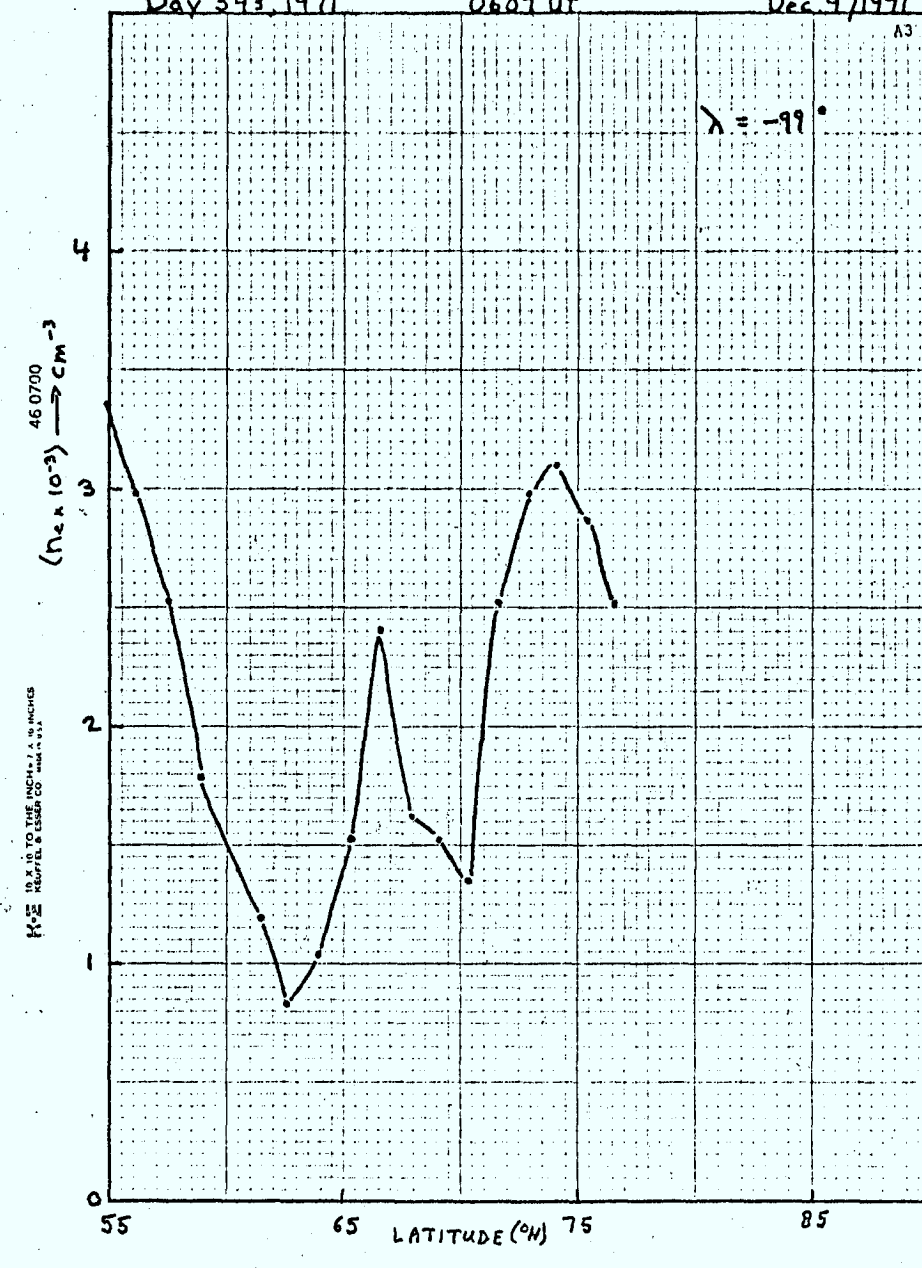


Day 343, 1971

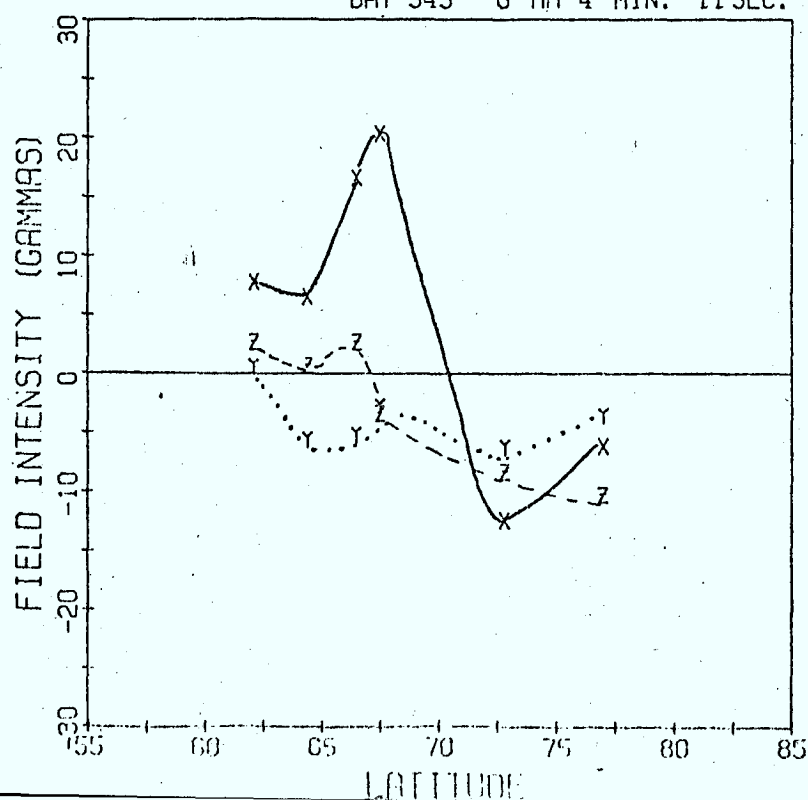
0607 UT

Dec 9/1971

A3

 $\lambda = -99^\circ$ 

DAY 343 6 HR 4 MIN. 11 SEC.

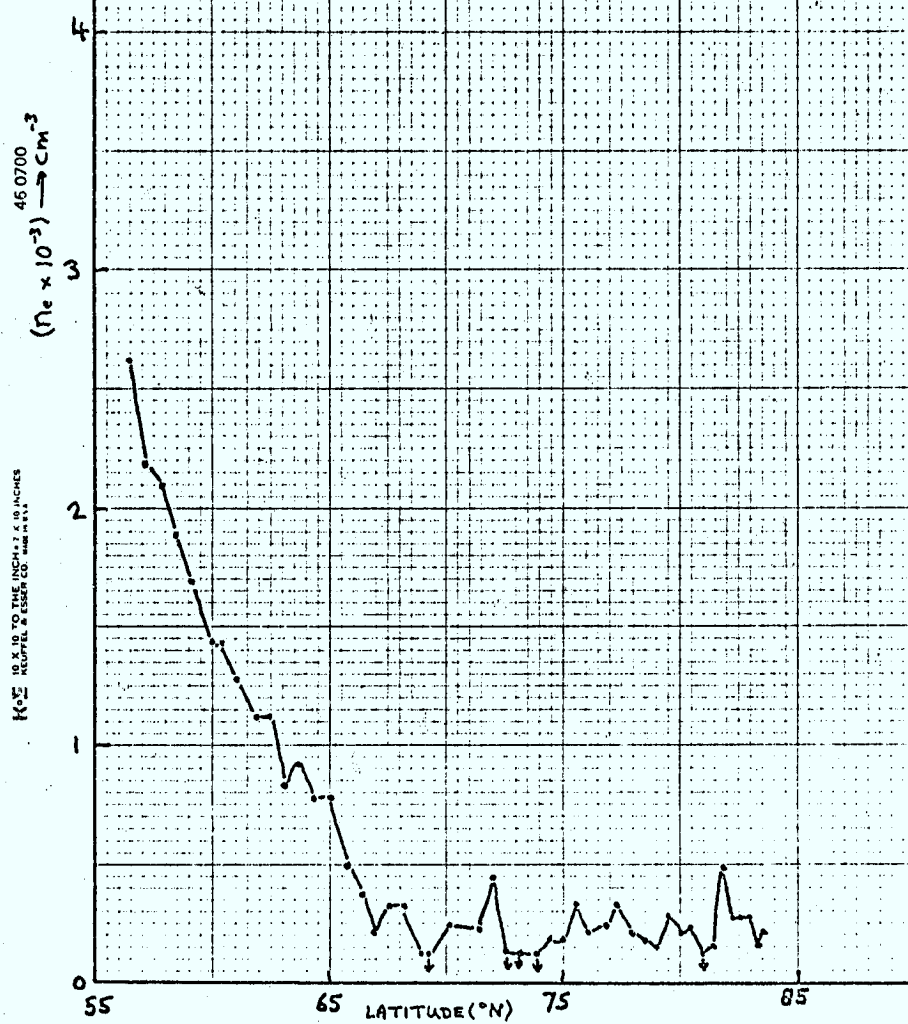


Day 344, 1971

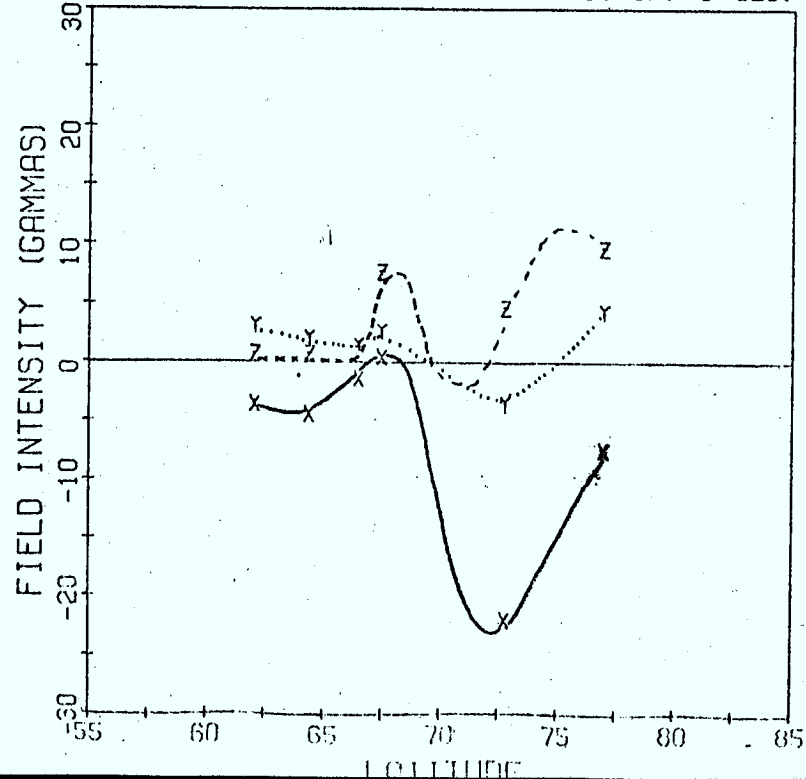
0641 UT

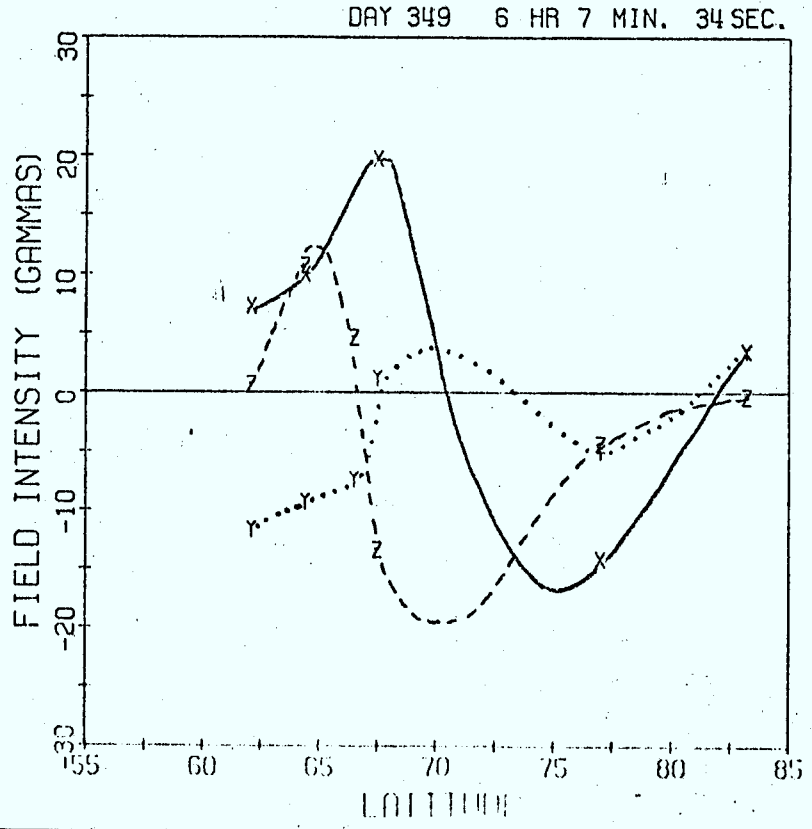
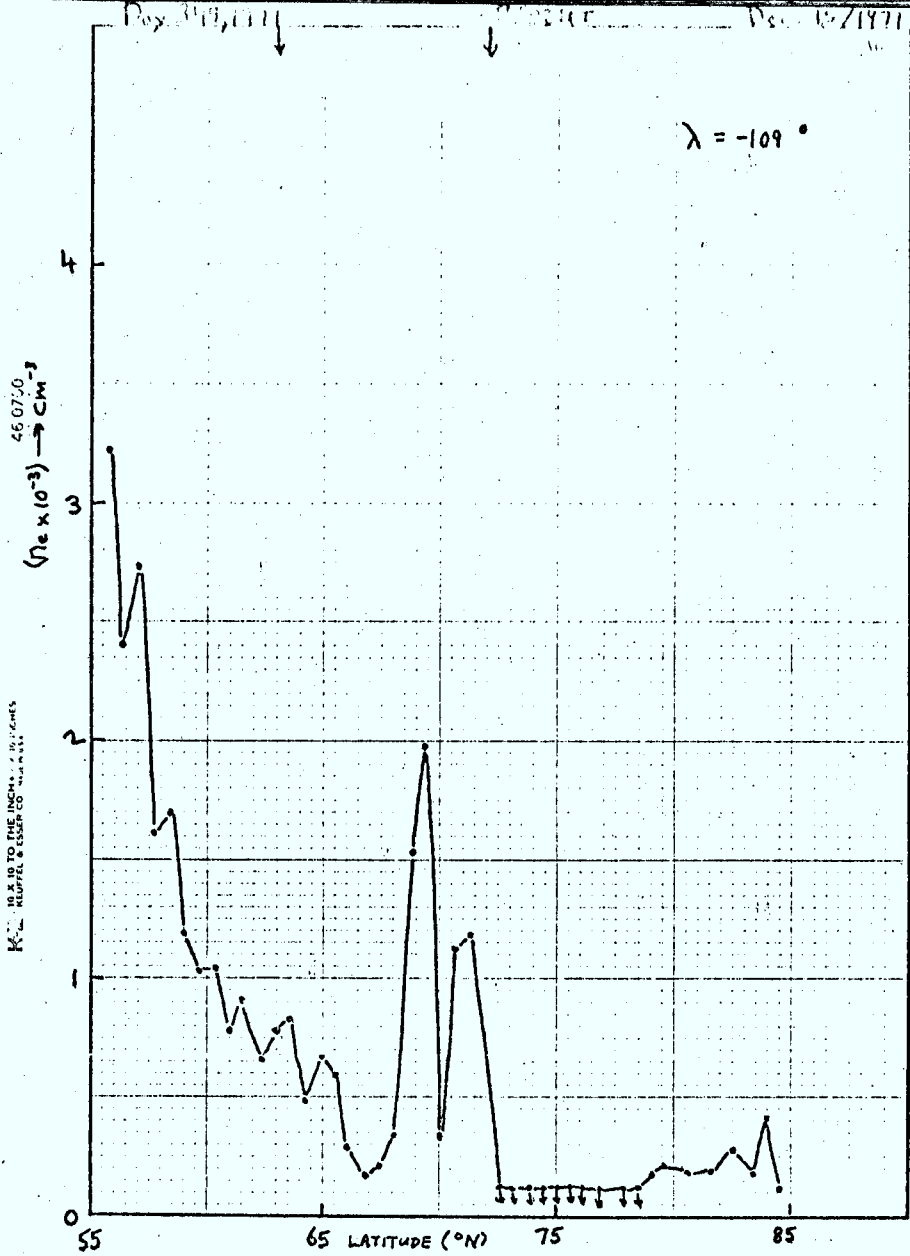
Dec. 10/1971

A9

 $\lambda = -111^\circ$ 

DAY 344 6 HR 38MIN. 5 SEC.



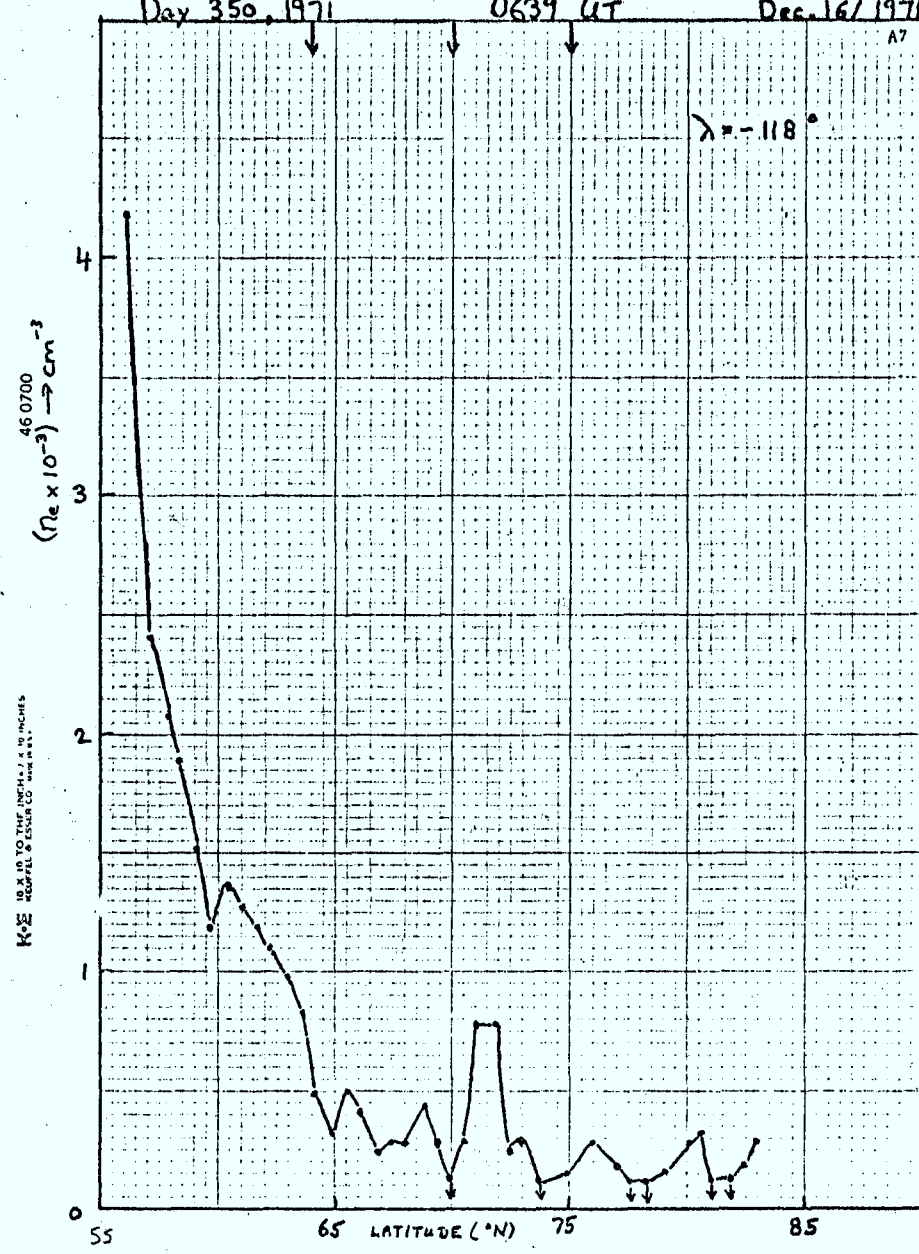


Day 350, 1971

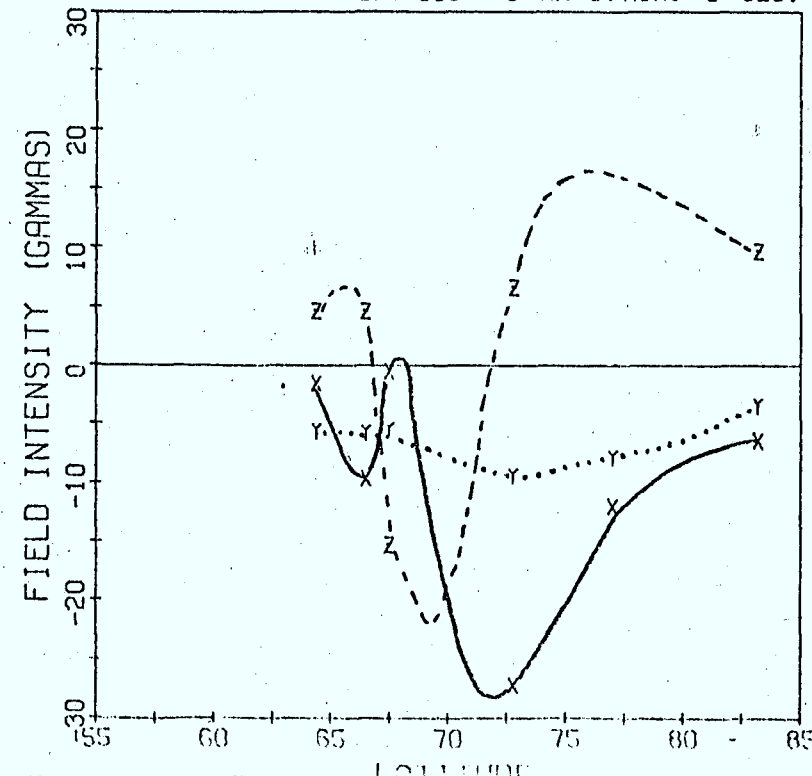
0639 UT

Dec. 16/1971

A7

 $\lambda = -118^\circ$ 

DAY 350 6 HR 37MIN. 5 SEC.

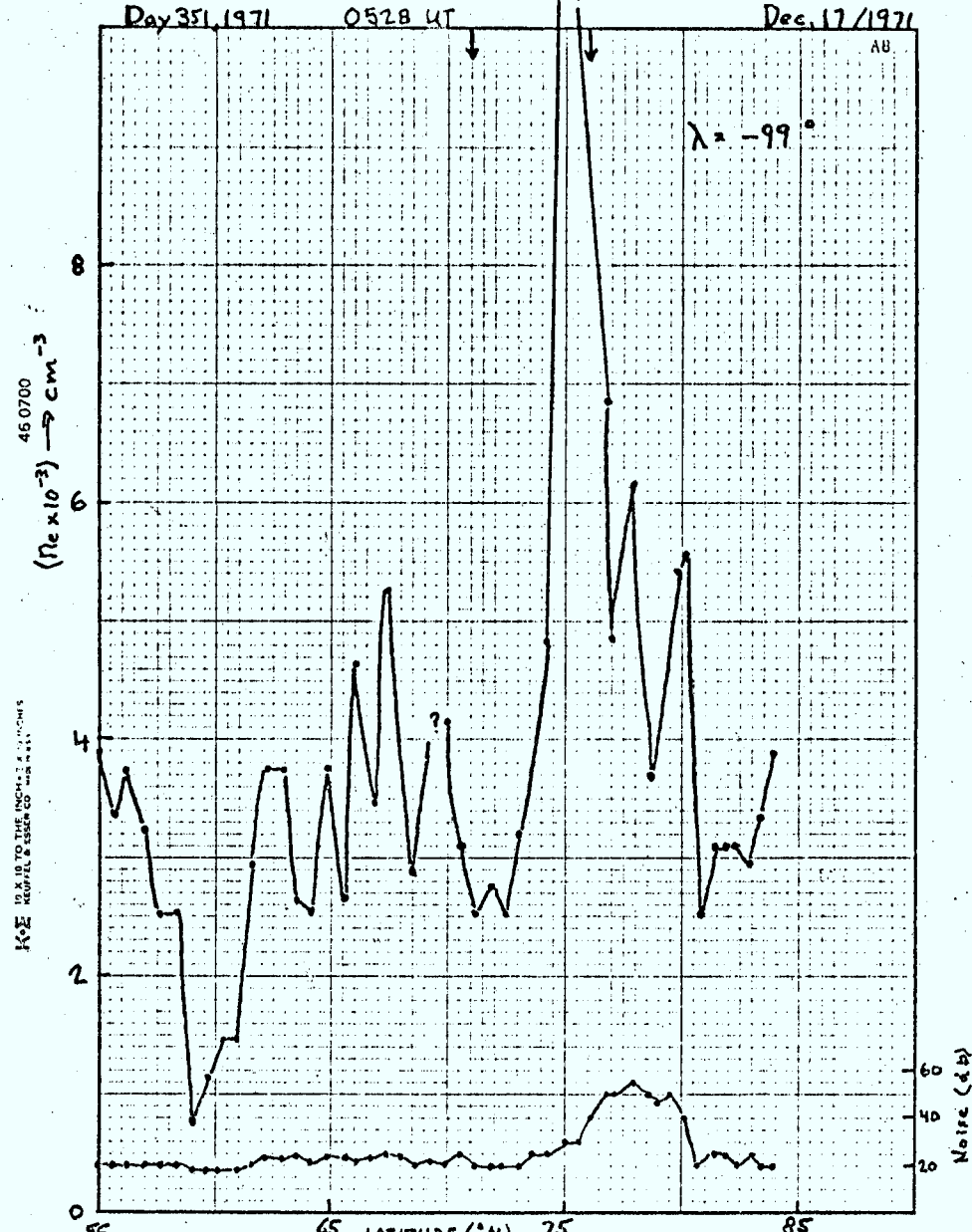


Day 351, 1971

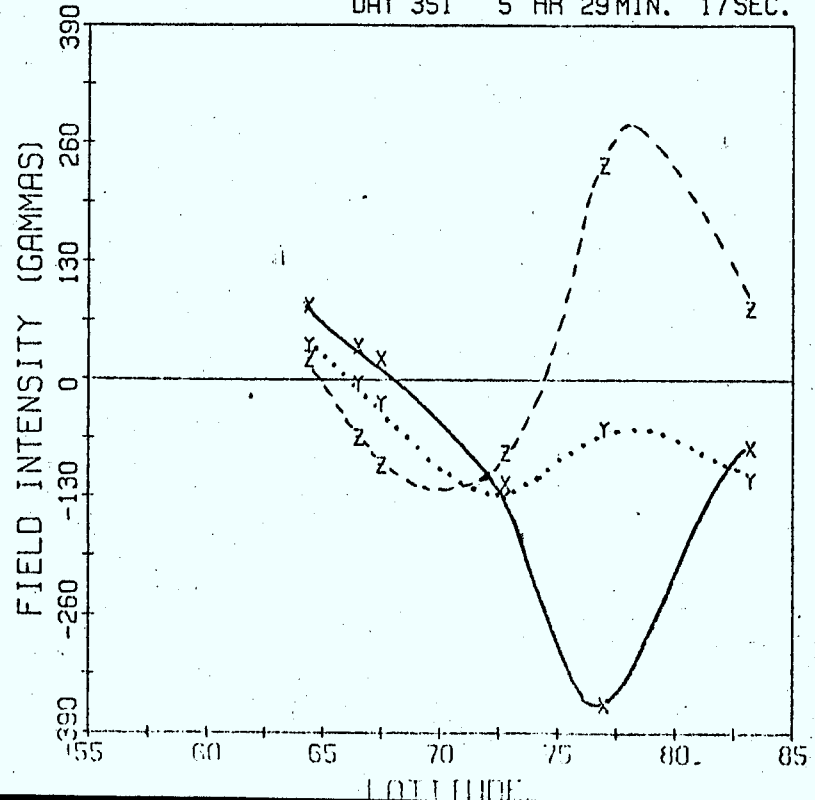
0528 UT

Dec. 17/1971

AB



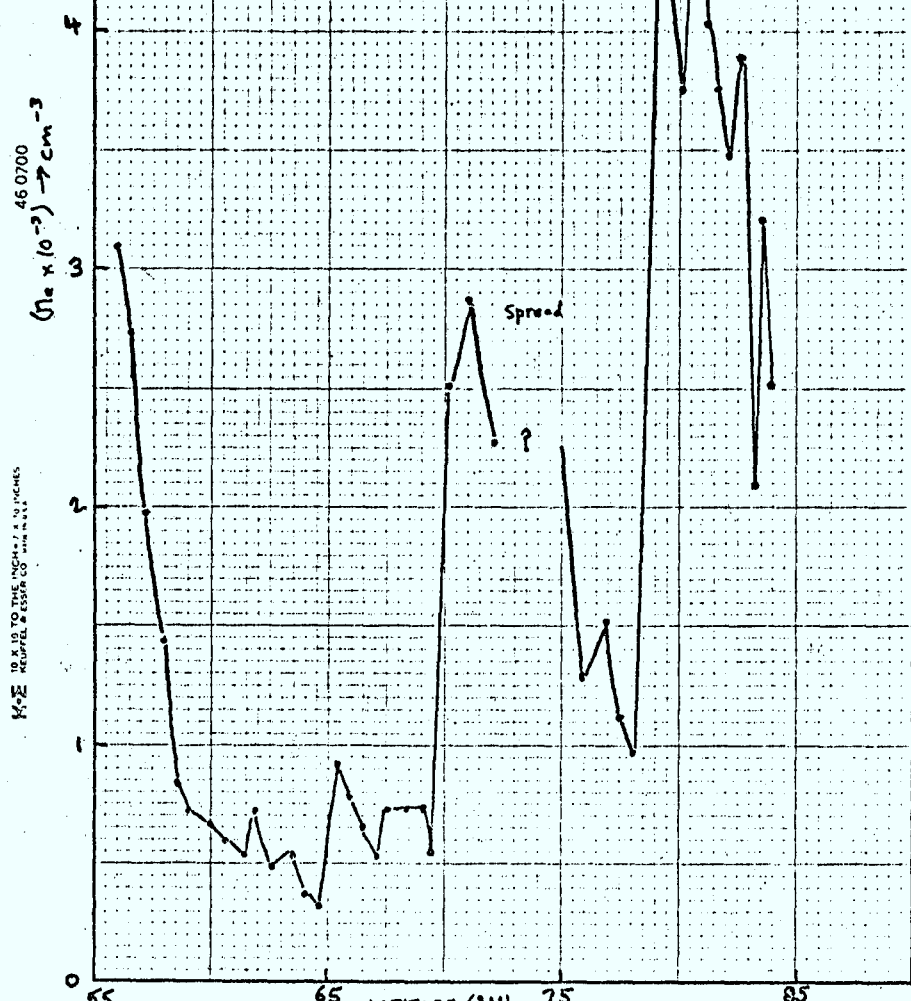
UHT 351 5 HR 29 MIN. 17 SEC.



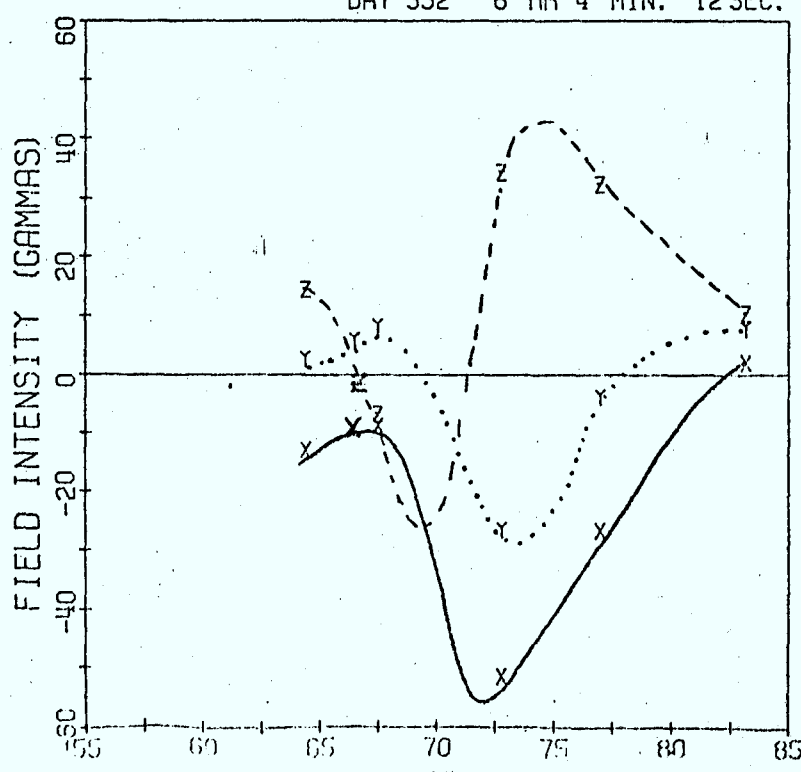
Day 352, 1971

0608 UT

Dec. 19 / 1971



DAY 352 6 HR 4 MIN. 12 SEC.

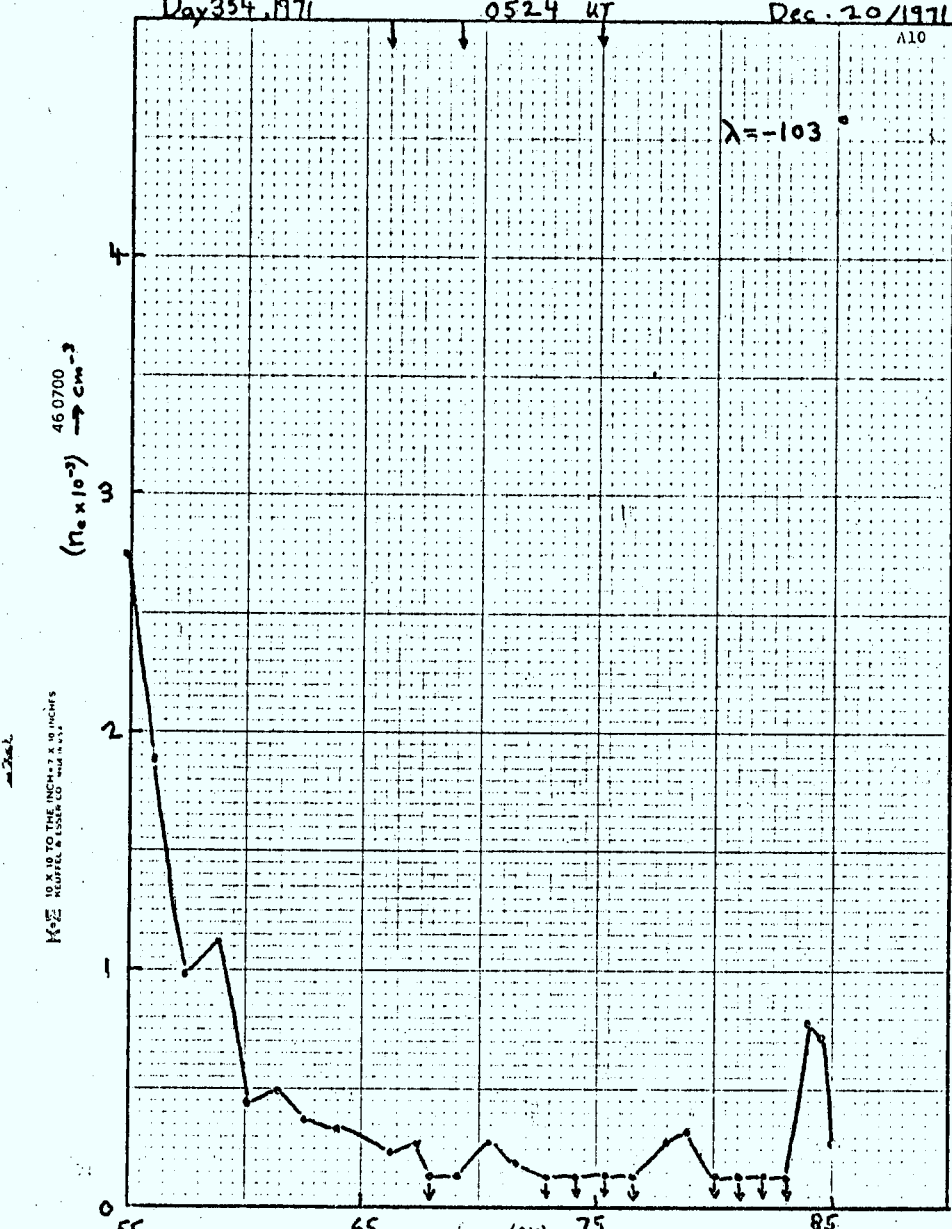


Day 354, 1971

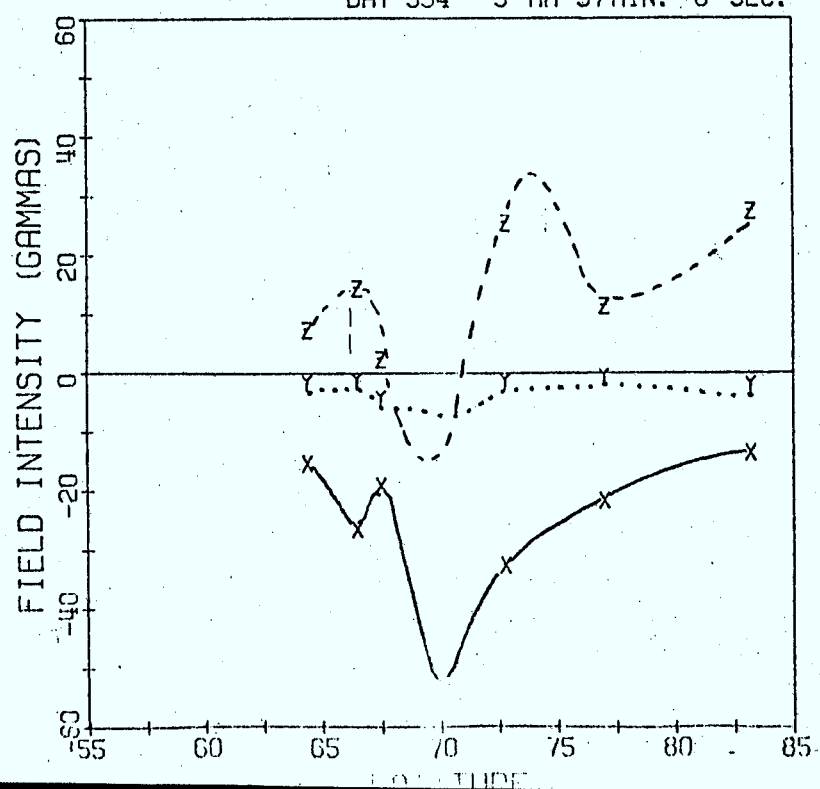
0524 UT

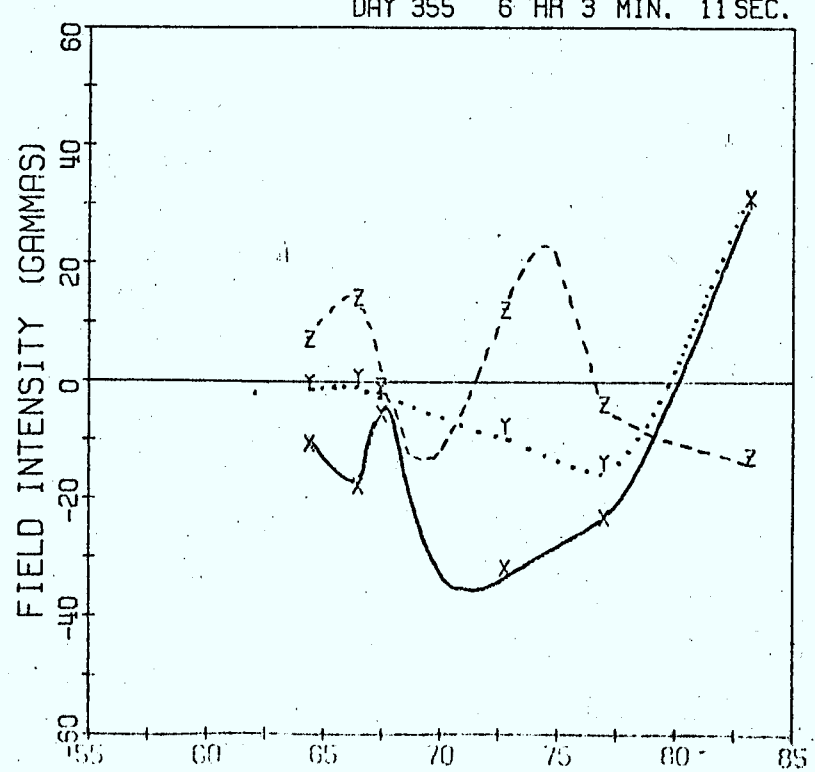
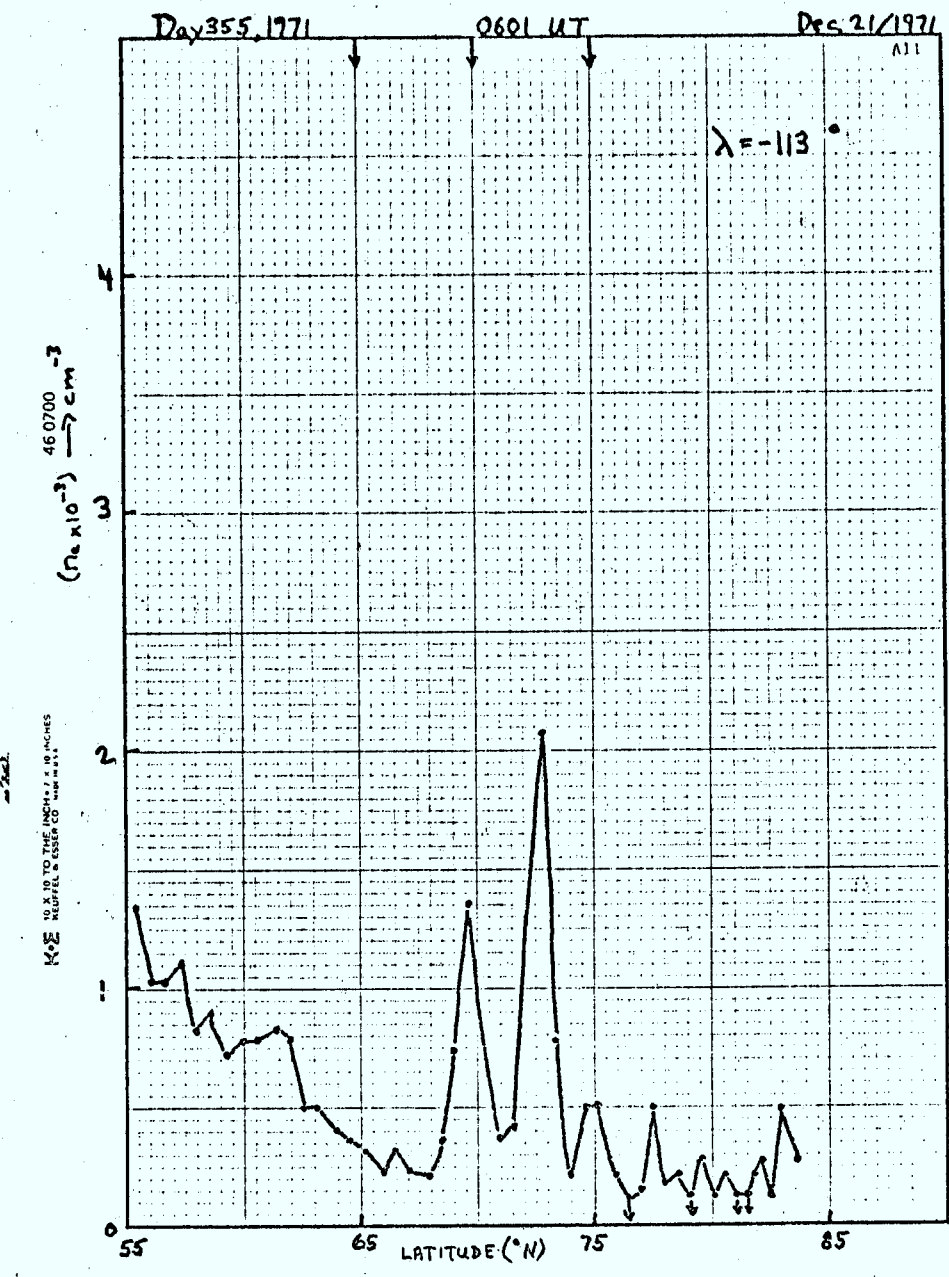
Dec. 20/1971

A10

 $\lambda = -103^\circ$ 

DAY 354 5 HR 37 MIN. 0 SEC.



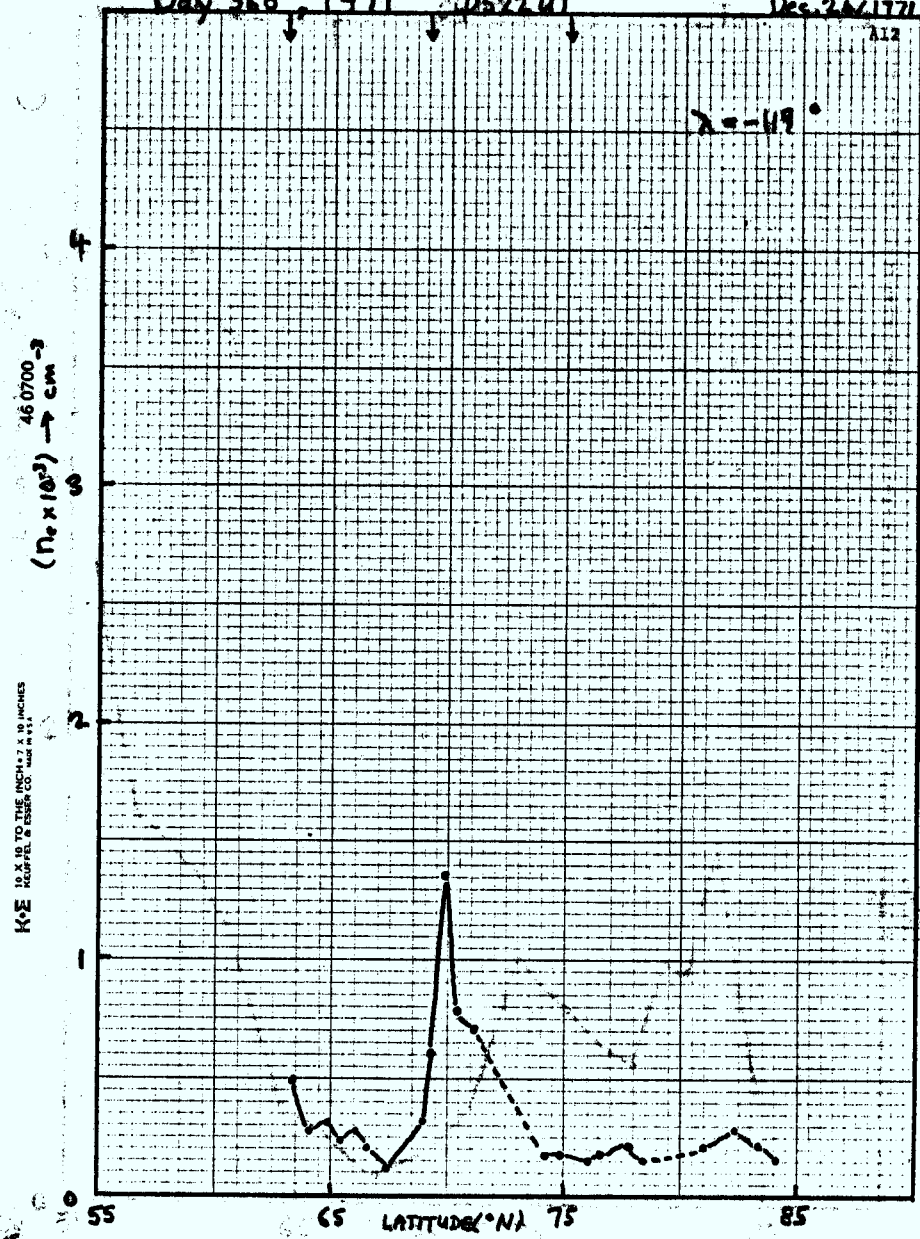


Day 360 1971 0522 UT

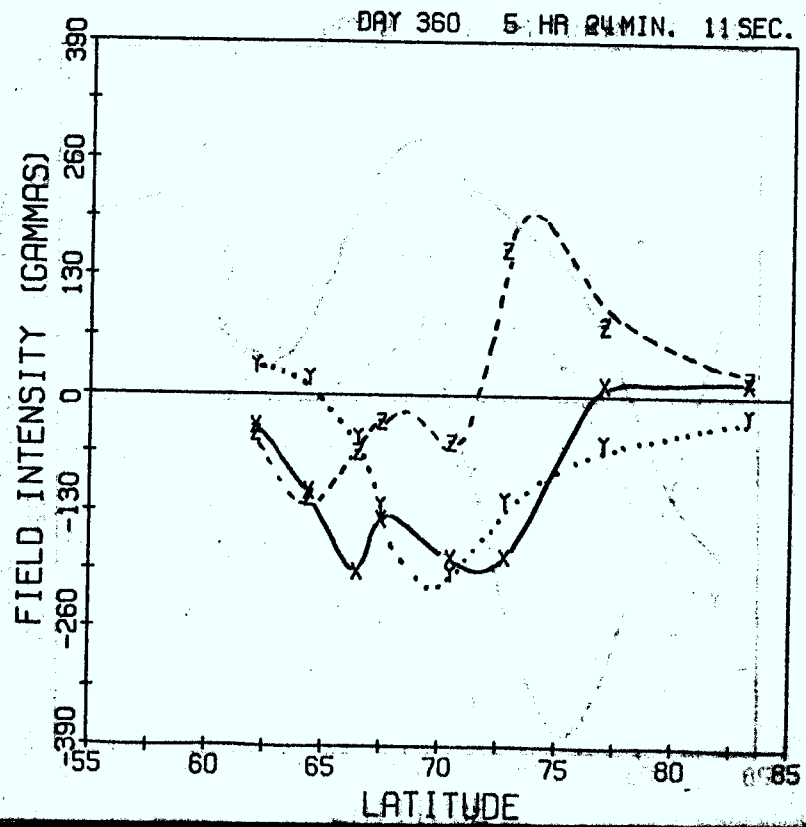
Vec. 20/1172

312

$\lambda = -119^\circ$



DAY 360 5 HR 24 MIN. 11 SEC.



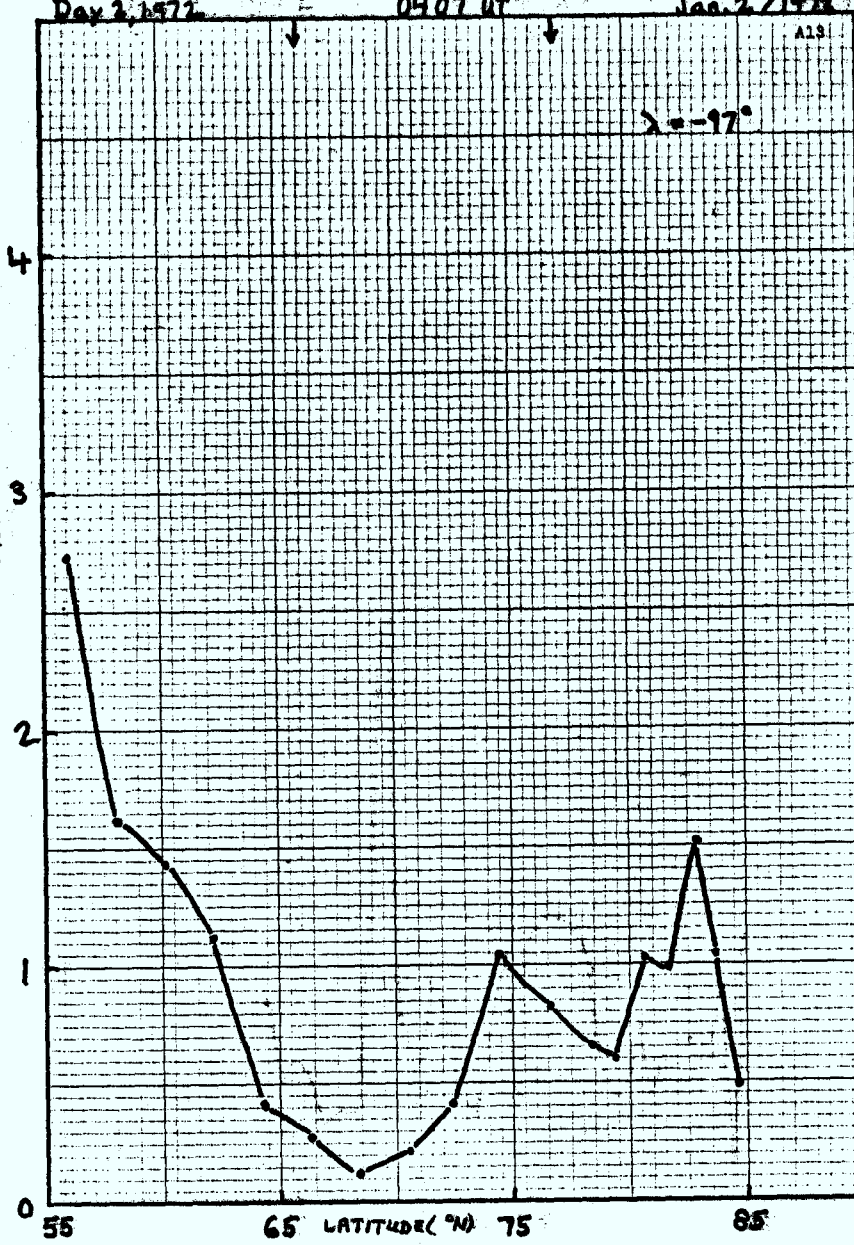
Day 2, 1972

0407 UT

Jan. 2, 1972

A13

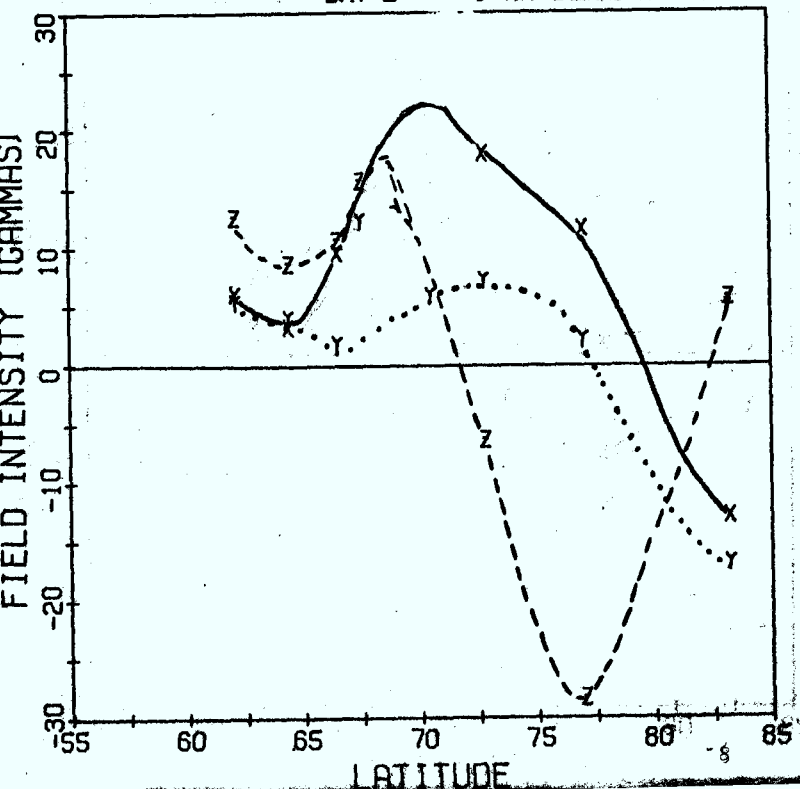
Lat -97°

(n_a × 10⁻³) → cm⁻³K-E RATIO TO THE INCHES X 10⁻³ INCHES

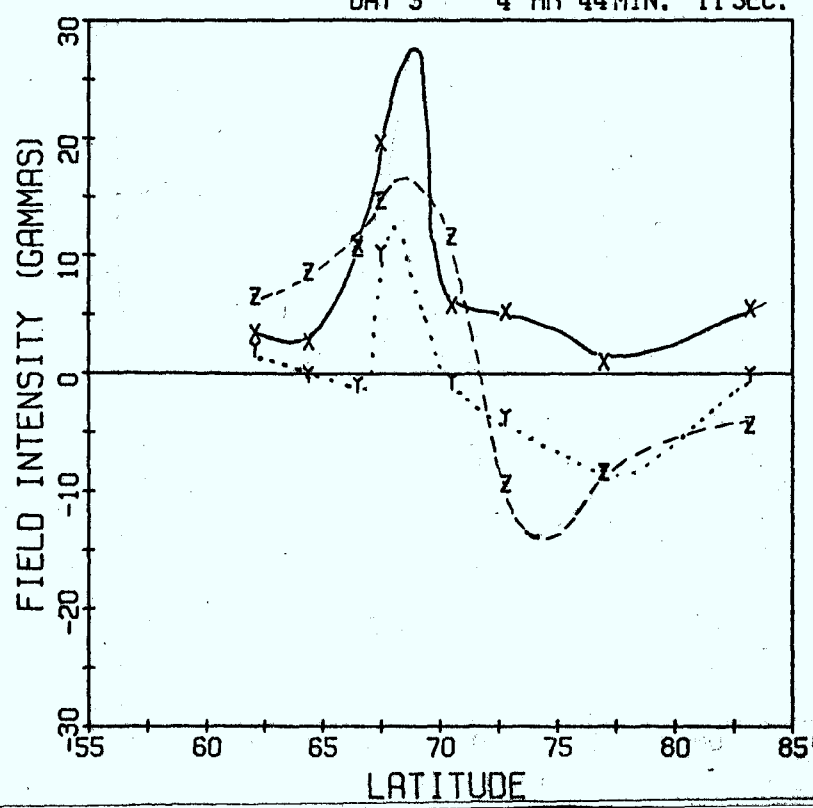
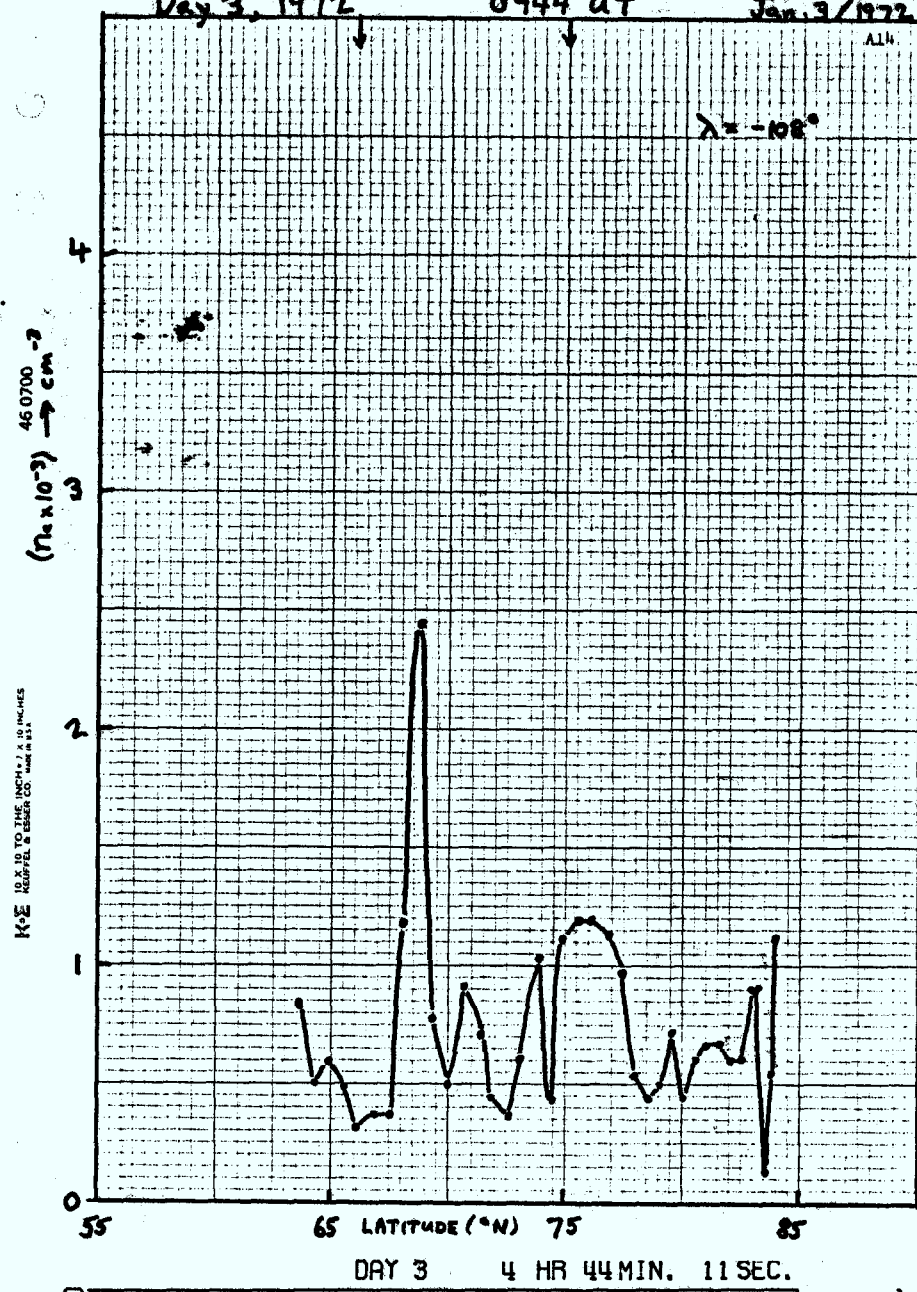
DAY 2 4 HR 10MIN. 17 SEC.

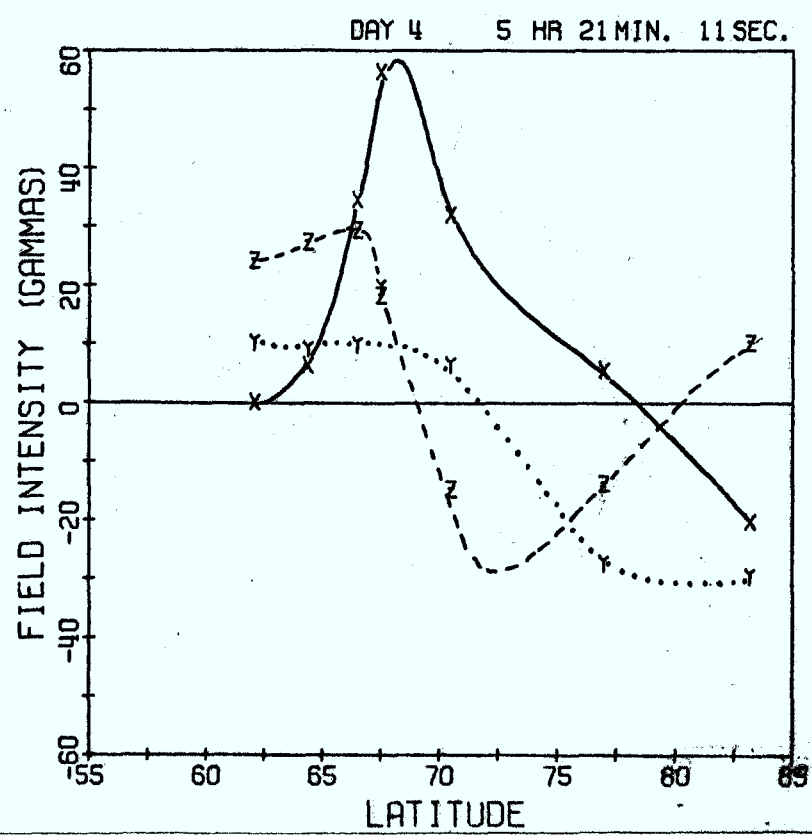
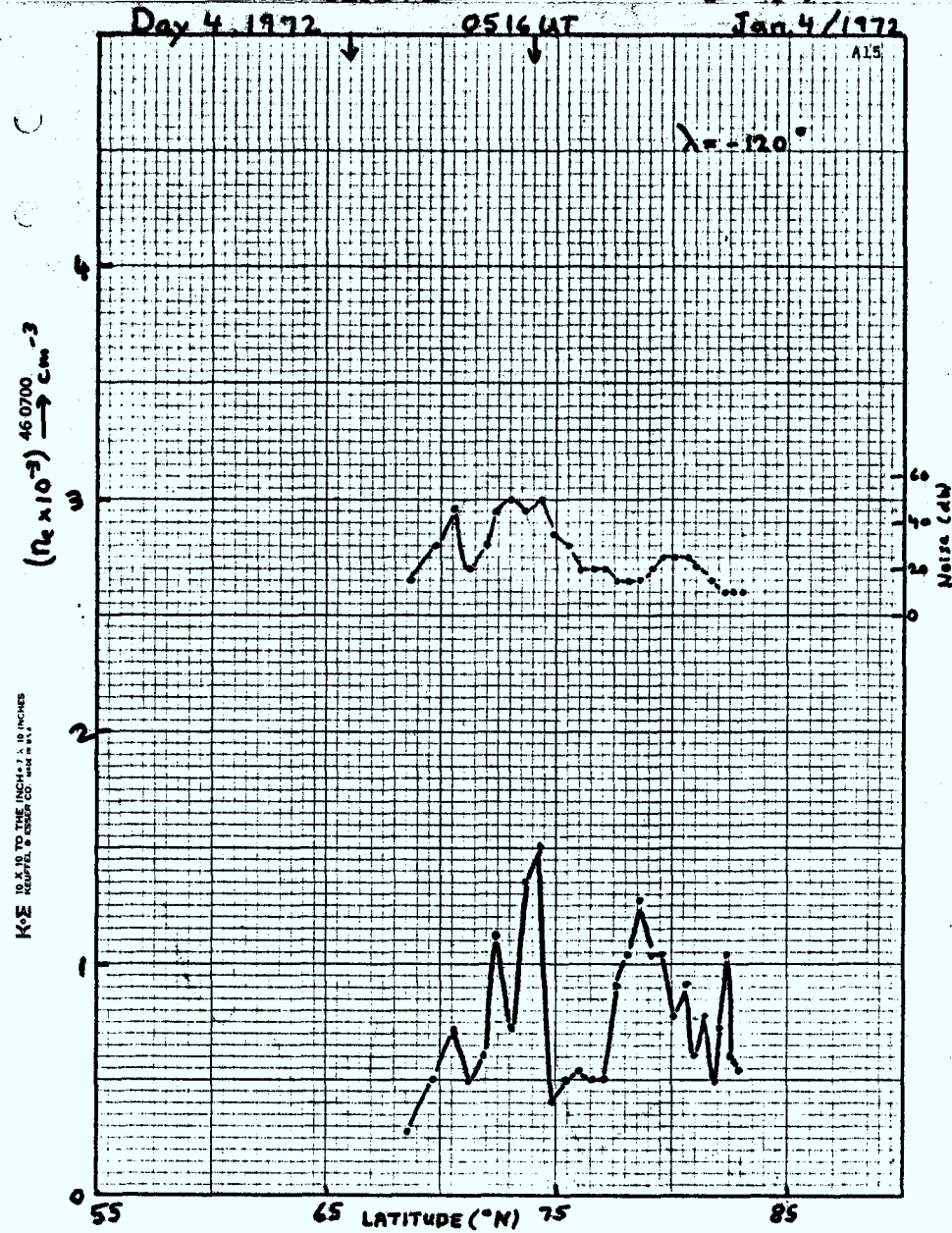
FIELD INTENSITY (GAMMAS)

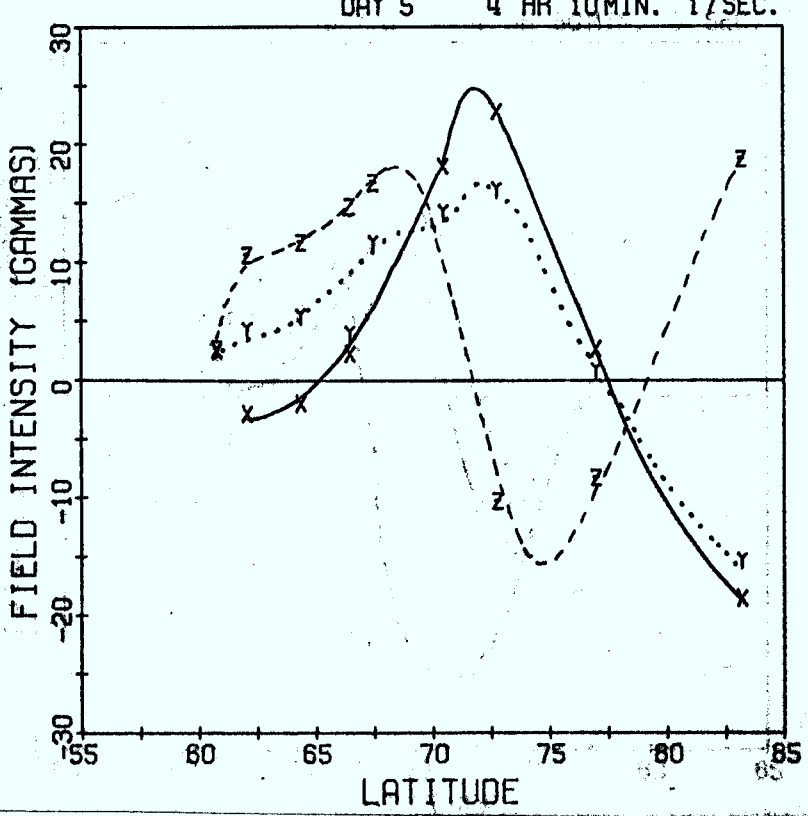
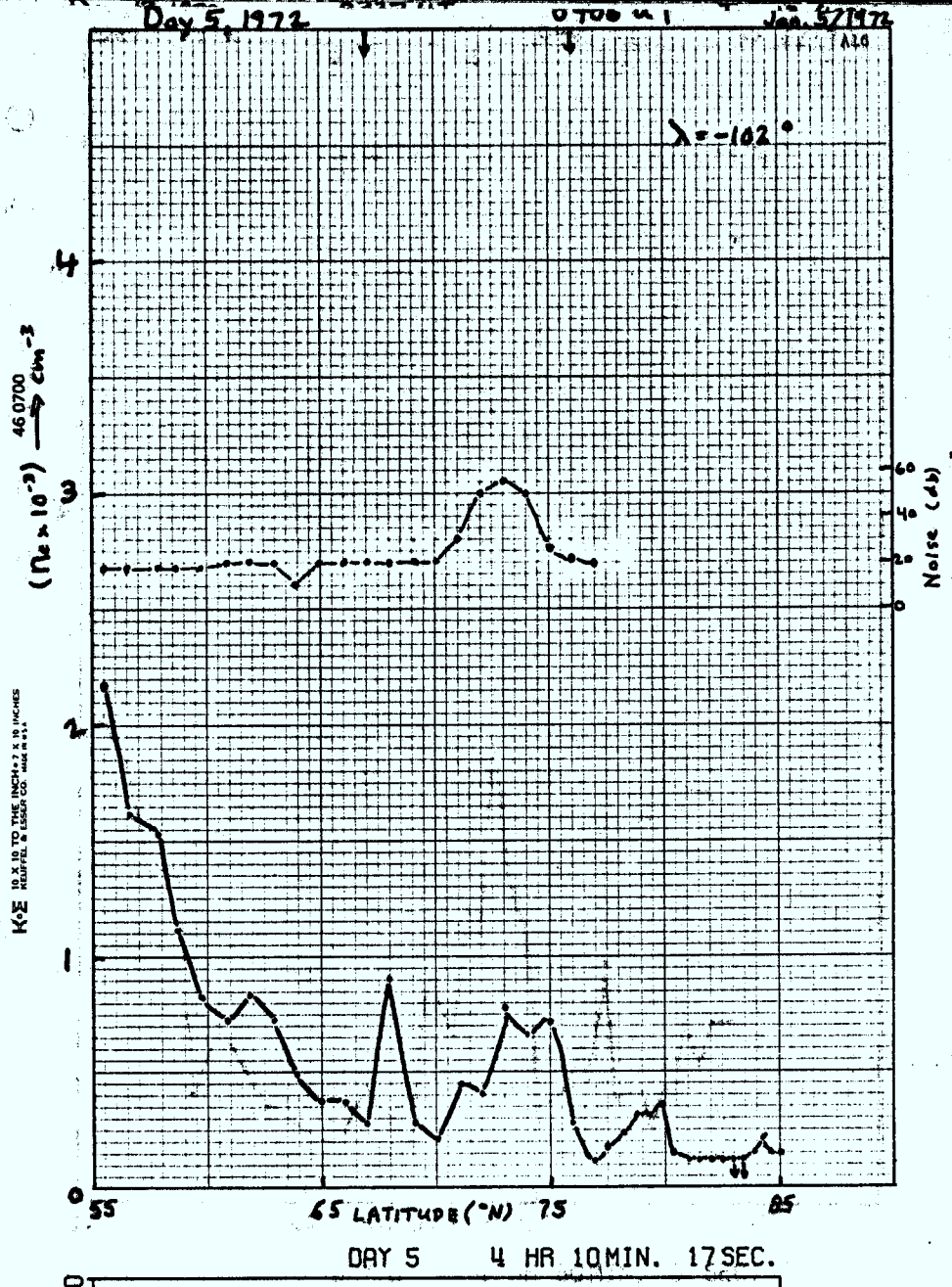
LATITUDE

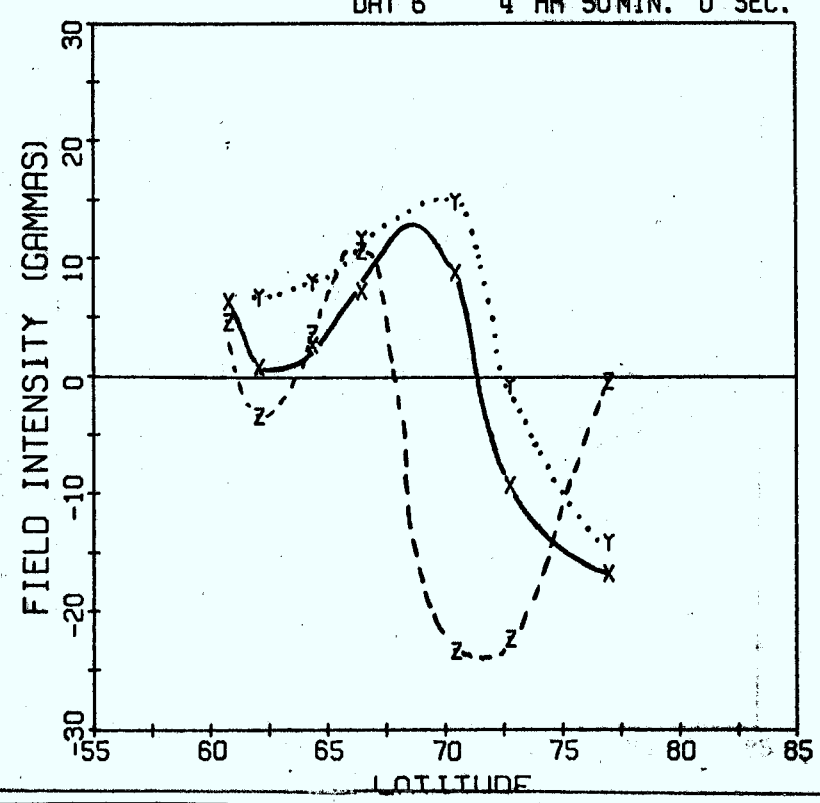
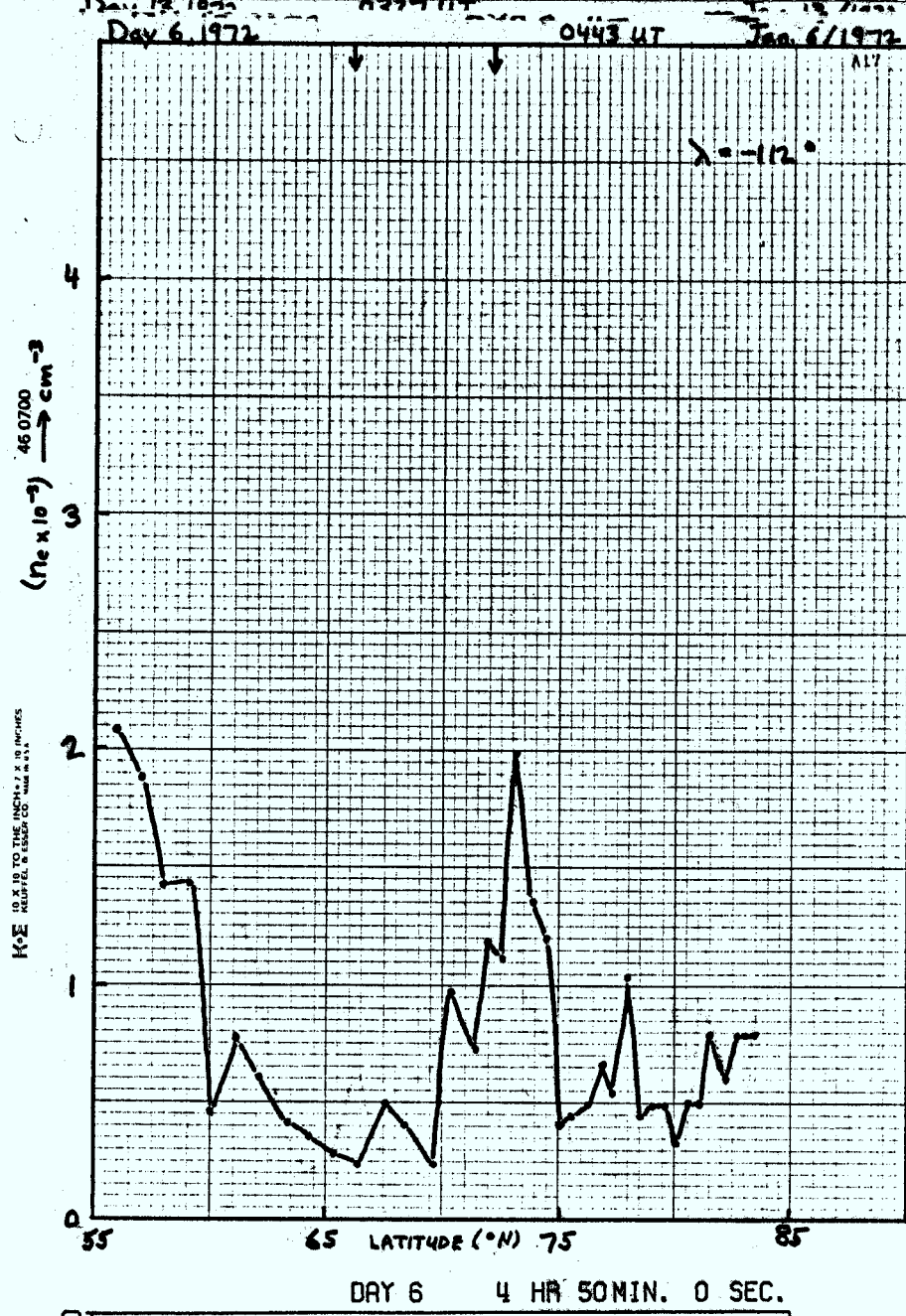


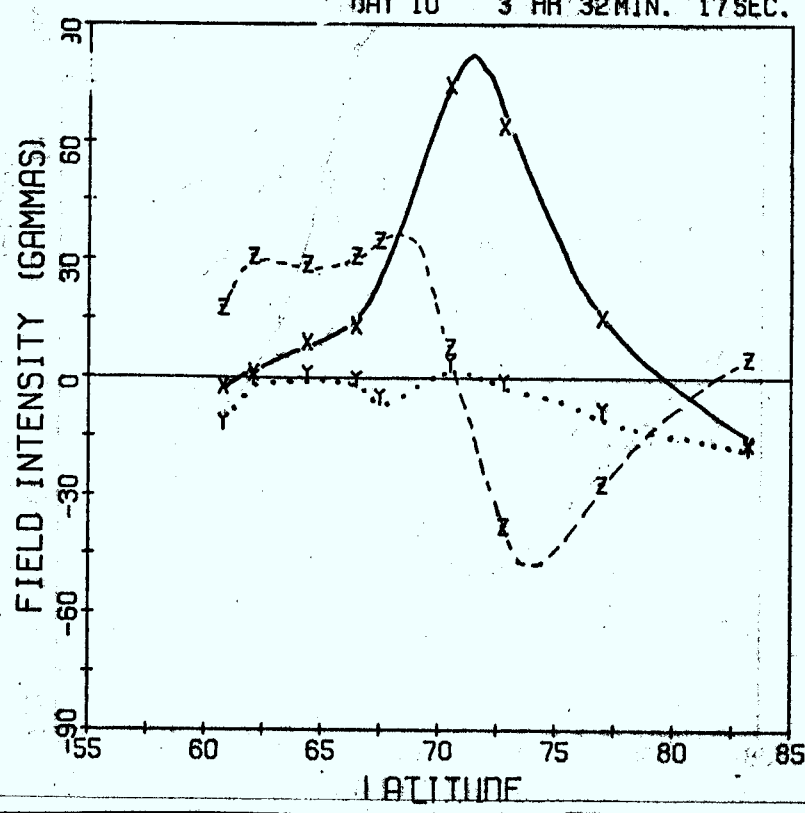
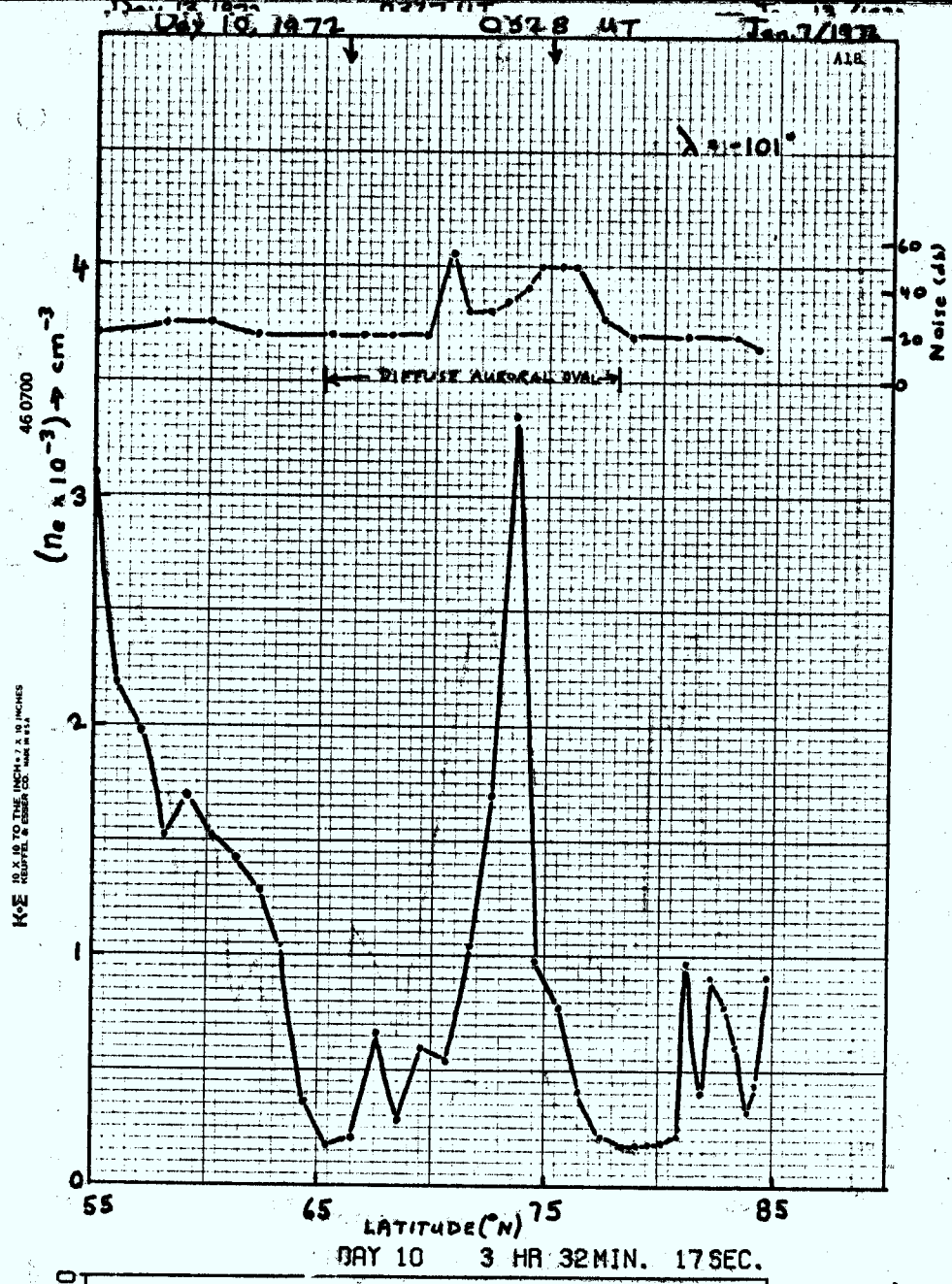
Day 3, 1972 0444 UT Jan. 3/1972









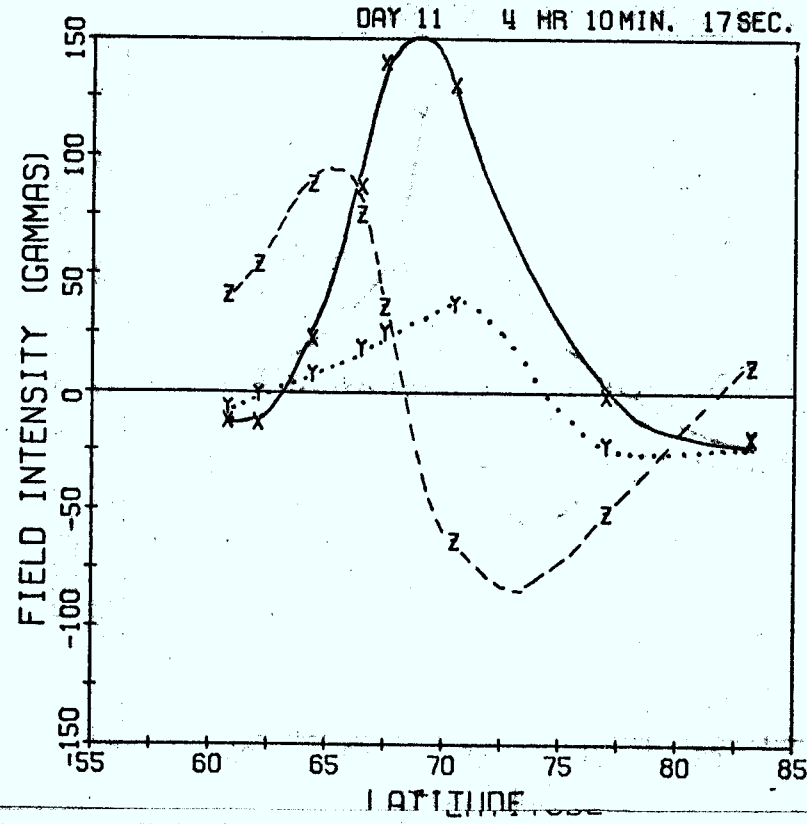
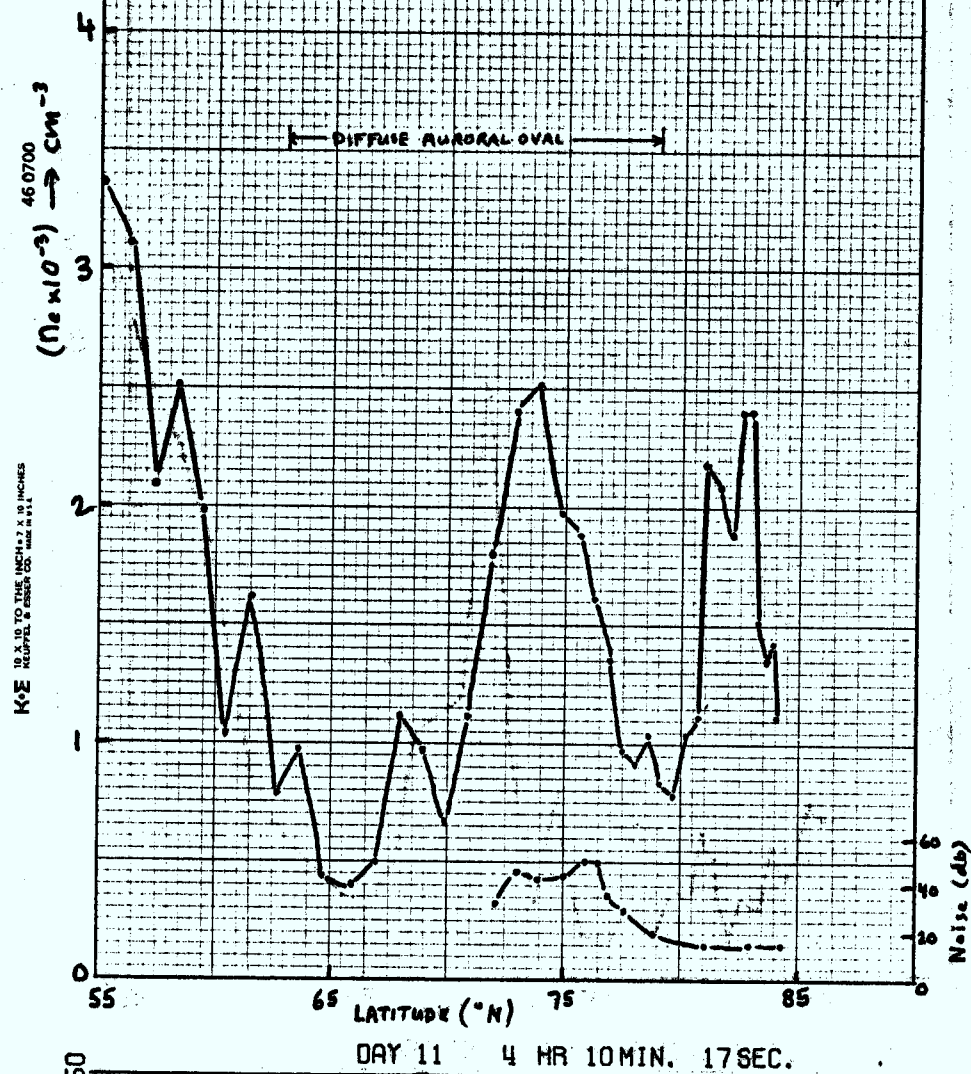


May 11, 1972

0405 UT

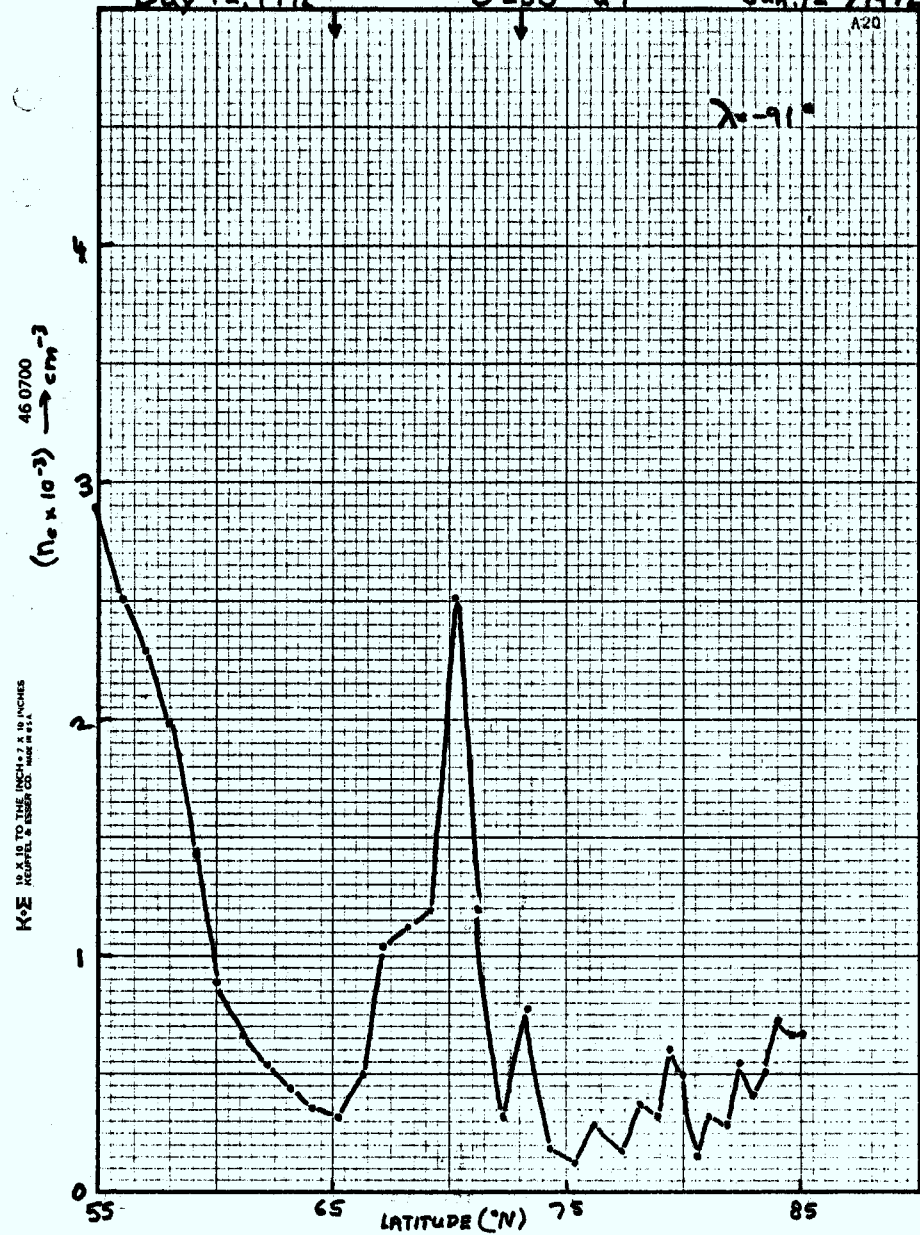
Jan. 11/1972

A19

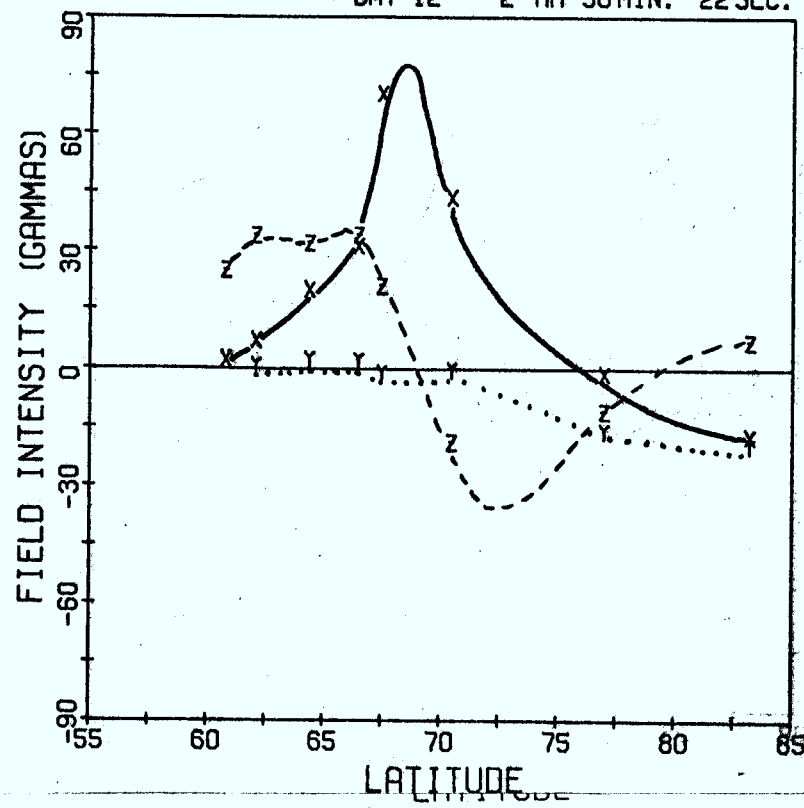
 $\lambda = -108^\circ$ 

Day 12, 1972 0250 UT Jan. 12 / 1972

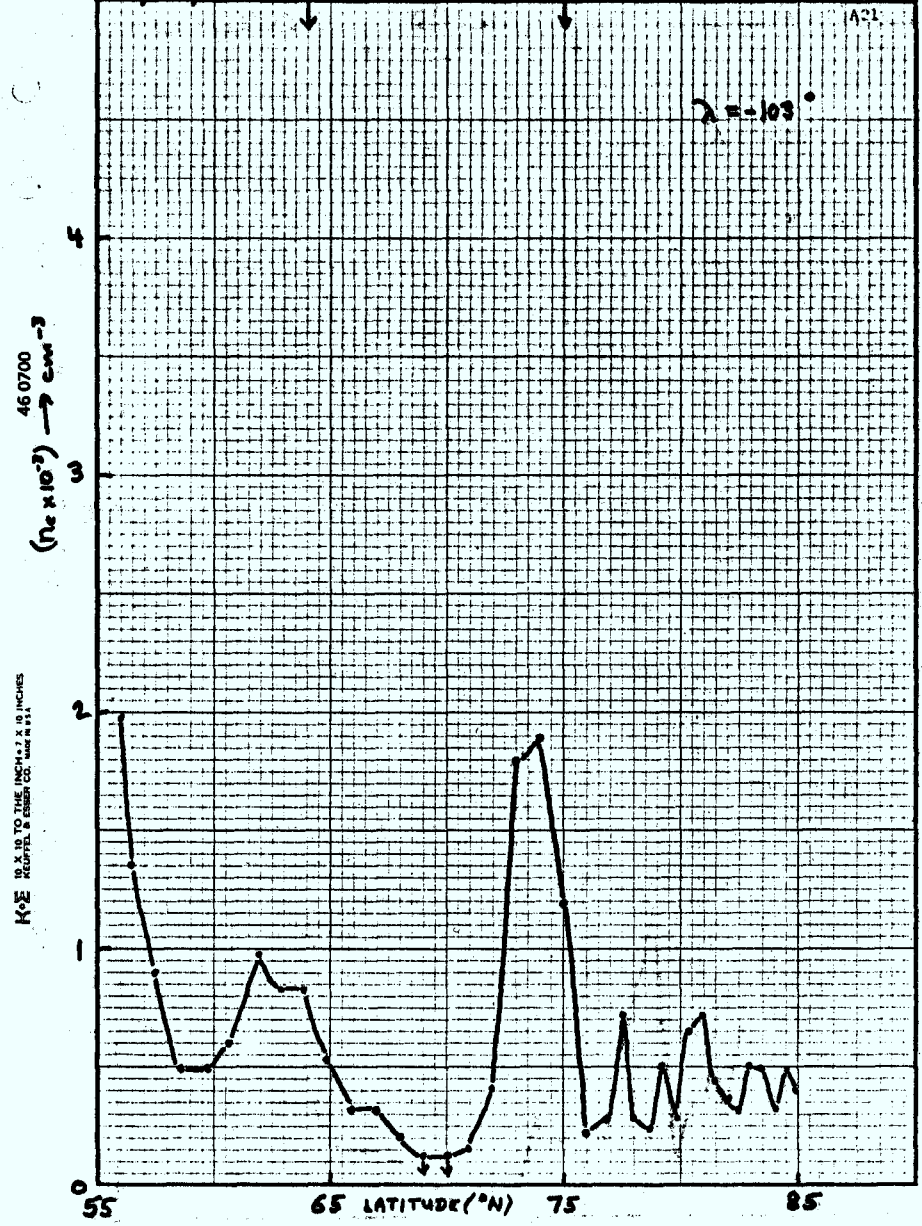
A20



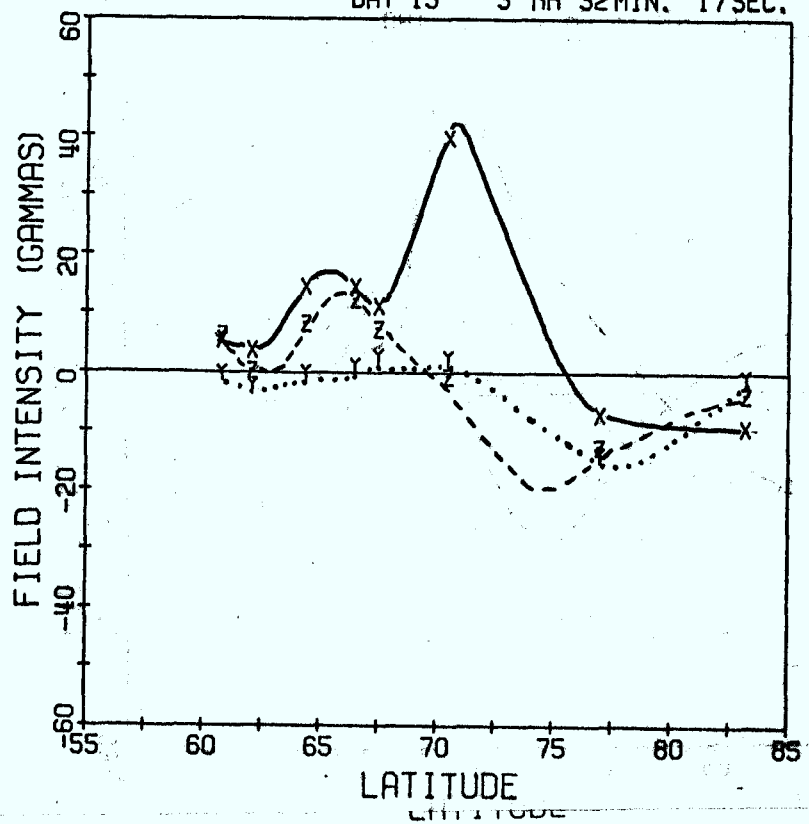
DAY 12 2 HR 58 MIN. 22 SEC.



Day 13, 1972 0327 UT Jan 13 / 1972



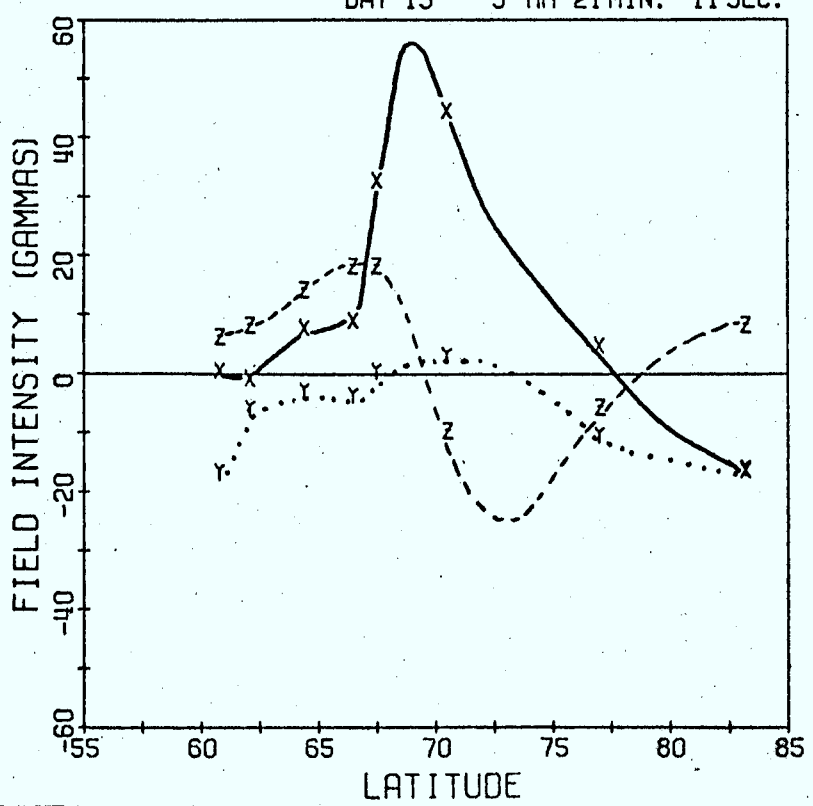
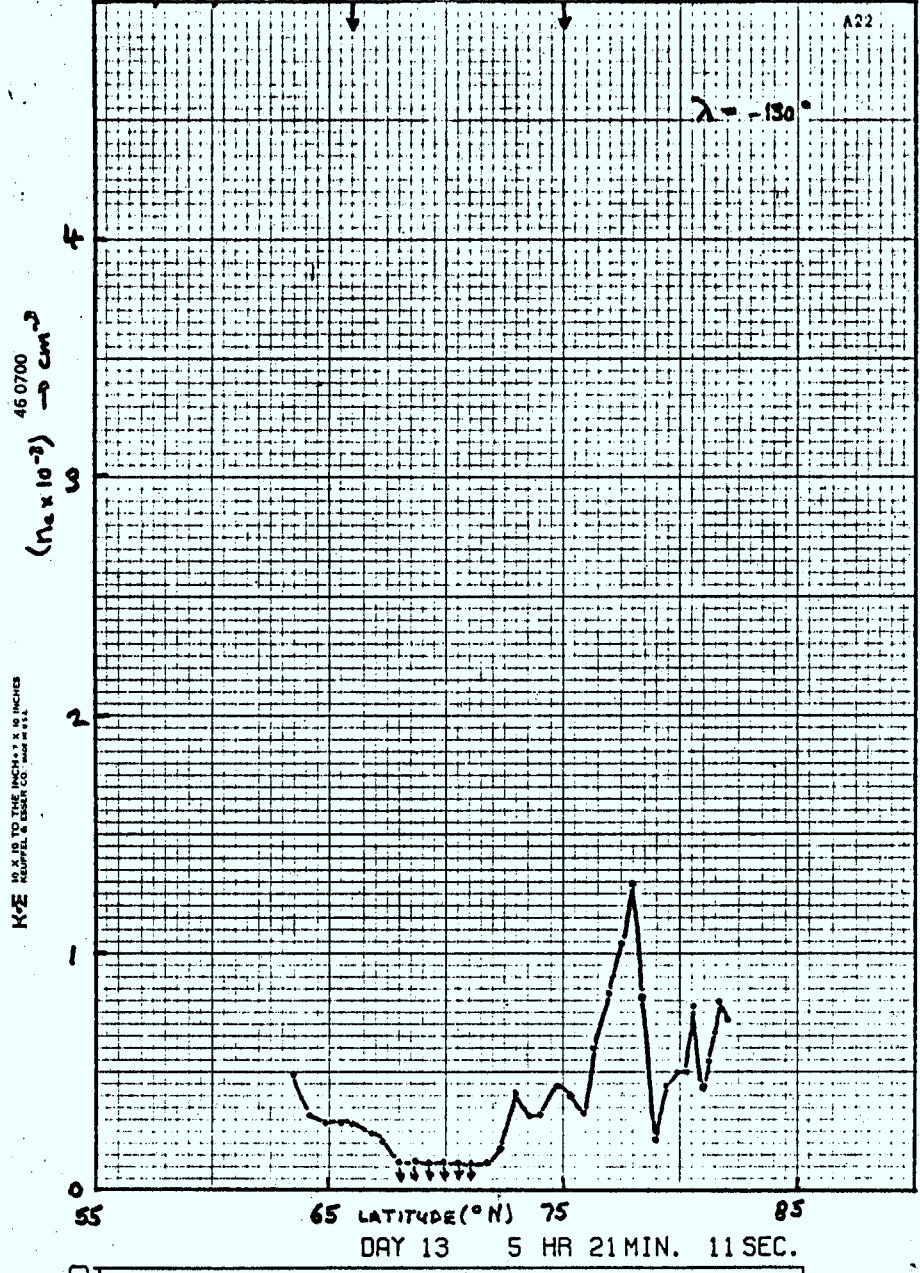
DAY 13 3 HR 32 MIN. 17 SEC.



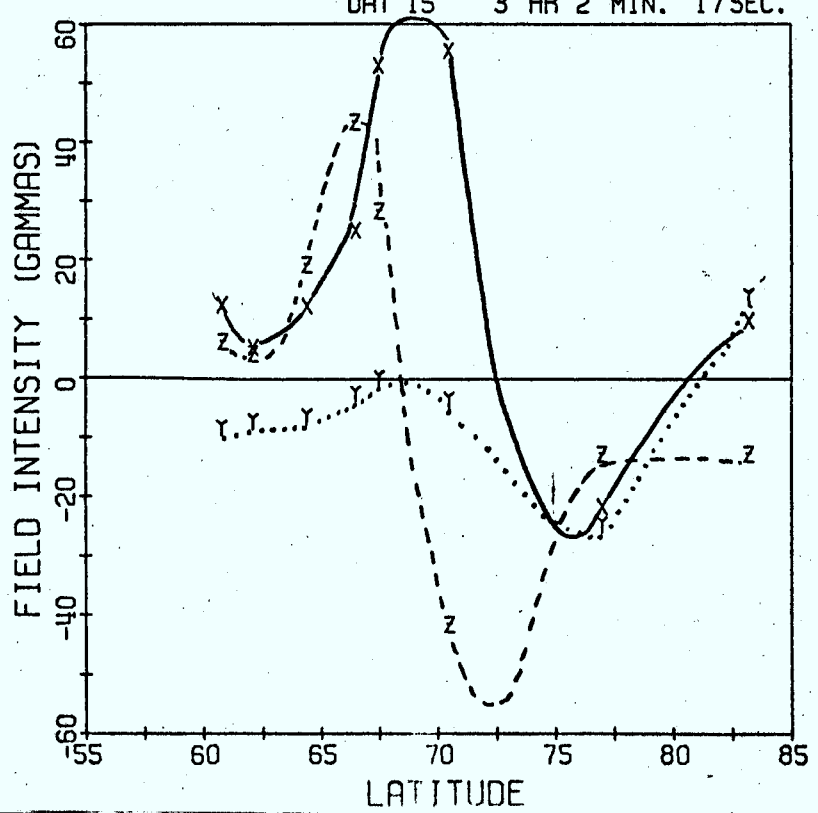
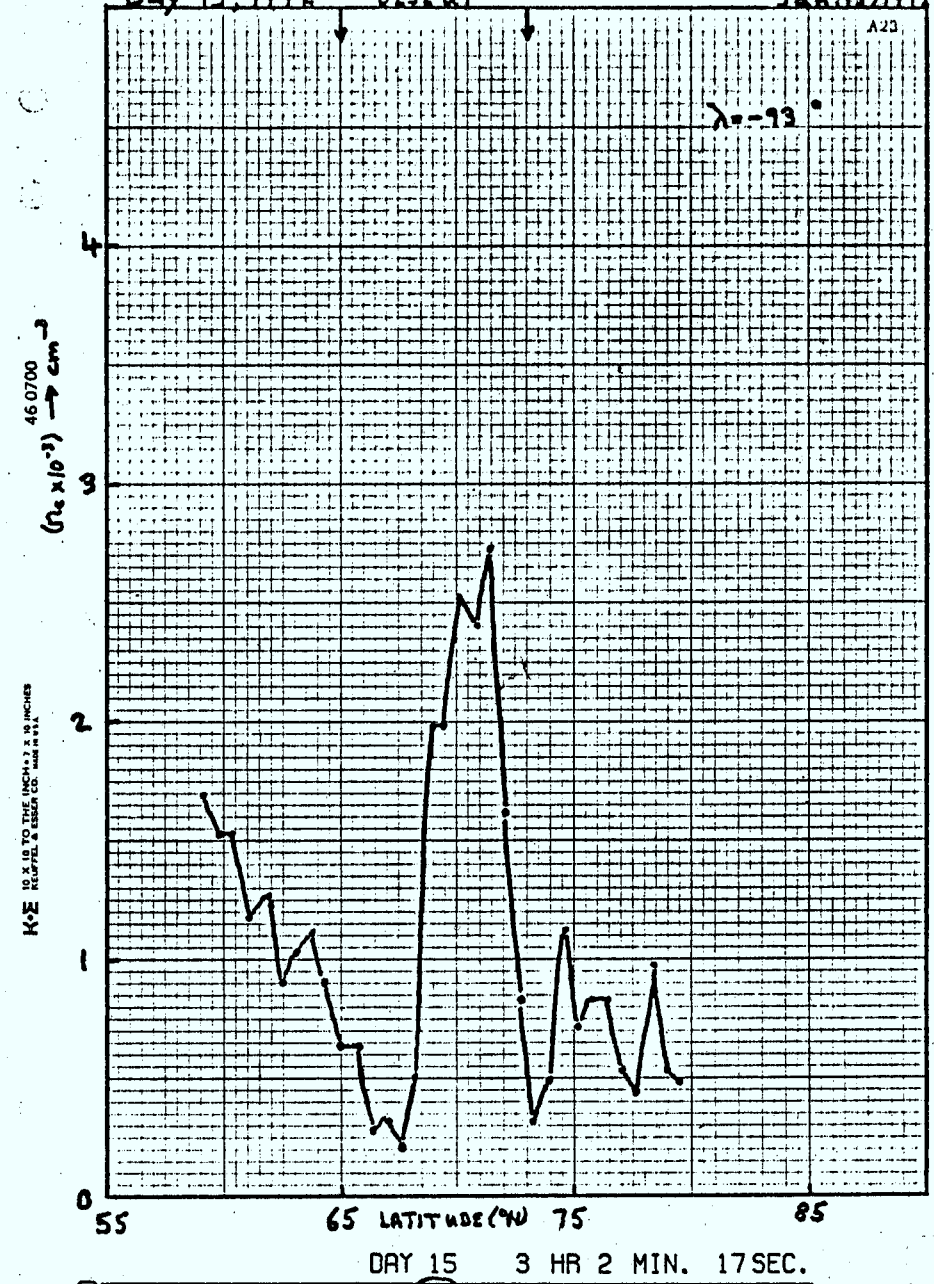
Day 13, 1972

0519 UT

Jan. 13 / 1972



Day 15, 1972 0252 UT Jan 15/1972

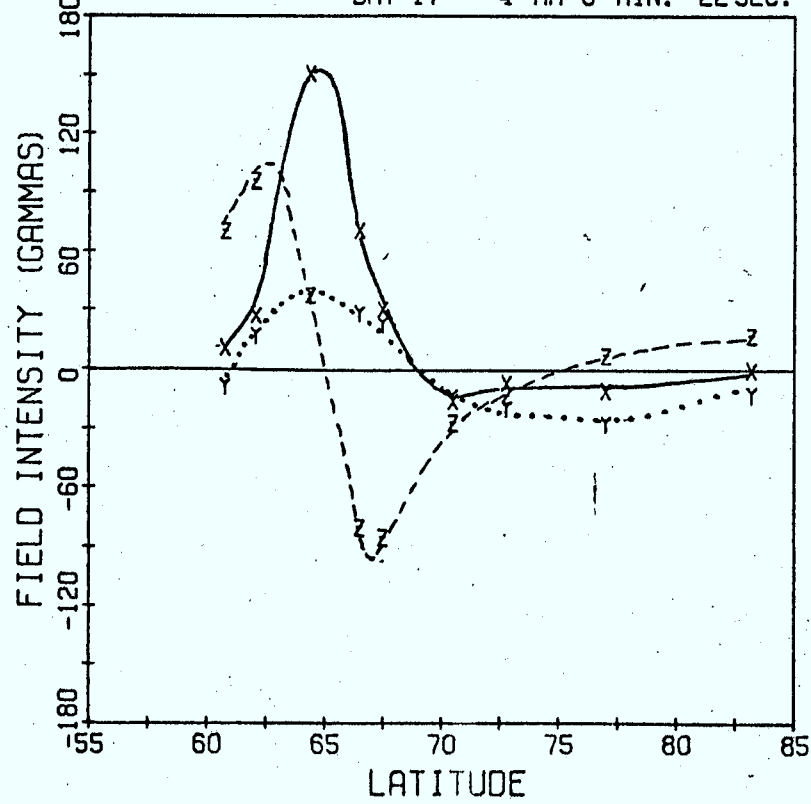
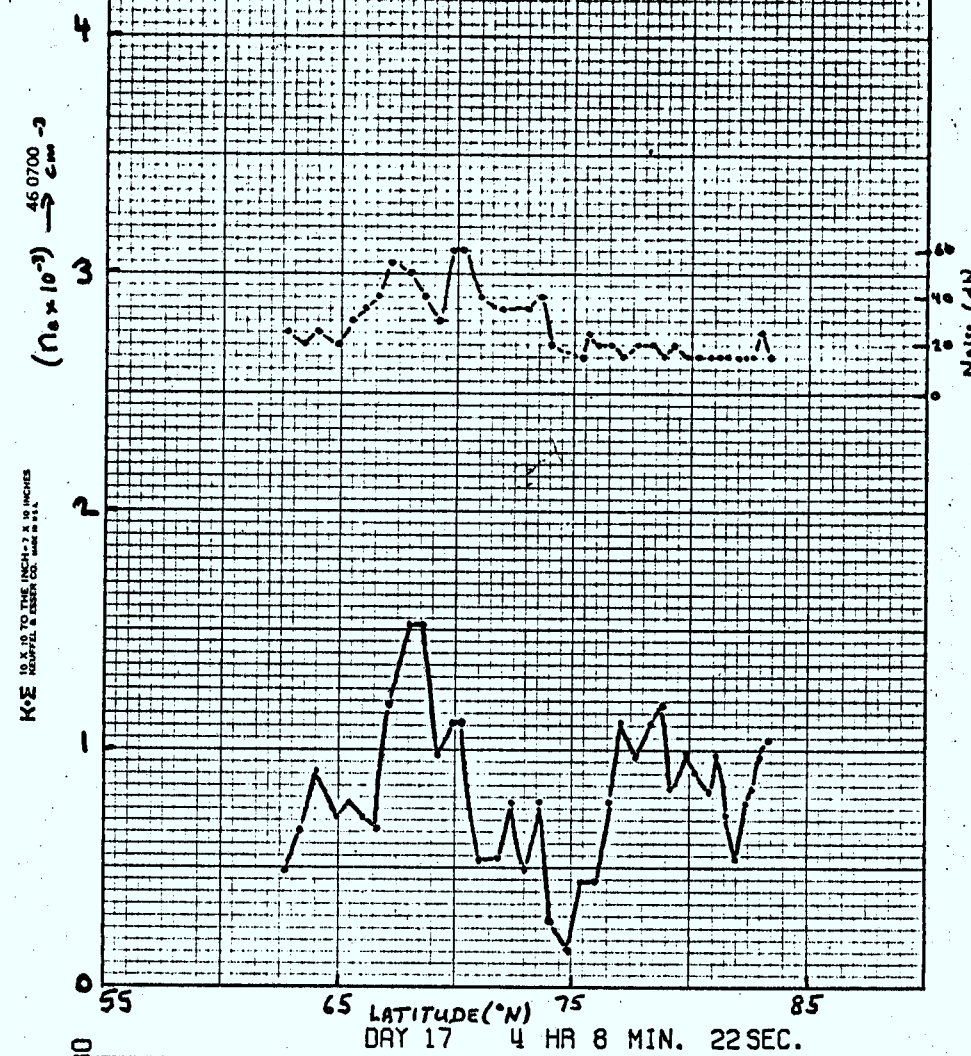


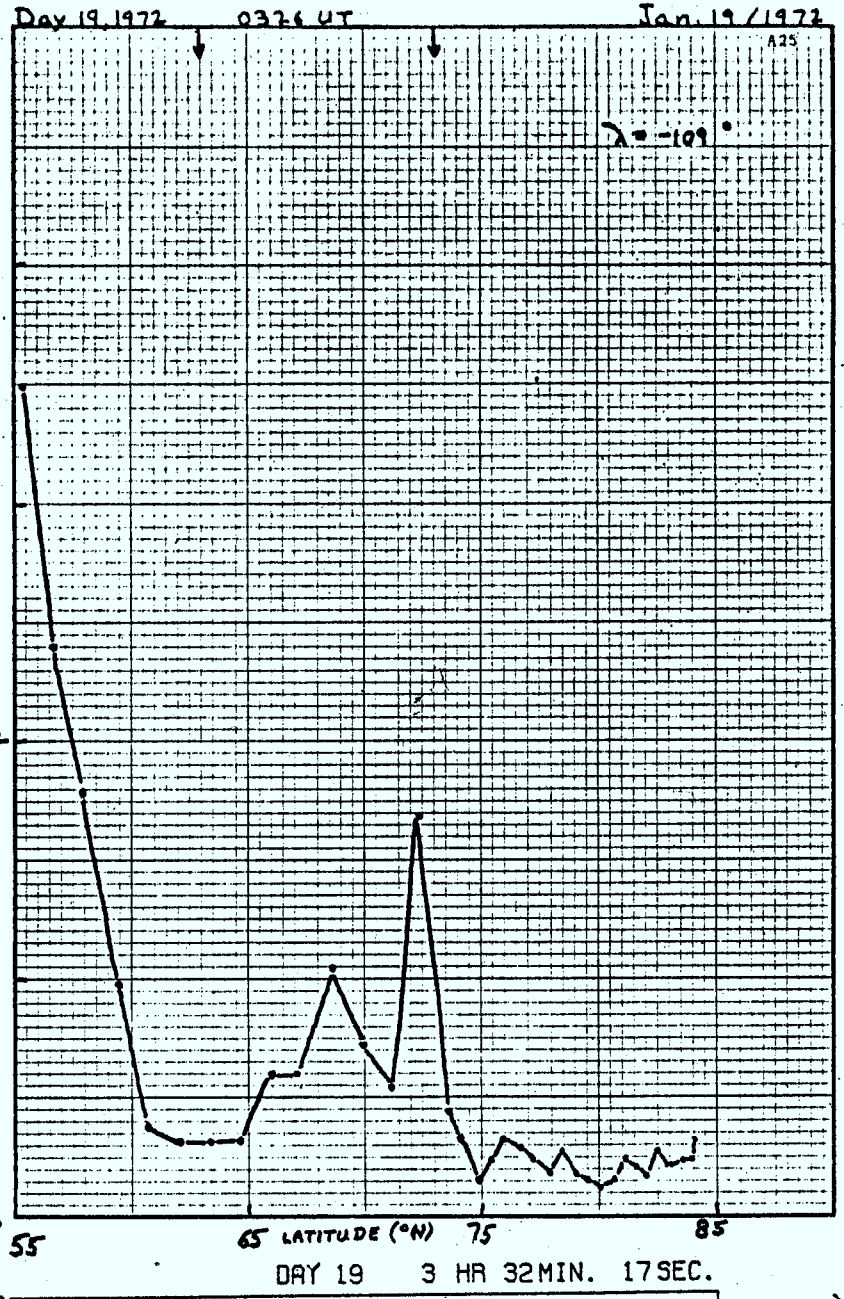
Day 17, 1972

0403 UT

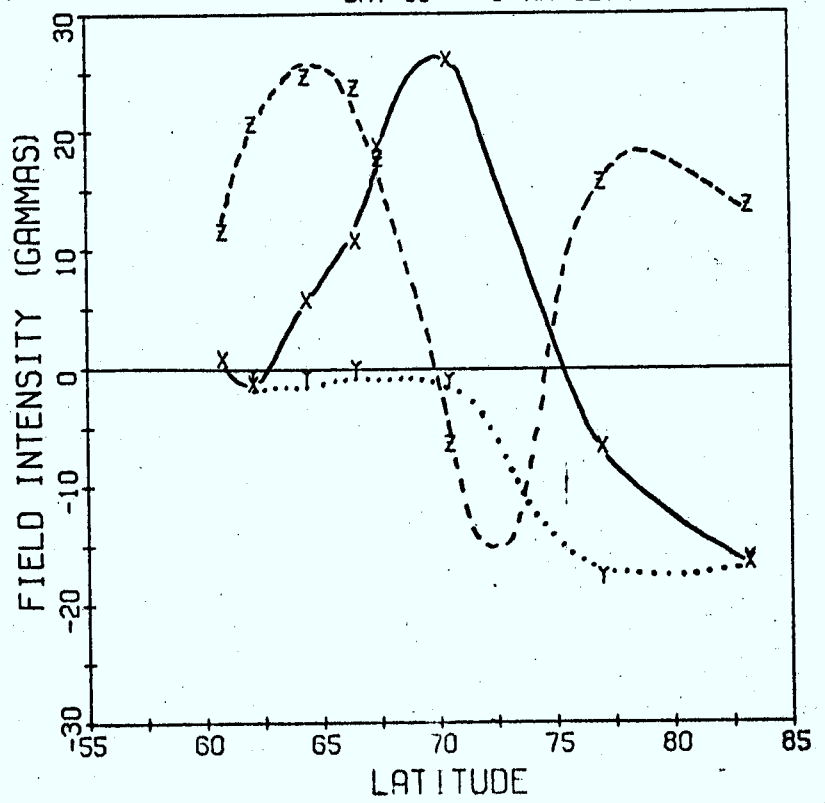
Jan. 17/1972

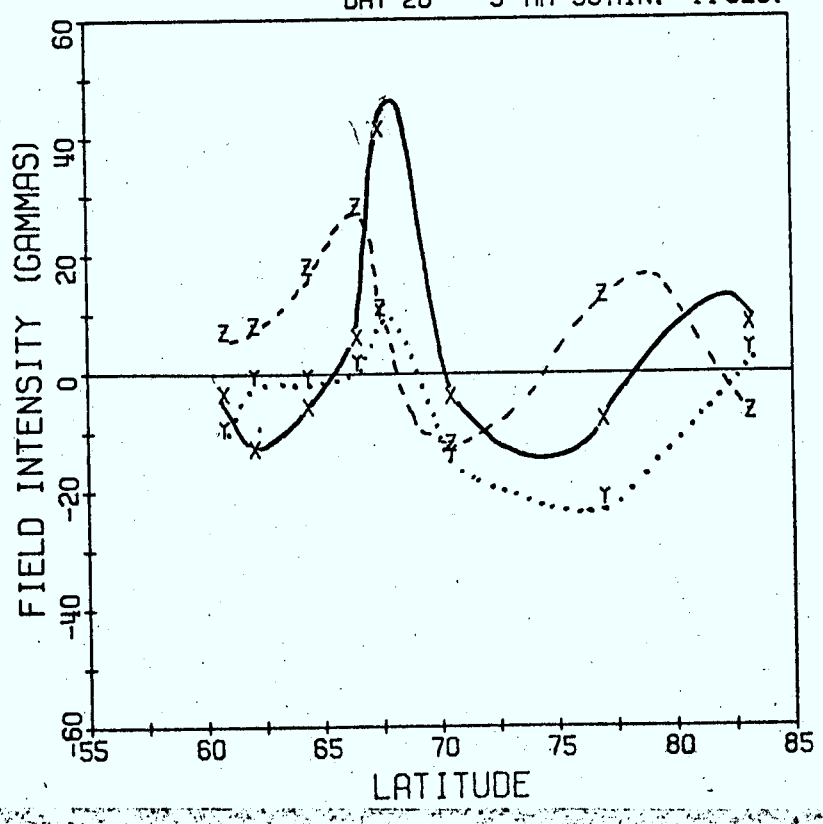
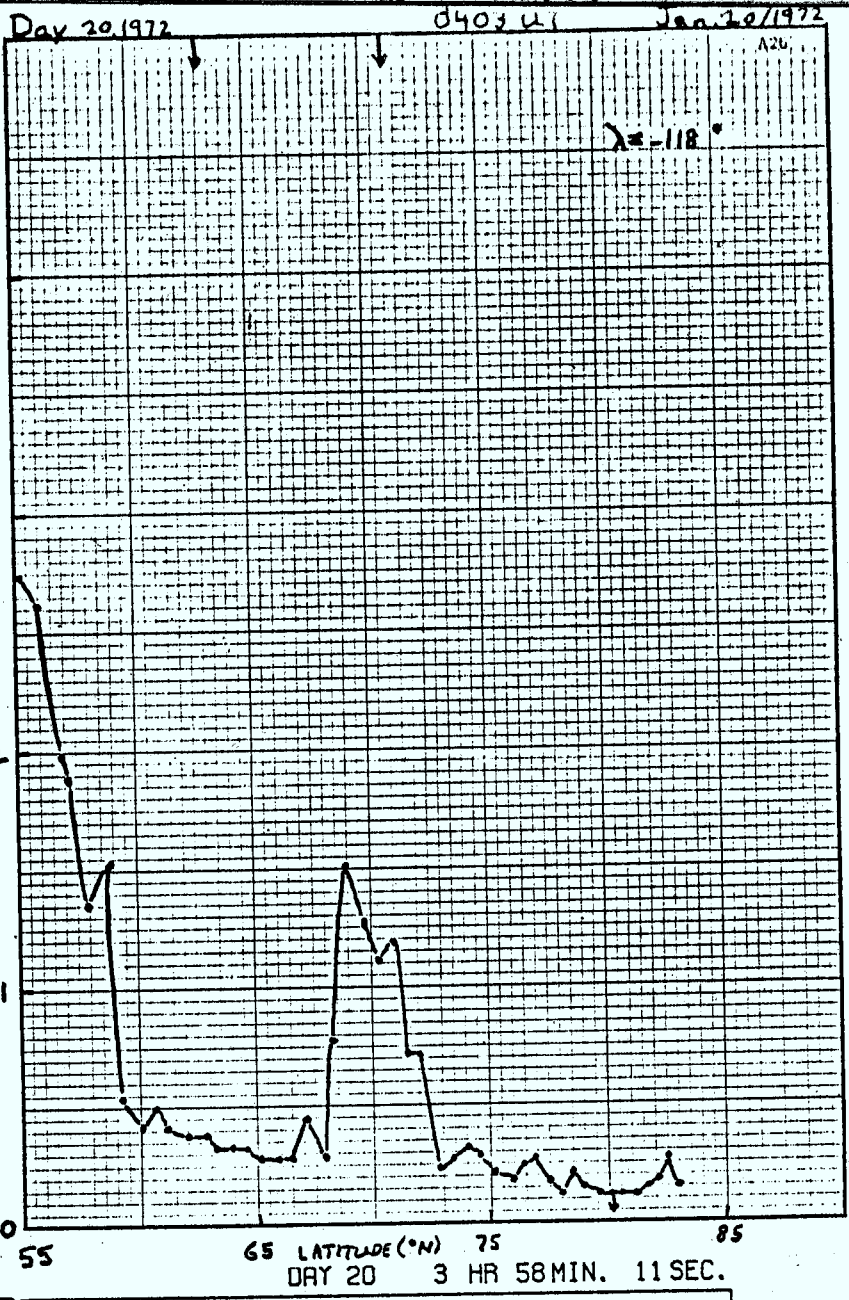
A24

 $\lambda = 115^\circ$ 

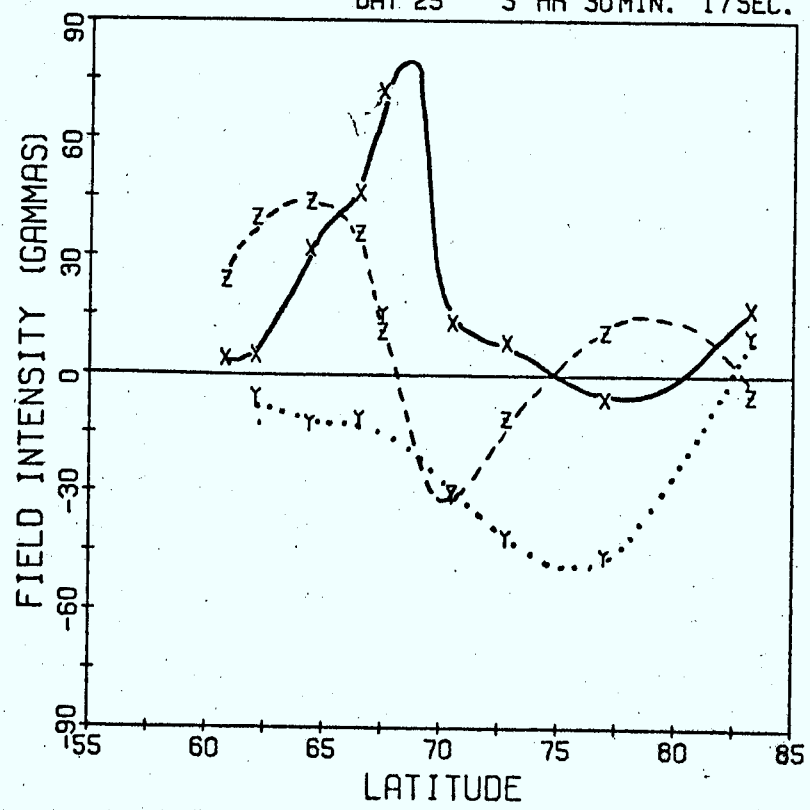
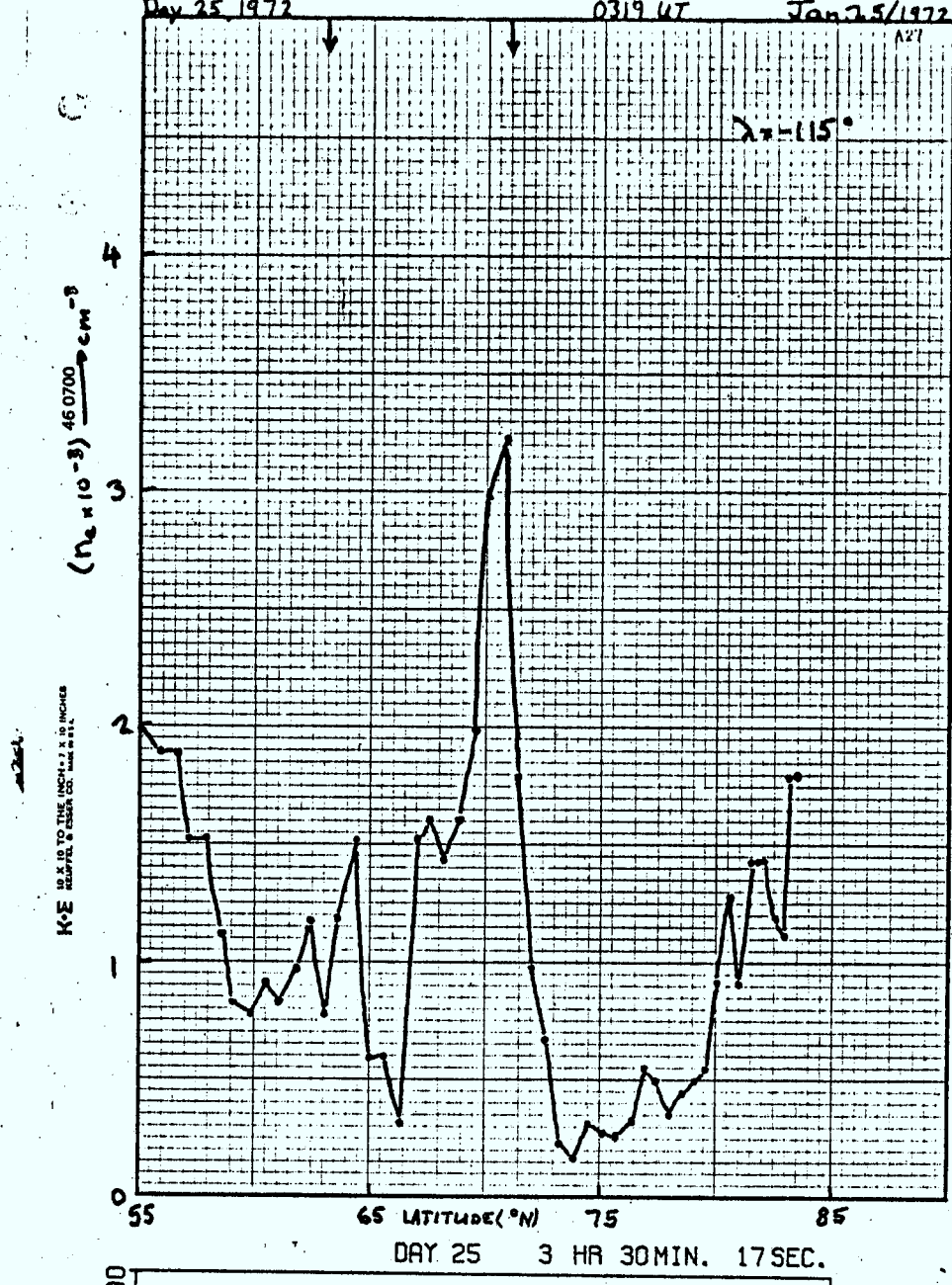


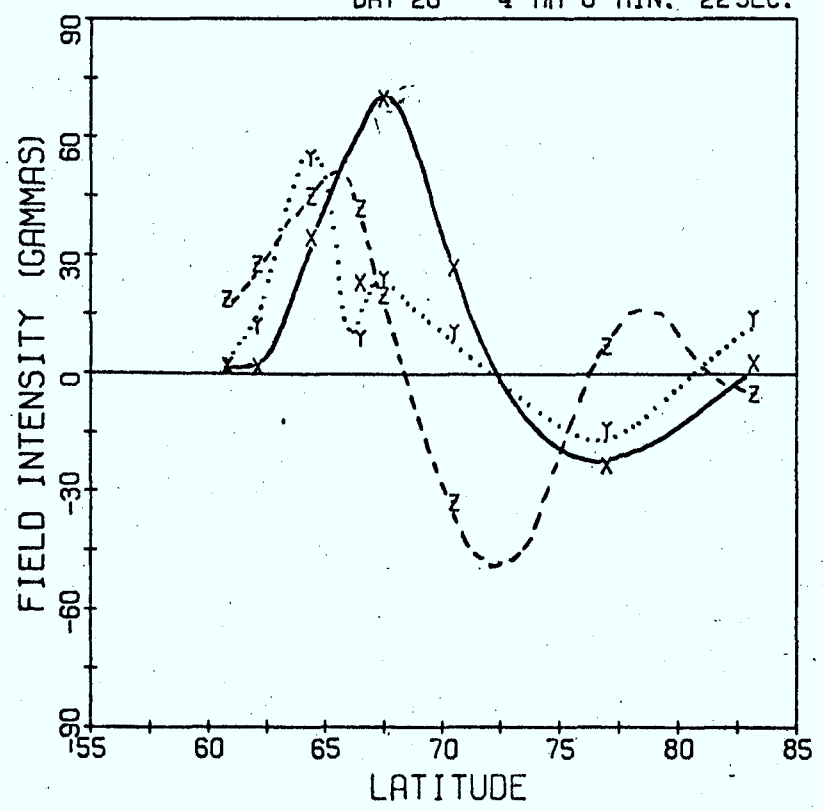
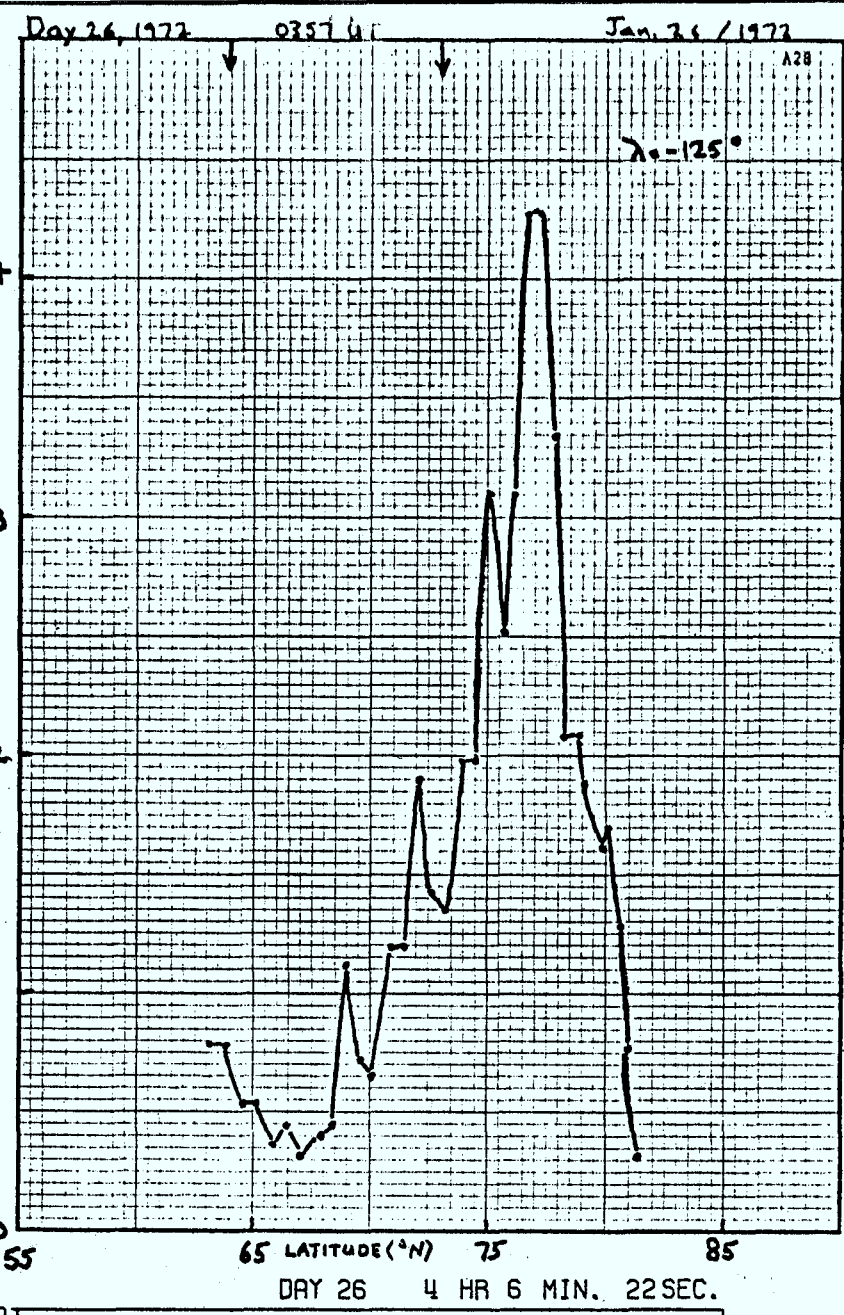
DAY 19 3 HR 32MIN. 17SEC.

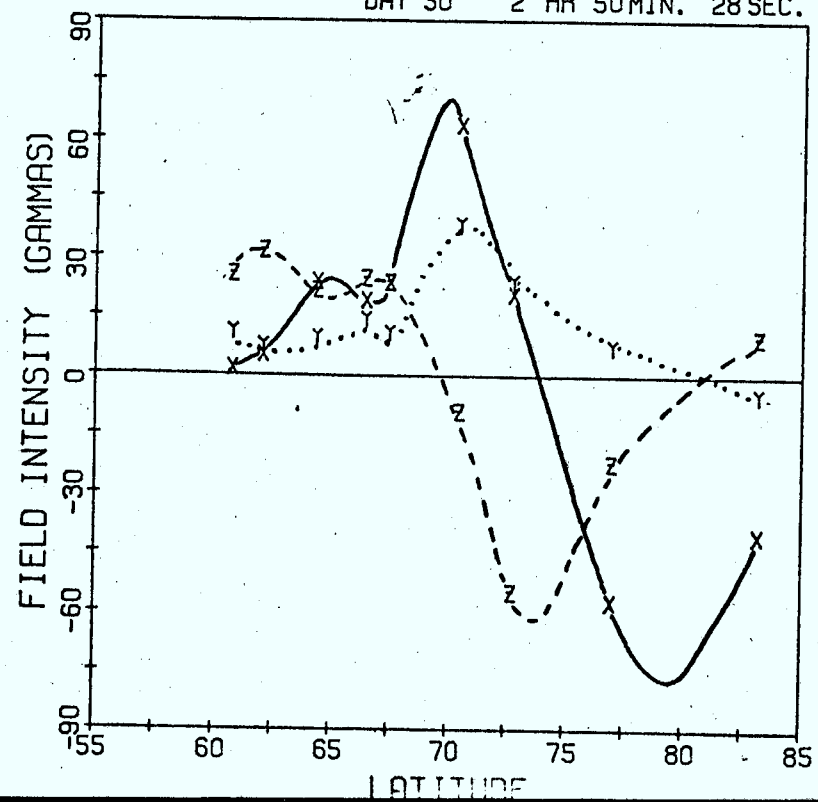
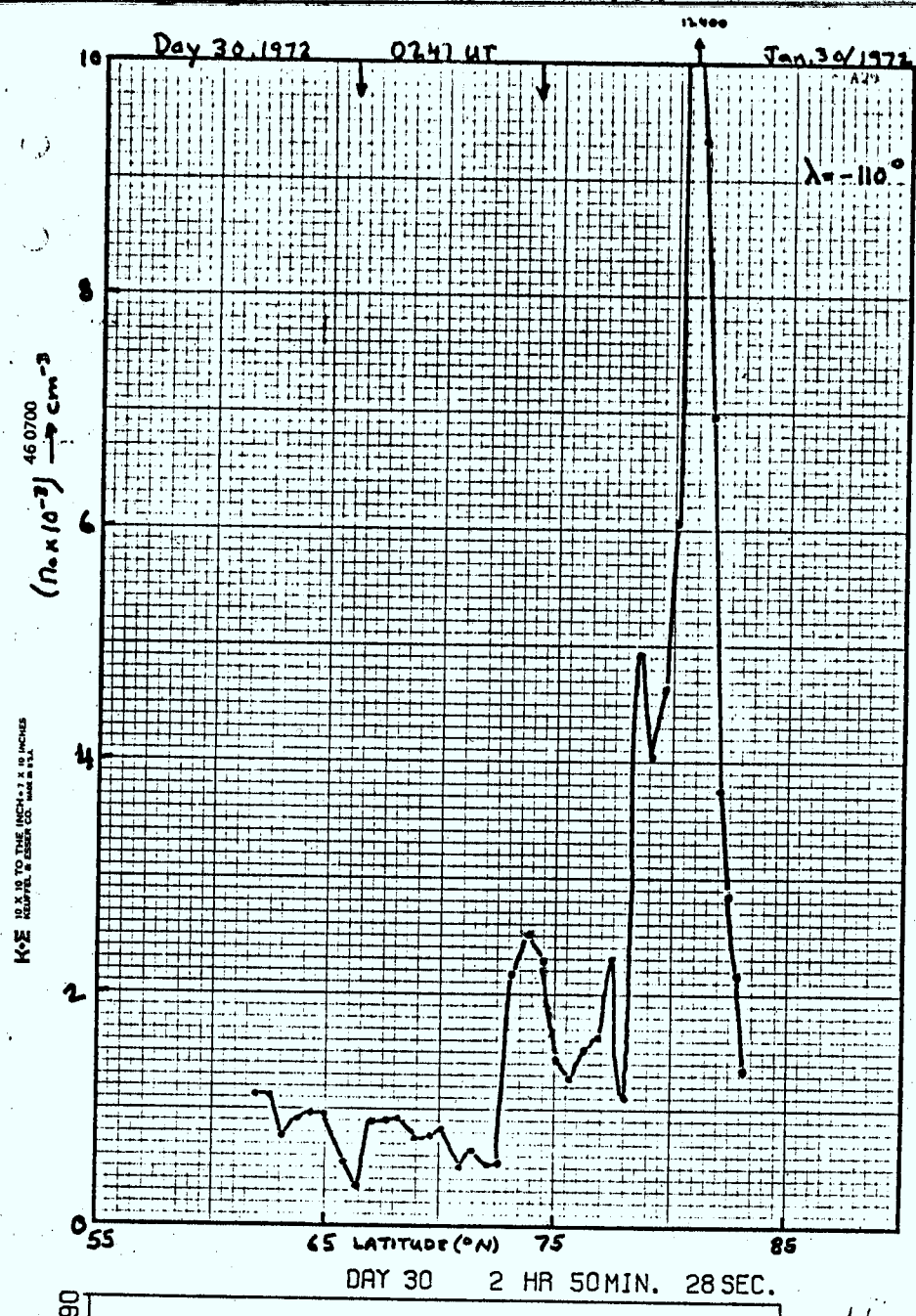




Day 25 1972 0319 UT Jan 25/1972



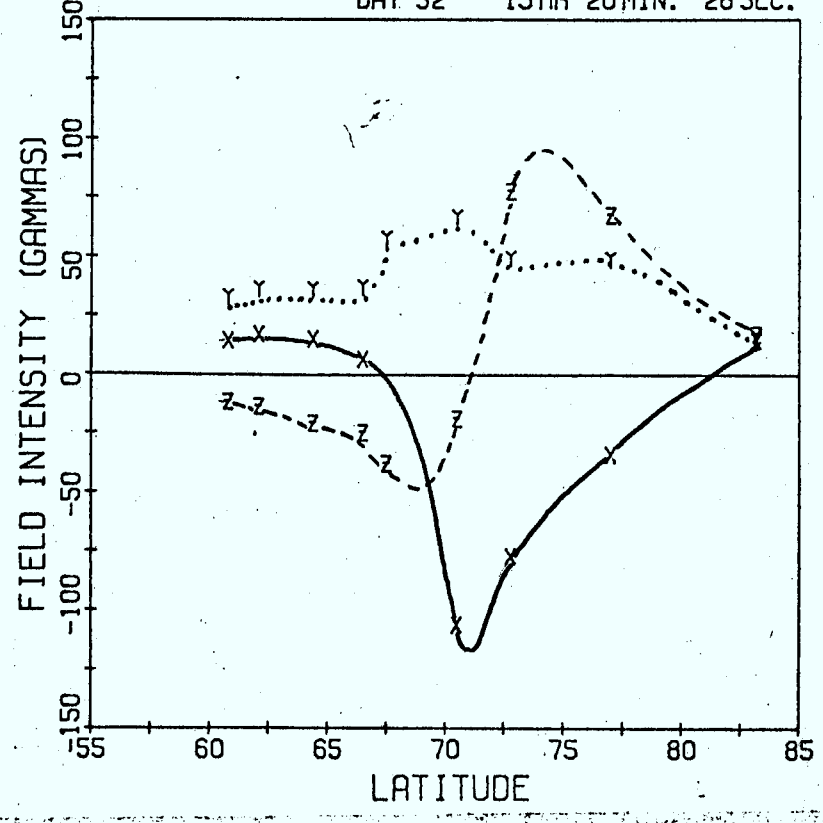
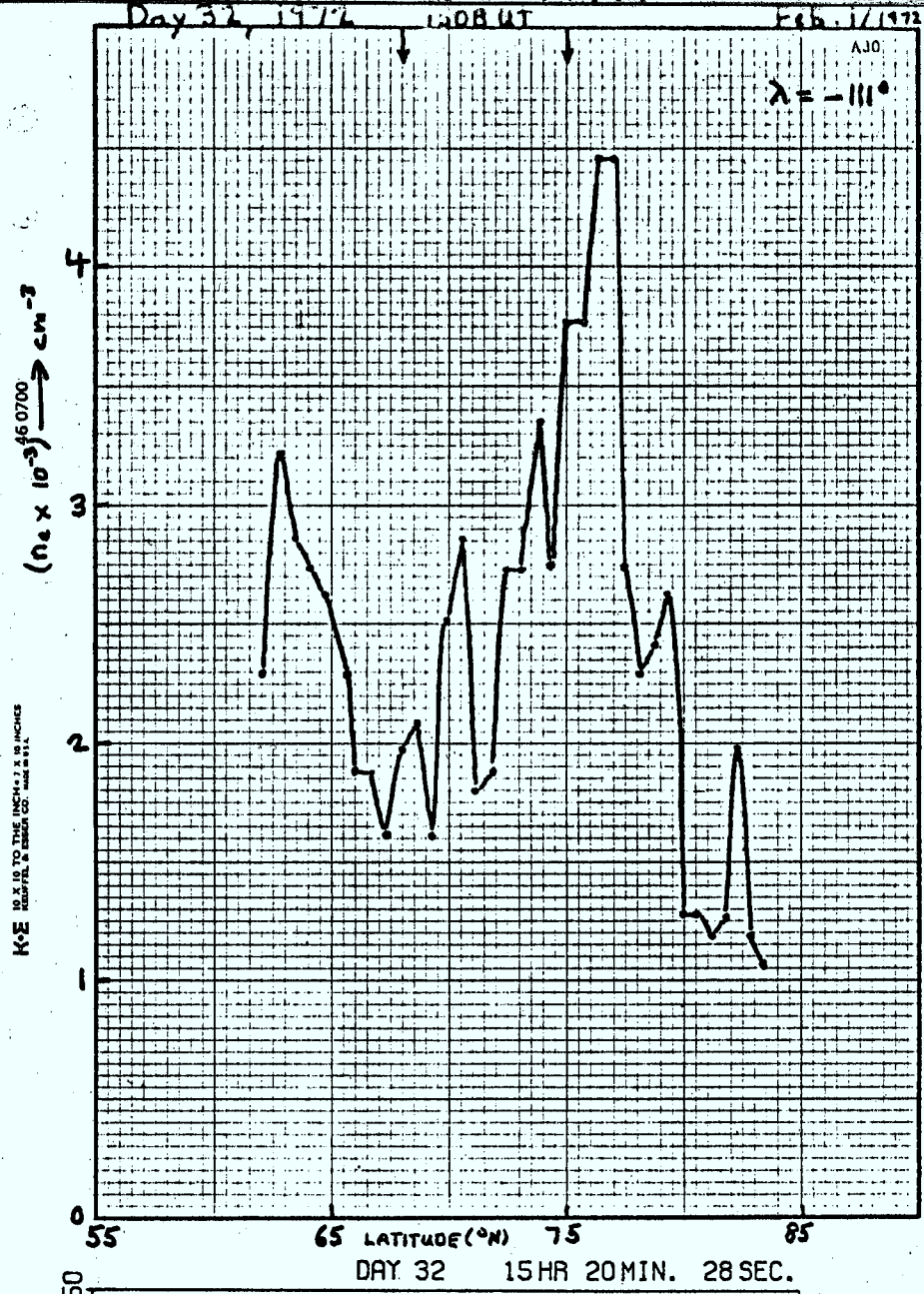




Day 32, 1972 WDB UT Feb. 1, 1972

AJO

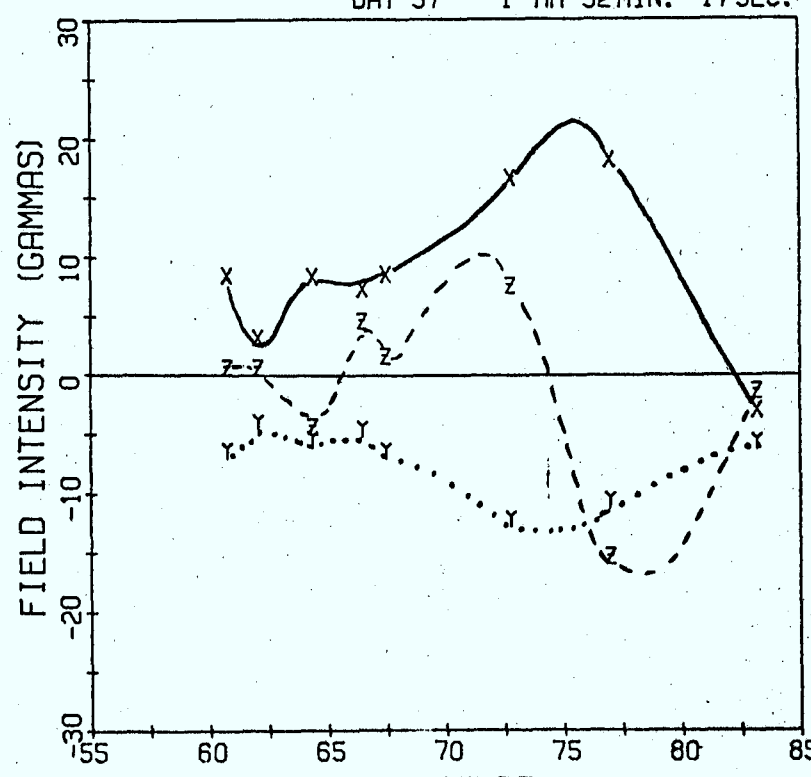
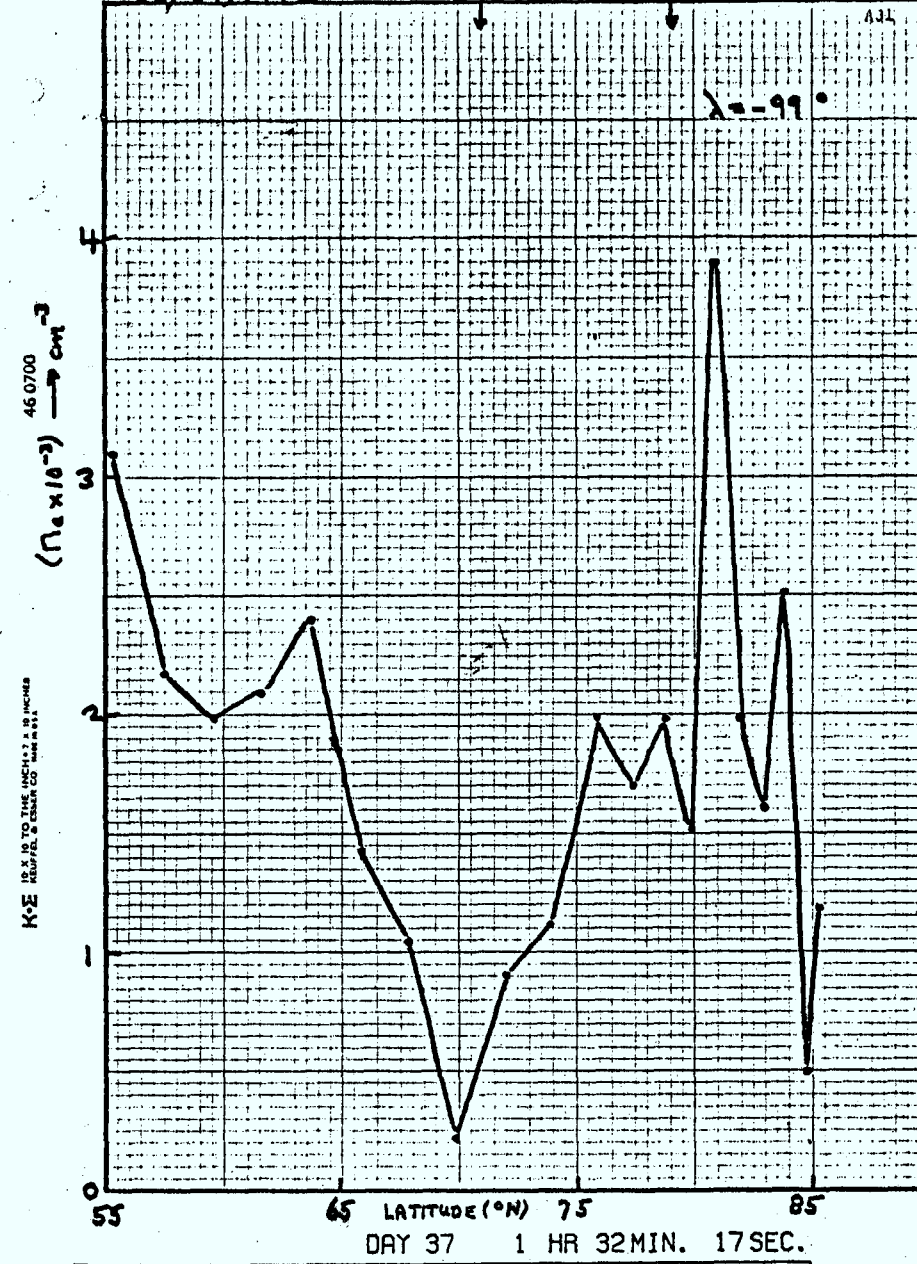
$\lambda = -111^\circ$



Day 37, 1972

0139 UT

Feb. 6/1972



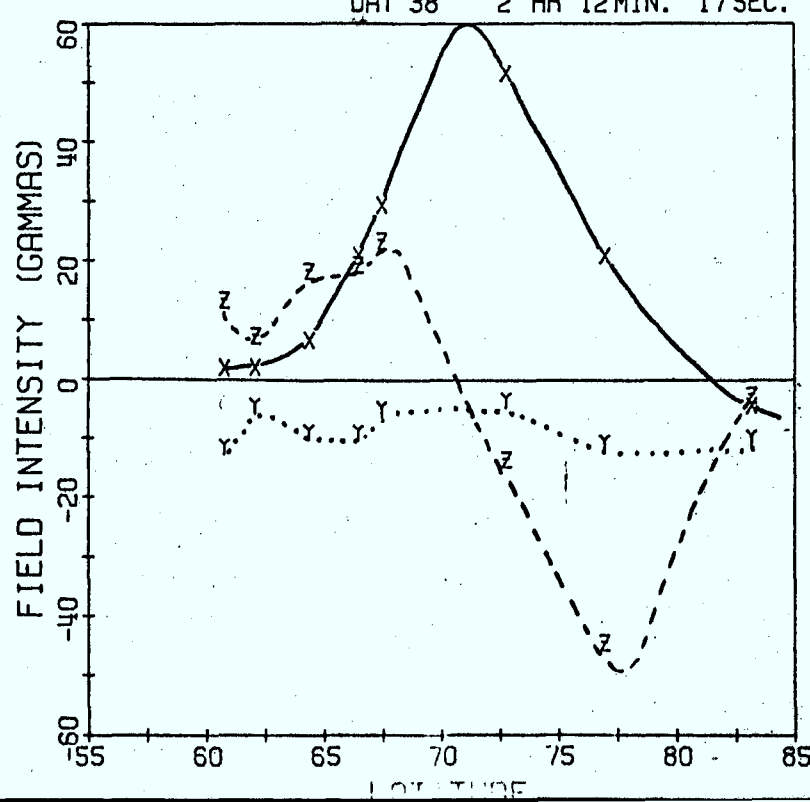
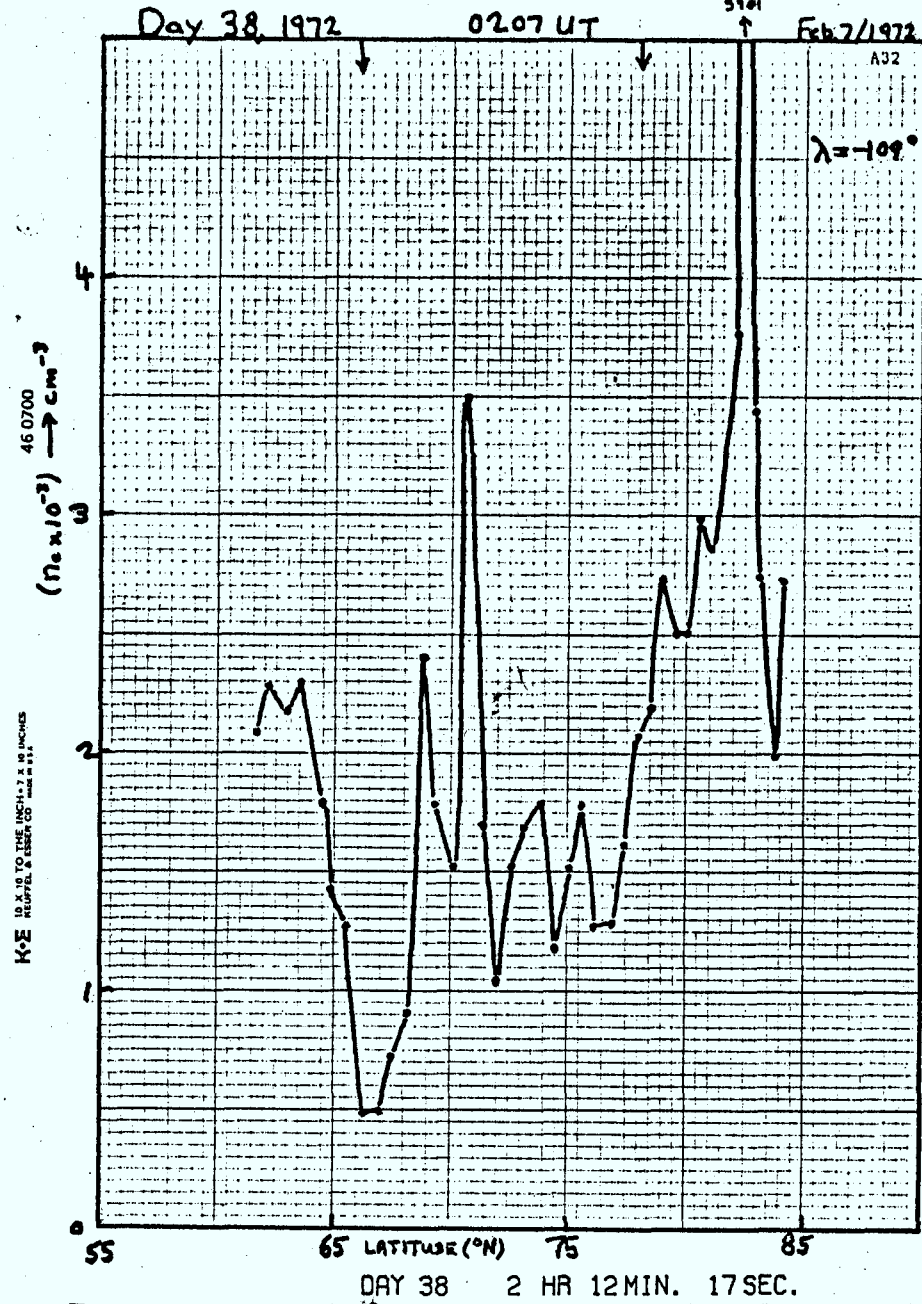
Day 38, 1972

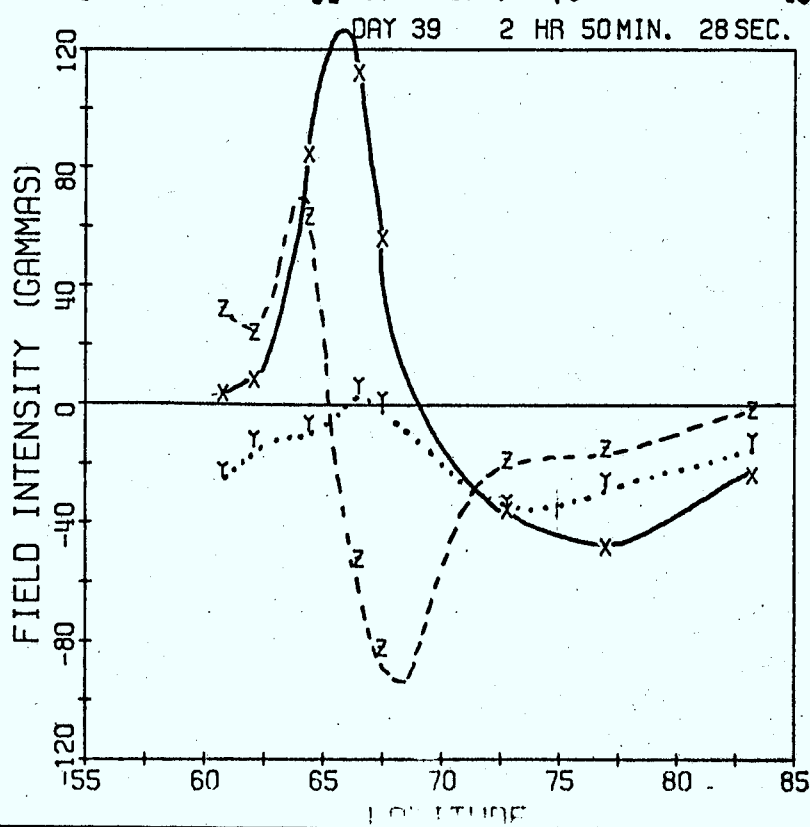
0207 UT

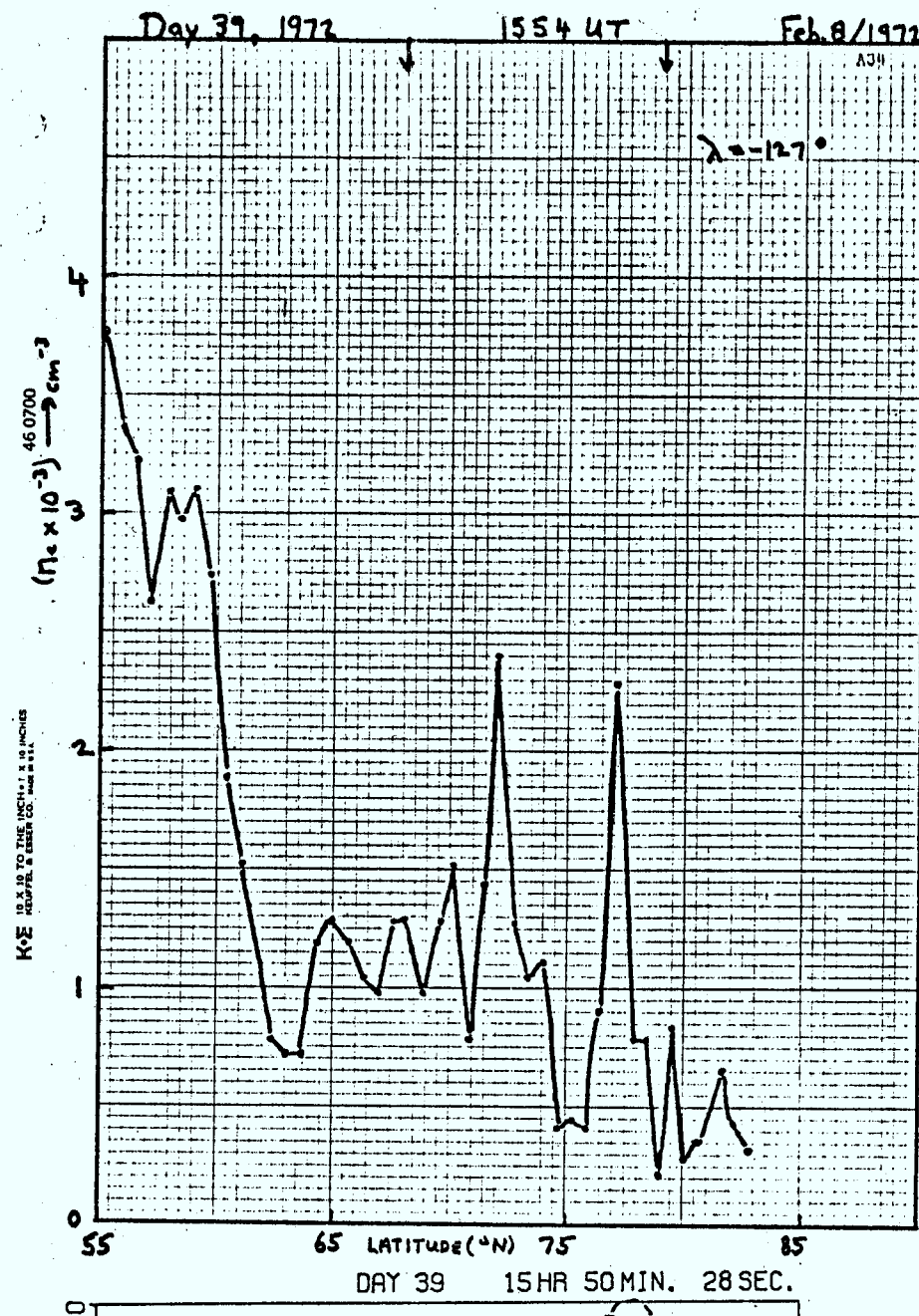
↑ Feb 7/1972

A32

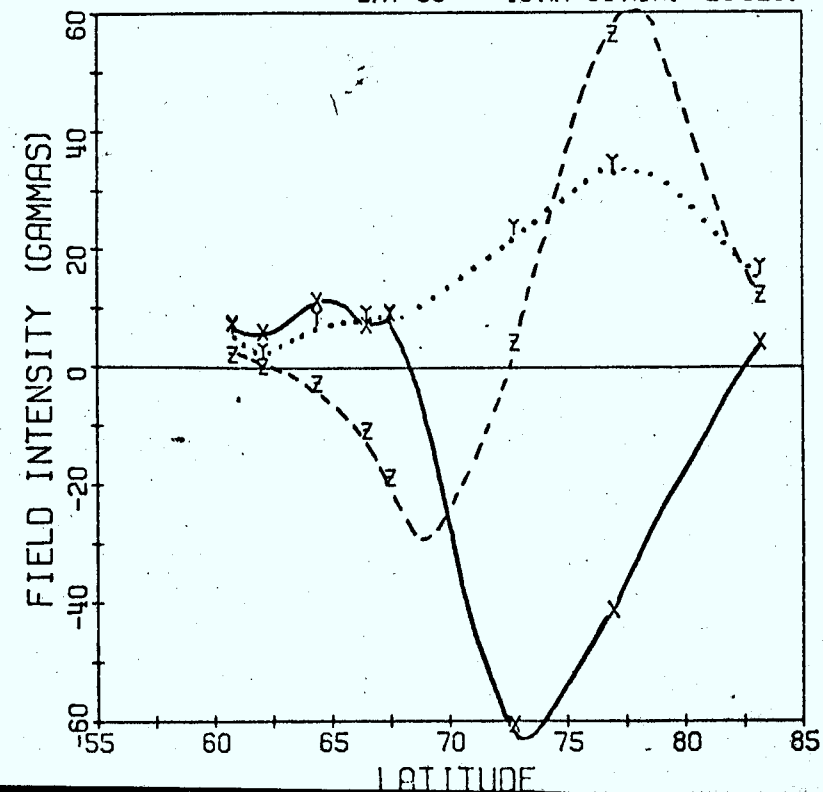
$\lambda = -102^\circ$

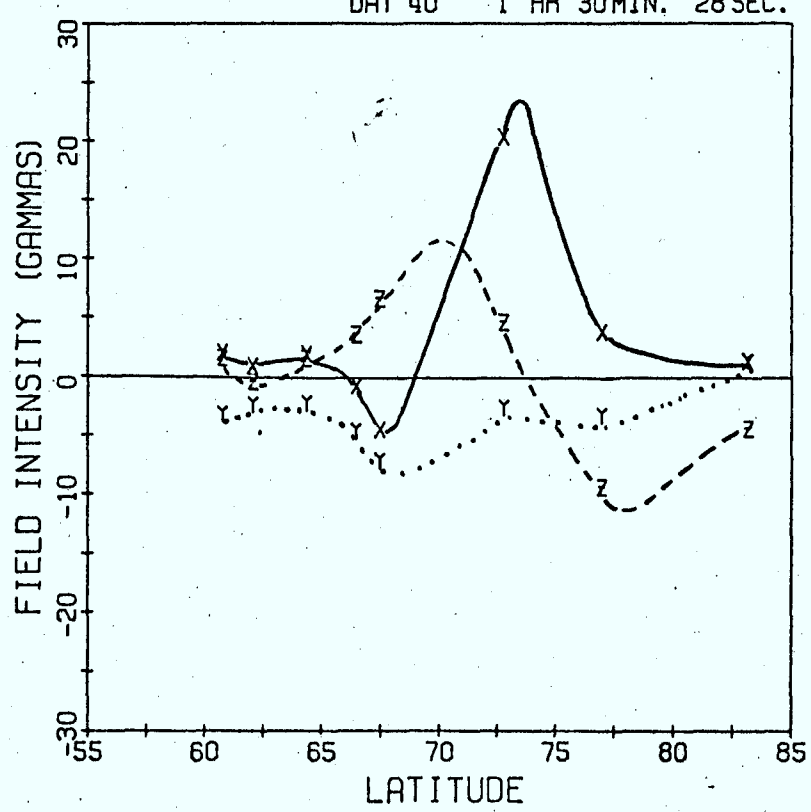
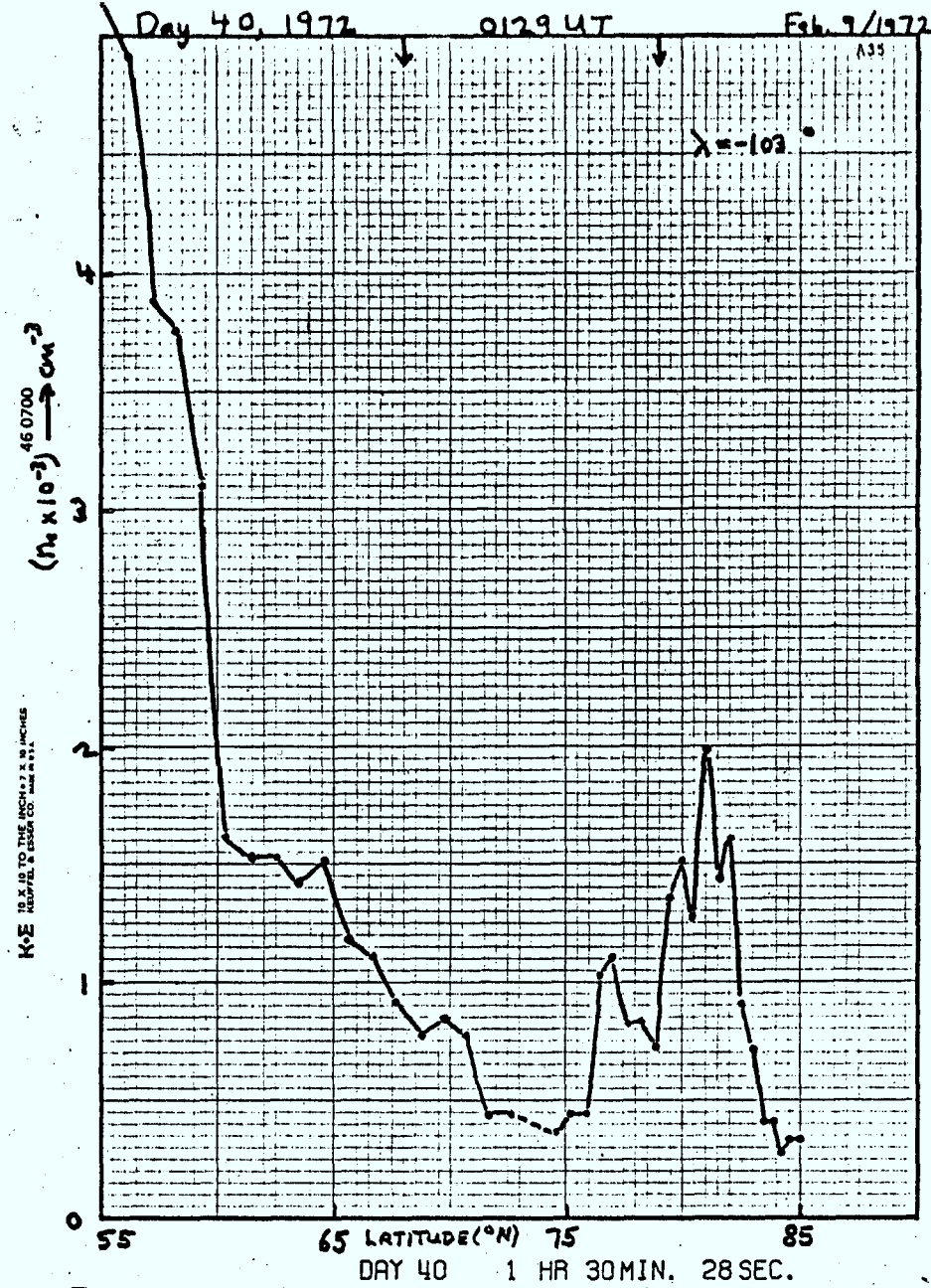


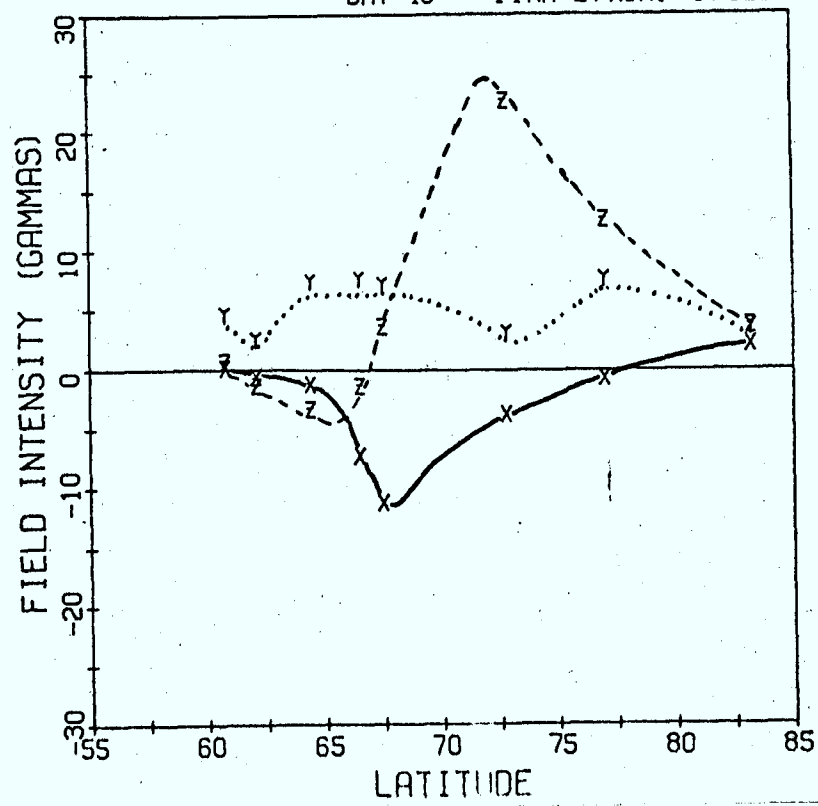
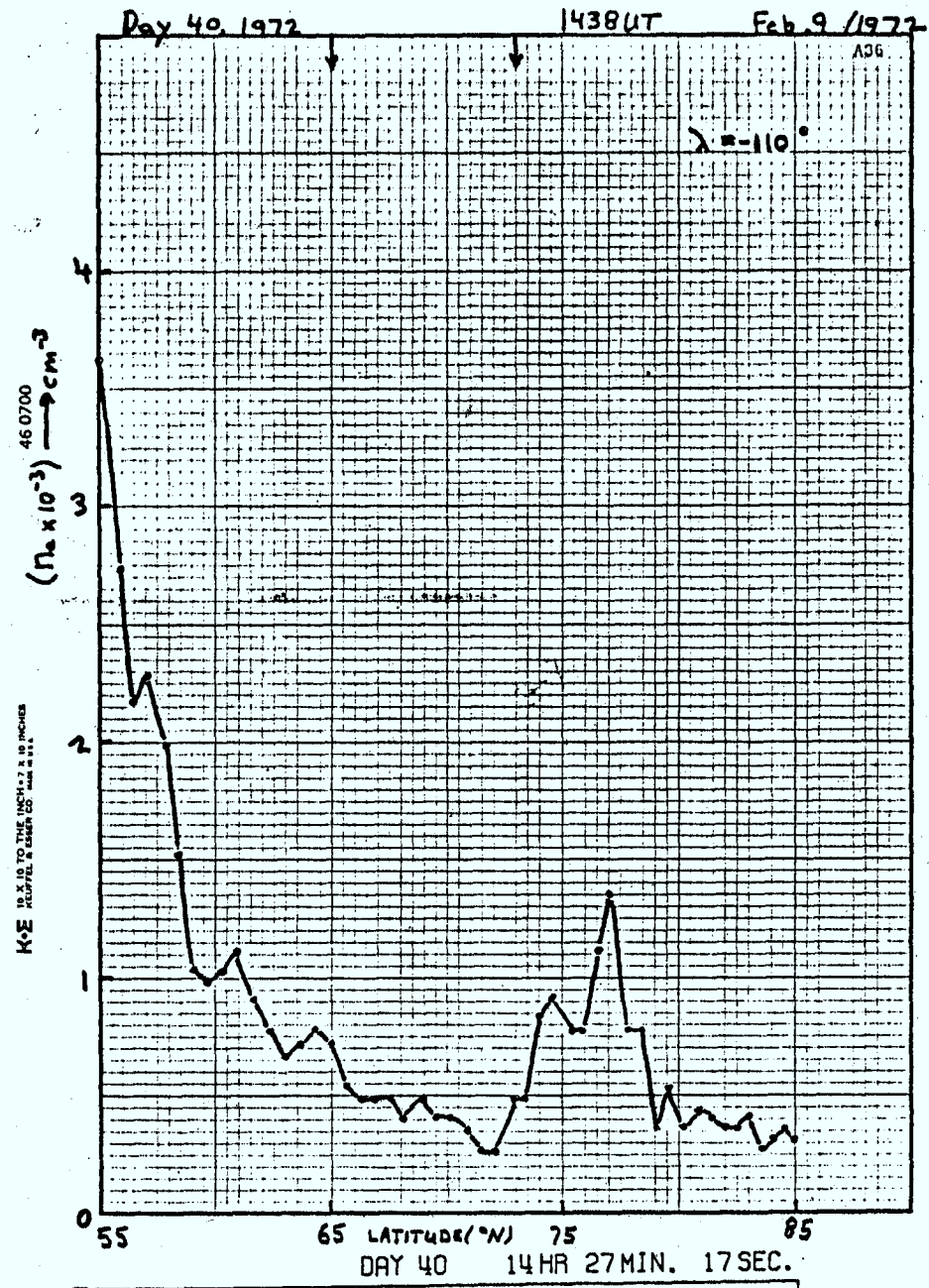




DAY 39 15HR 50 MIN. 28 SEC.





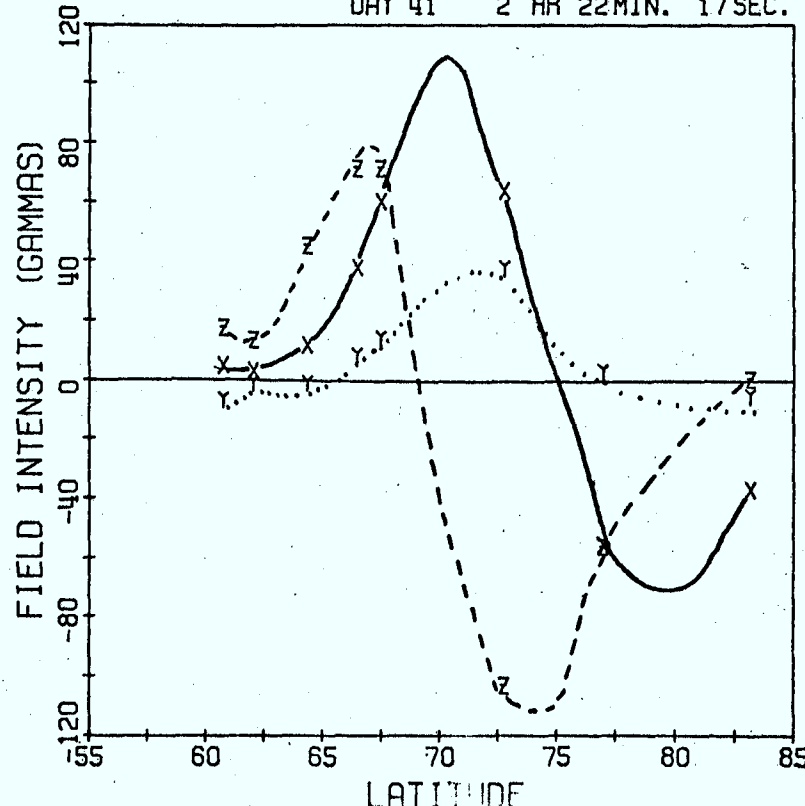
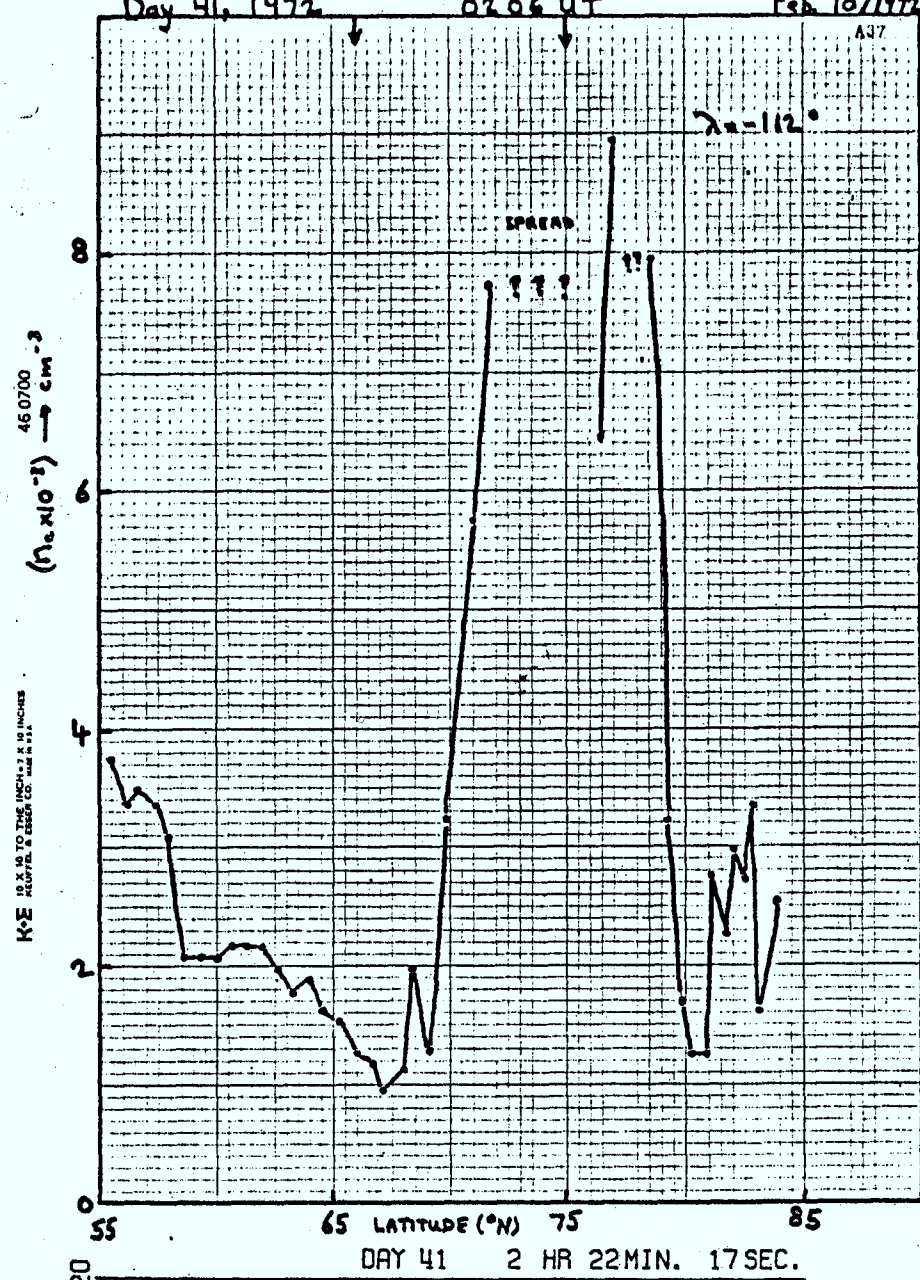


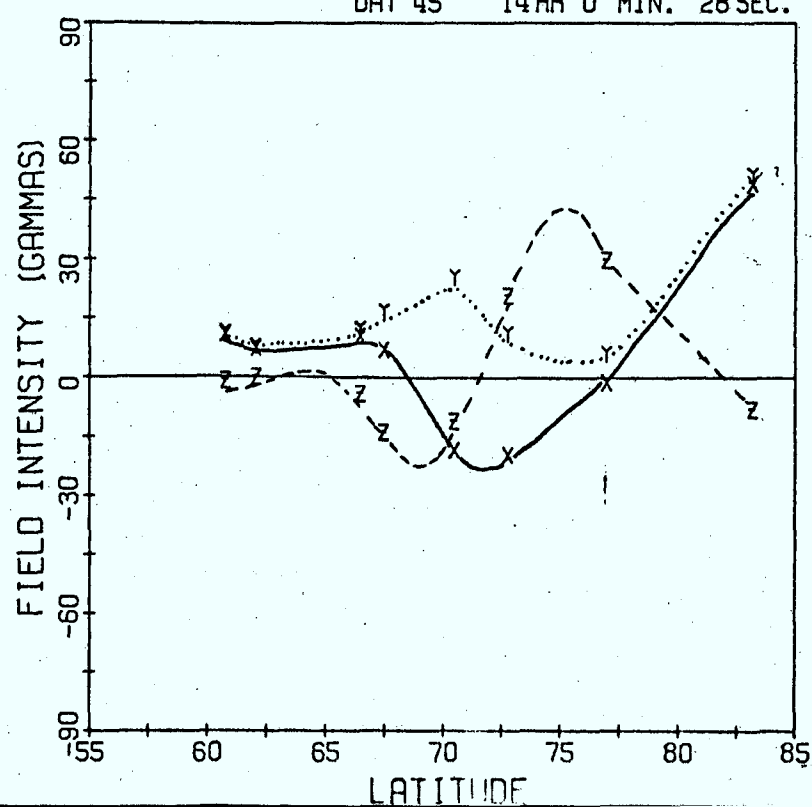
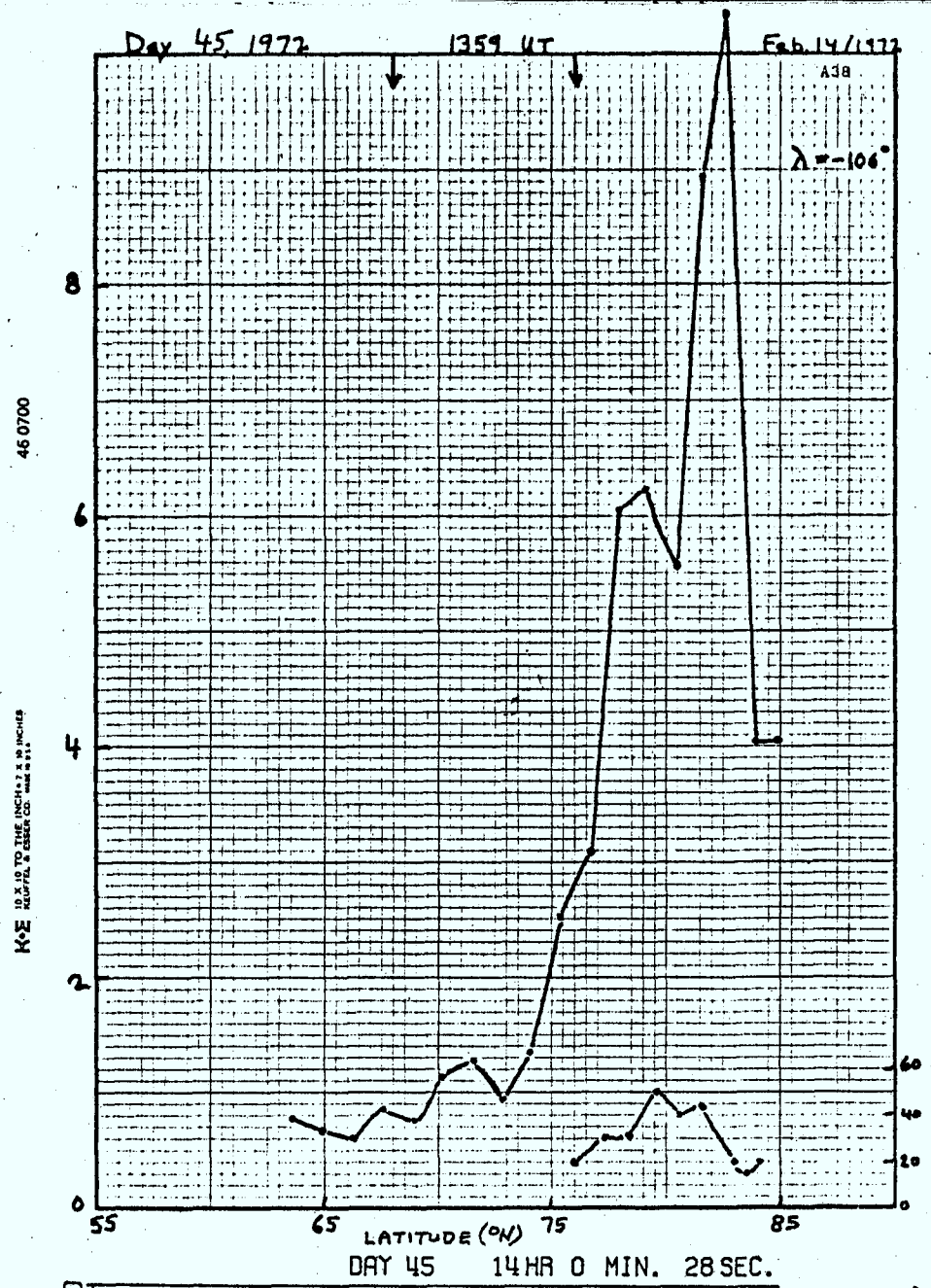
Day 41, 1972

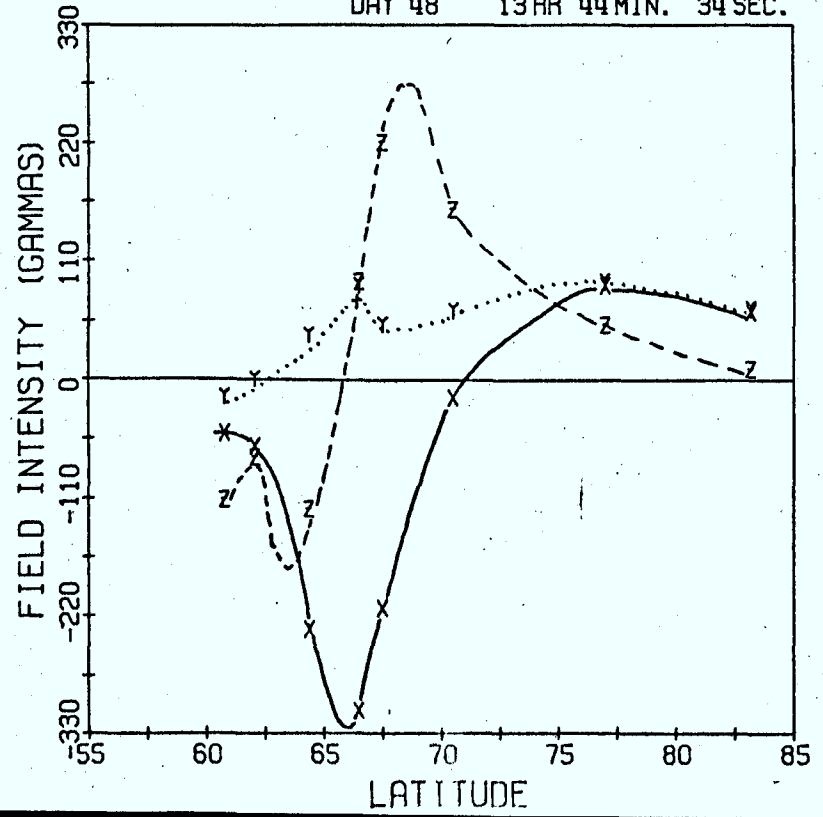
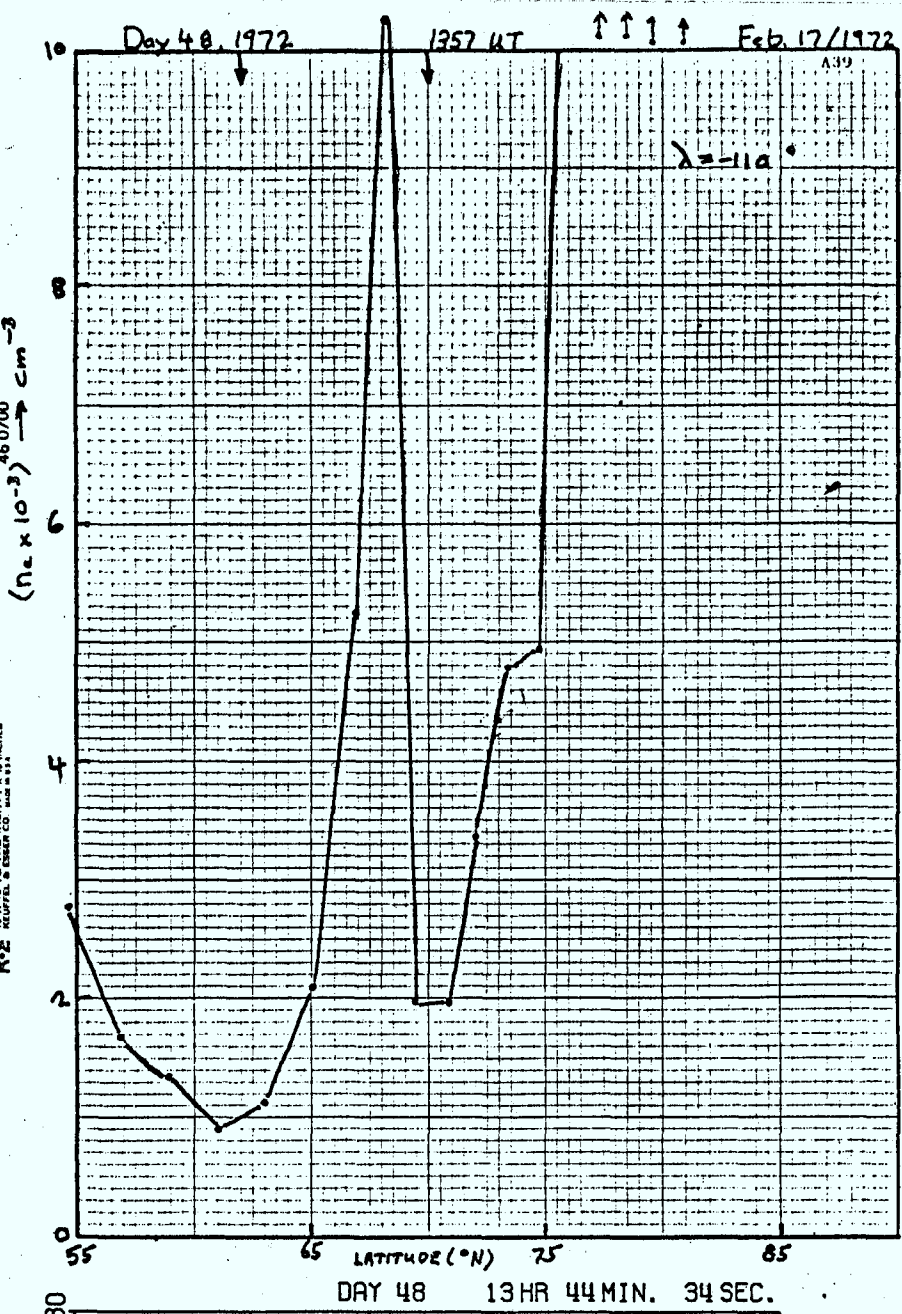
0206 UT

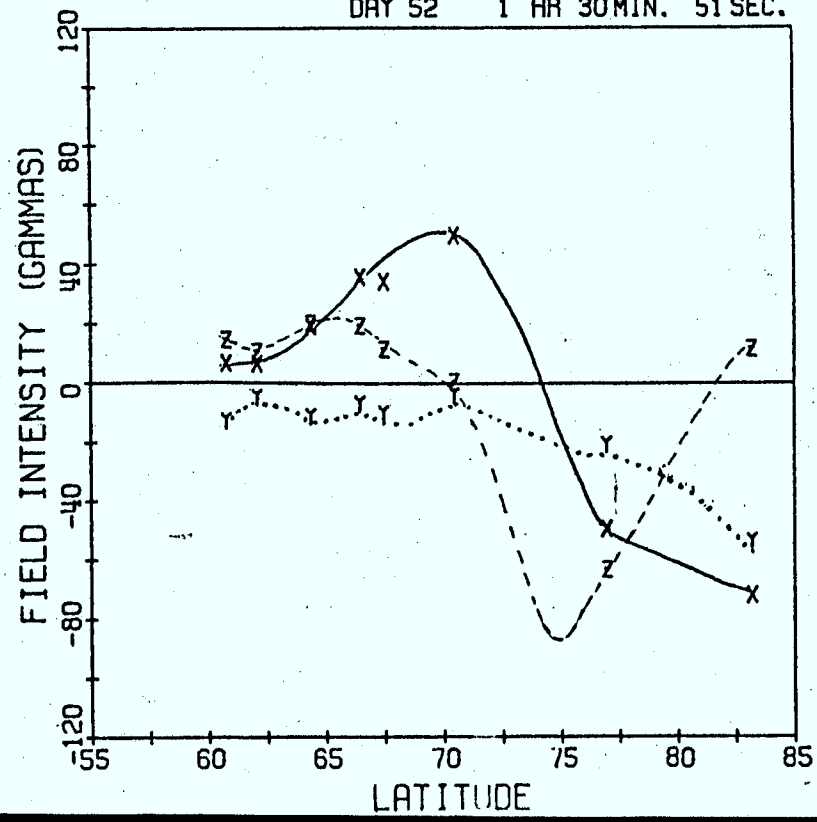
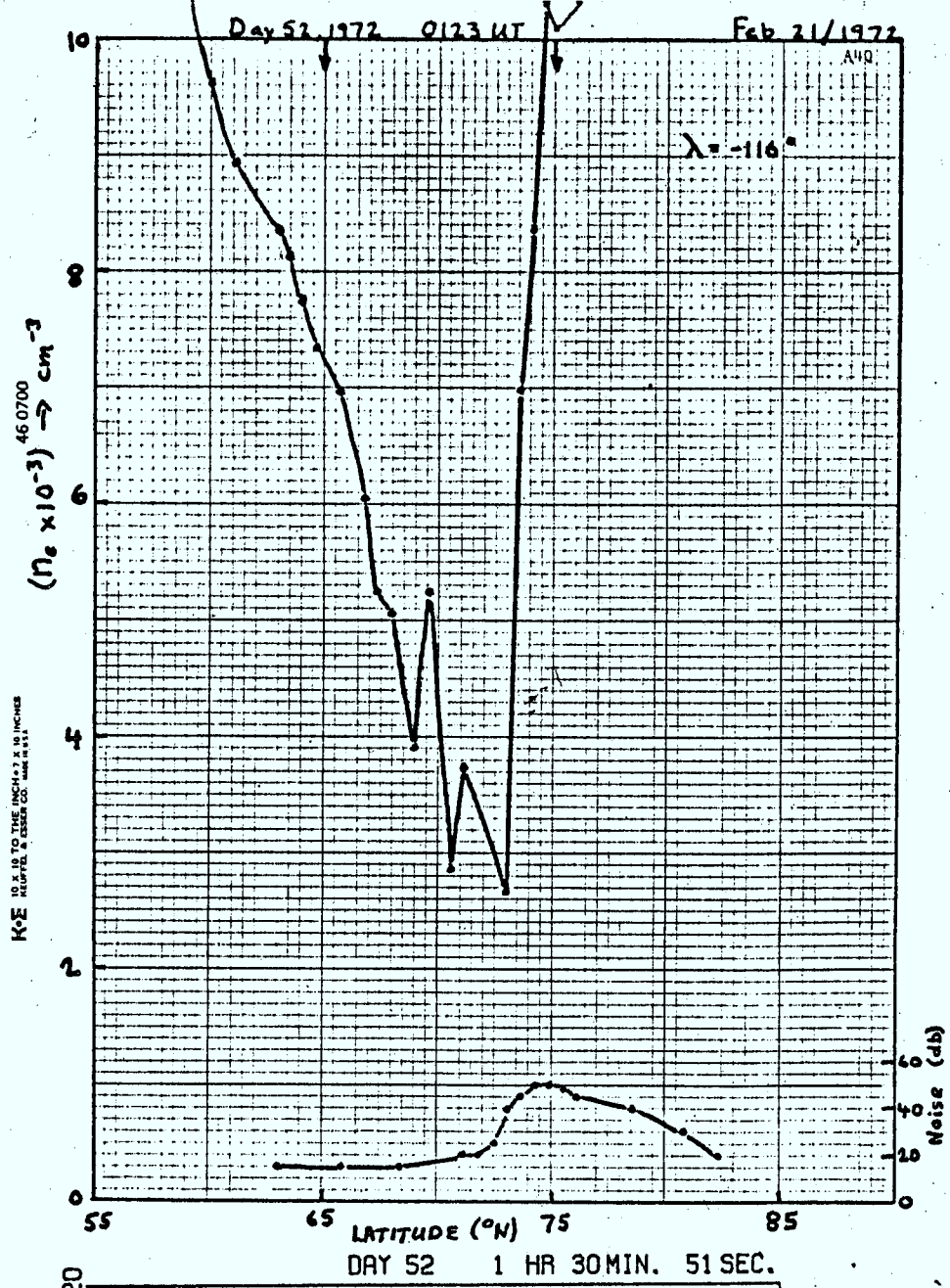
Feb 10/1972

A47

 $\lambda = 112^\circ$ 







Day 53, 1972

1319 UT

Feb 22/1972

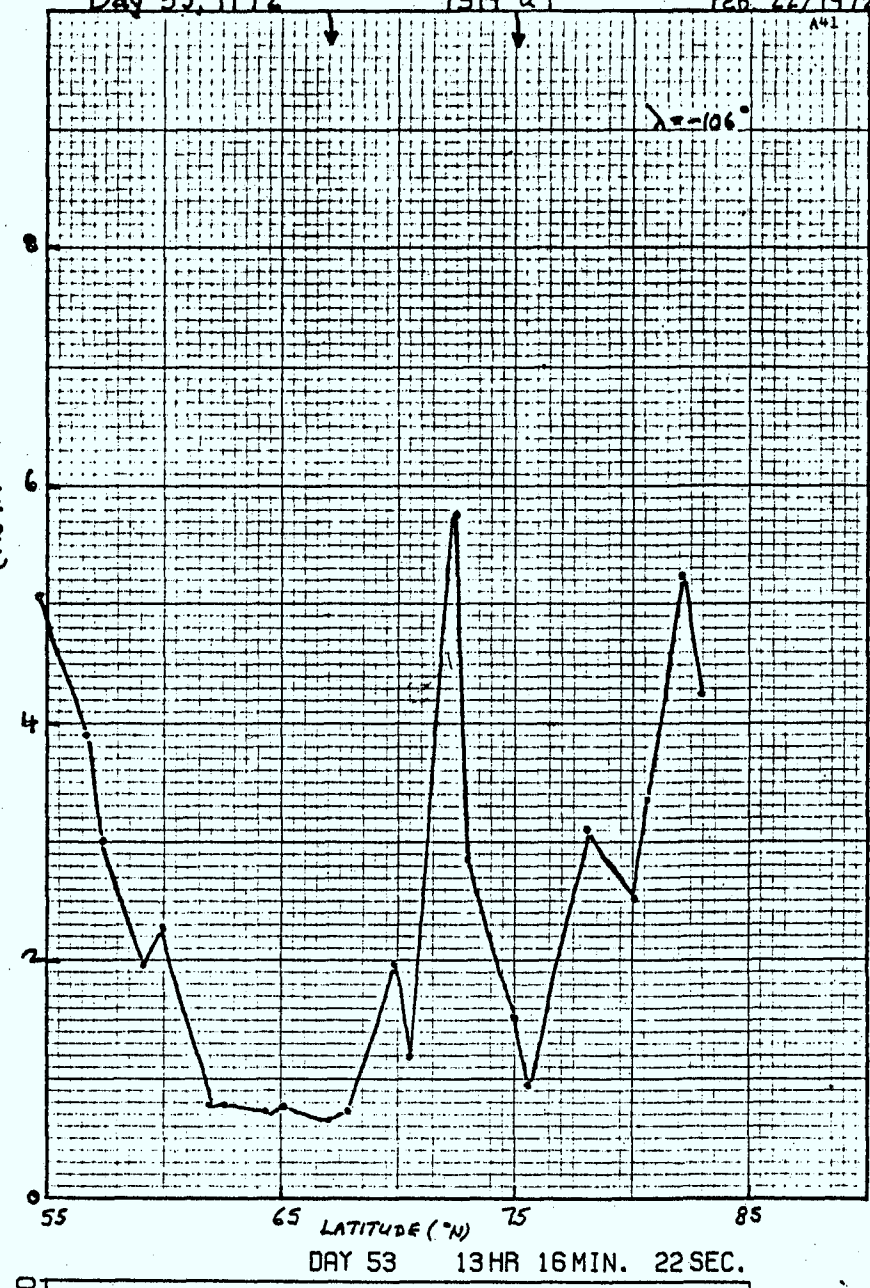
↓

↓

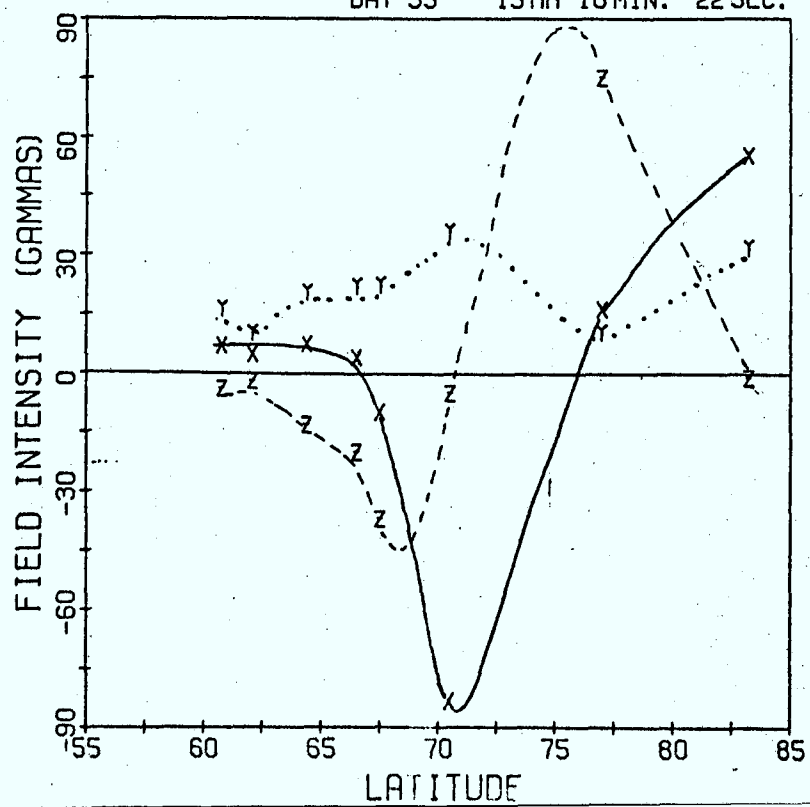
↓

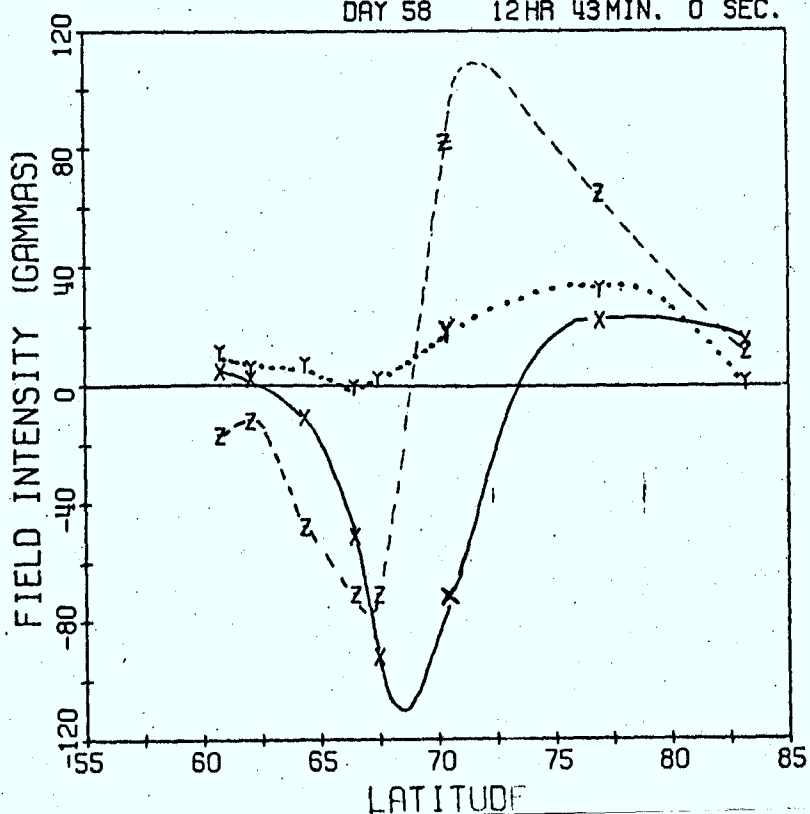
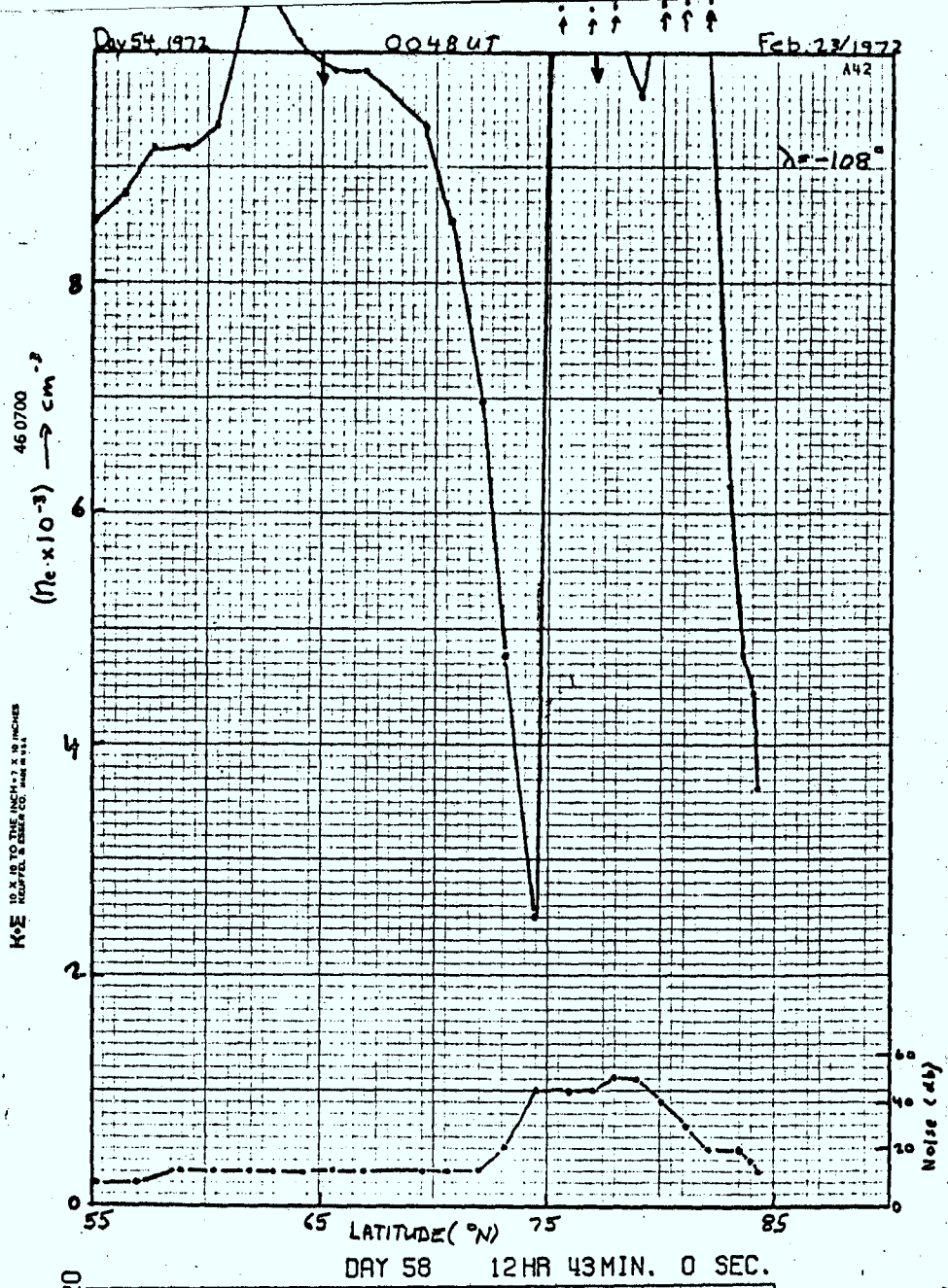
(no. $\times 10^{-3}$) 46.0700 \rightarrow cm $^{-3}$

KOE 10.56 TO THE INCH 7.7 X 10 INCHES



DAY 53 13HR 16MIN. 22SEC.

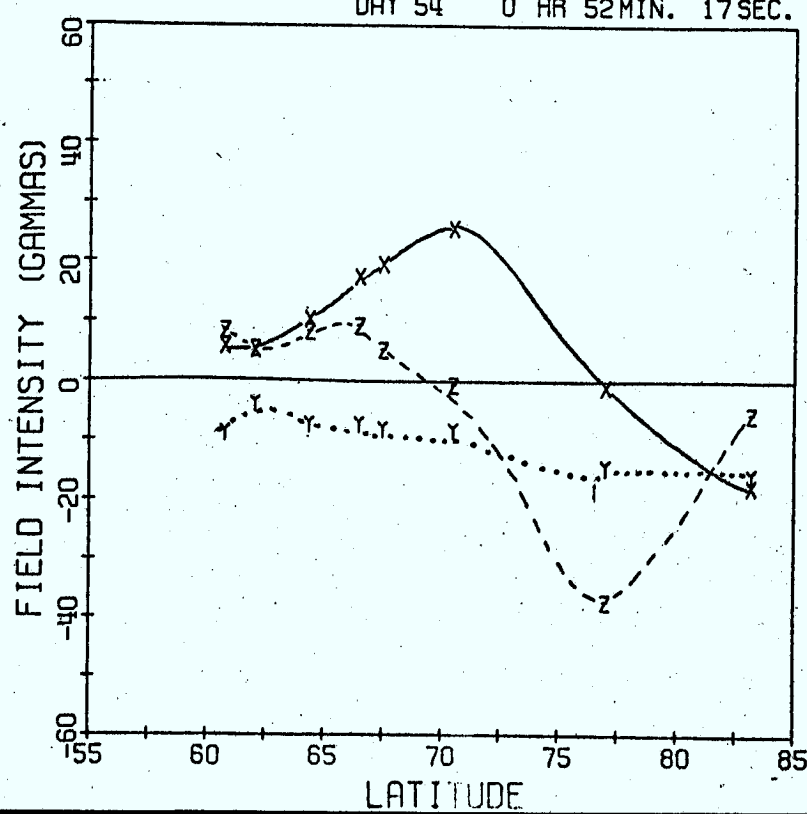
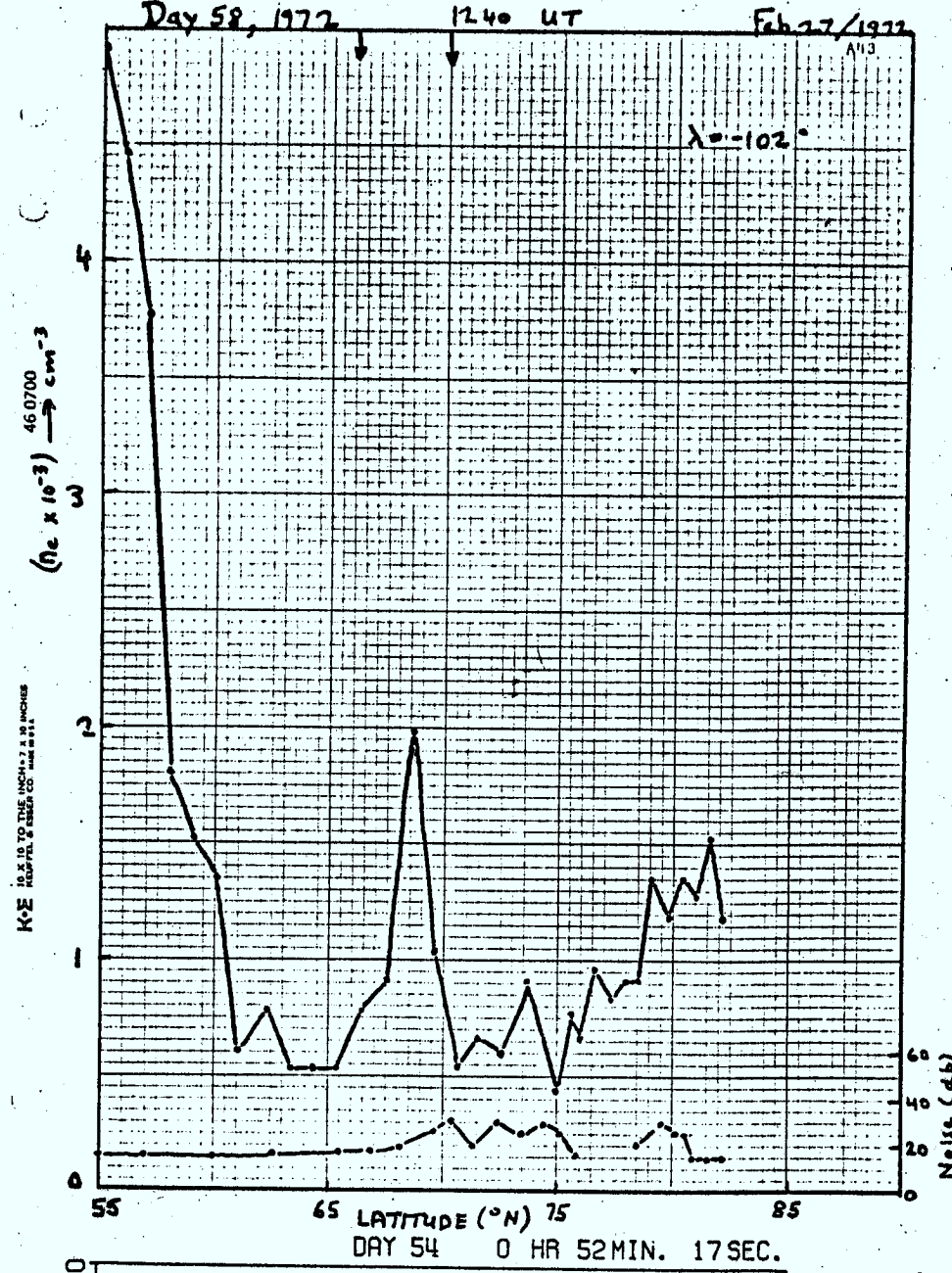




Day 52, 1972

1240 UT

Feb 27/1972





ROSTOKER, GORDON
Research on the correlation of
Alouette-Isis satellite data...

P
91
C655
R688
1975

DATE DUE
DATE DE RETOUR

LOWE-MARTIN No. 1137

CRL-2243
extra